THE PREPARATION AND CHARACTERIZATION OF DENDRIMER COATED MAGNETIC NANOPARTICLES FOR TARGETED CANCER THERAPY

A THESIS SUBMITTED TO
THE GRADUATE SCHOOL OF NATURAL AND APPLIED SCIENCES OF
MIDDLE EAST TECHNICAL UNIVERSITY

BY

ROUHOLLAH KHODADUST

IN PARTIAL FULFILLMENT OF THE REQUIREMENTS
FOR
THE DEGREE OF DOCTOR OF PHILOSOPHY
IN
BIOTECHNOLOGY

SEPTEMBER 2013

Approval of the thesis:

THE PREPARATION AND CHARACTERIZATION OF DENDRIMER COATED MAGNETIC NANOPARTICLES FOR TARGETED CANCER THERAPY

submitted by **ROUHOLLAH KHODADUST** in partial fulfillment of the requirements for the degree of **Doctor of Philosophy in Department of Biotechnology, Middle East Technical University** by,

Prof. Dr. Canan Özgen
Dean, Graduate School of **Natural and Applied Sciences** _____

Prof. Dr. Nesrin Hasırcı
Head of Department, **Biotechnology** _____

Prof. Dr. Ufuk Gündüz
Supervisor, **Department of Biotechnology, METU** _____

Prof. Dr. Güngör Gündüz
Co-Supervisor **Department of Chemical Eng., METU** _____

Examining Committee Members:

Assoc. Prof. Dr. Çağdaş Son
Department of Biological Sciences, METU _____

Prof. Dr.Ufuk Gündüz
Department of Biotechnology,METU _____

Assoc. Prof. Dr. Ayşen Tezcaner
Department of Engineering Sciences, METU _____

Assoc. Prof. Dr. Sreeparna Banerjee
Department of Biotechnology,METU _____

Assoc. Prof. Dr. Bora Maviş
Dept. of Mechanical Engineering, Hacettepe University _____

Date: 4th September 2013

I hereby declare that all information in this document has been obtained and presented in accordance with academic rules and ethical conduct. I also declare that, as required by these rules and conduct, I have fully cited and referenced all material and results that are not original to this work.

Name, Last name: Rouhollah KHODADUST

Signature :

ABSTRACT

THE PREPARATION AND CHARACTERIZATION OF DENDRIMER COATED MAGNETIC NANOPARTICLES FOR TARGETED CANCER THERAPY

Khodadust, Rouhollah
Ph.D., Department of Biotechnology
Supervisor: Prof. Dr. Ufuk Gündüz
Co-Supervisor: Prof. Dr. Güngör Gündüz

September 2013, 109 pages

Nanotechnology is a promising alternative to overcome the limitations of classical chemotherapy. This technology has enabled the development of particles with nano sizes that can be fabricated from a multitude of materials in a variety of compositions. These nanoparticles include; quantum dots (QDs), polymeric nanoparticles, gold nanoparticles, magnetic nanoparticles and dendrimeric nanoparticles.

In first section of this study, superparamagnetic iron oxide nanoparticles were synthesized by coprecipitation method. The nanoparticles were modified with aminopropyltrimethoxysilane and then were coated with PAMAM dendrimer. The detailed characterization of synthesized nanoparticles was performed by X-ray diffraction, X-ray photoelectron spectroscopy (XPS), Fourier transform infrared spectroscopy (FTIR), transmission electron microscopy (TEM), dynamic light scattering, and vibrating sample magnetometer (VSM) analyses. TEM images demonstrated that the DcMNPs have mono-disperse size distribution with an average particle diameter of 16 ± 5 nm. DcMNPs were found to be superparamagnetic through VSM analysis. The synthesis, aminosilane modification, and dendrimer coating of iron oxide nanoparticles were validated by FTIR and XPS analyses. Cellular internalization of nanoparticles was studied by inverted light scattering microscopy, and cytotoxicity was determined by XTT analysis. Results demonstrated that the synthesized DcMNPs, with their functional groups, symmetry perfection, size distribution, magnetic properties, and nontoxic characteristics could be suitable nano-carriers for targeted cancer therapy upon loading with various anticancer agents.

Poly (I: C), which is a synthetic double-stranded RNA, have significant toxicity on tumor cells. In the second part of this study, Poly (I:C) for the first time was efficiently bound onto the surface of different generations of newly synthesized PAMAM dendrimer coated magnetic nanoparticles (DcMNPs) which can be targeted to the tumor site under magnetic field. Poly (I:C) activation was achieved in the presence of EDC and 1-Methylimidazole. Binding of Poly (I:C) onto DcMNPs was followed by agarose gel electrophoresis. Acidic reaction conditions were found as superior to basic and neutral for binding of Poly (I:C). In addition, having more functional groups at the surface, higher generations (G_7, G_6, G_5) of PAMAM DcMNPs were found more suitable as a delivery system for Poly (I:C). In vitro cytotoxicity study on different breast-cancer cell lines demonstrated that Poly (I:C)-bound DcMNPs are more effective than free Poly (I:C). However, highest cytotoxicity of Poly (I:C)-bound DcMNPs was observed in Doxorubicin resistant MCF7 cells. Therefore, Poly (I:C)-bound DcMNPs seem to be a suitable for the treatment of Doxorubicin resistant cells.

In the third part of the study, Doxorubicin loading, release, and stability on nanoparticles (NPs) were analyzed. Doxorubicin could be loaded on G_2, G_3 and G_4DcMNPs with 97% efficiency. The release studies demonstrated that low-generation NPs obtained in this study have pH-sensitive drug release characteristics. G_4DcMNPs, which released most of the drug in lower pH, seems to be the most suitable generation for efficient Doxorubicin delivery. *In vitro* cytotoxicity study on Doxorubicin resistant MCF7 cells demonstrated that application of Doxorubicin-loaded DcMNPs are five times more effective than free Doxorubicin. Therefore, application of Doxorubicin-loaded G_4DcMNPs may help to overcome Doxorubicin resistance in MCF7/Dox cells. On the contrary, G_2 and G_3DcMNPs would be suitable for the delivery of drugs such as Vinca alkaloids and Taxenes, which show their effects in cytoplasm. The results also provide new insights in the development of pH-sensitive targeted drug delivery systems to overcome drug resistance during cancer therapy.

In the last section of the research Poly (I:C) binding on Doxorubicin-loaded G_4DcMNPs at pH 6 and pH 6.5 were studied. Results demonstrated that Doxorubicin loading on lower generation of DcMNPs make them more suitable for Poly (I:C) binding. Loading of Doxorubicin into the cavities of G_4DcMNPs increases the binding efficiency of Poly (I:C) to the surface functional groups up to ten fold. Amine groups at the surface of DcMNPs are the main reasons for the toxicity of these nanoparticles in blood. Binding of Poly (I:C) to amine groups on the surface of Doxorubicin-loaded DcMNPs will decrease the cytotoxicity of the system in the blood and increase its biocompatibility. TEM results demonstrated that Poly (I:C) binding on DcMNPs increases their dispersivity too. When we compared the *in vitro* cytotoxicity of Doxorubicin, Poly (I:C) and Poly (I:C)-bound Doxorubicin-loaded DcMNPs, it was observed that Poly (I:C)-bound Doxorubicin-loaded DcMNPs show the highest cytotoxic effect on Doxorubicin resistant cells. The results demonstrated that Poly (I:C)-bound, Doxorubicin loaded- G_4DcMNPs may be a useful delivery system by the biocompatibility of the complex in blood stream, and by their high toxicity inside tumor cells. These nanoparticles can also be a suitable targeted system to overcome the Doxorubicin resistance in cancer cells.

Keywords: DcMNPs, Poly (I:C), TLR3, Doxorubicin, Breast Cancer

ÖZ

KANSER TEDAVİSİNDE, İLAÇ HEDEFLENMESİ İÇİN KULLANILACAK DENDRIMER KAPLI MANYETİK NANOPARÇACIKLARIN SENTEZİ VE İLAÇ TAŞIMA ÖZELLİKLERİNİN İNCELENMESİ

Rouhollah, Khodadust
Doktora, Biyoteknoloji Bölümü
Tez Yöneticisi: Prof. Dr. Ufuk Gündüz
Ortak Tez Yöneticisi: Prof. Dr. Güngör Gündüz

Eylül 2013, 109 sayfa

Nanoteknoloji klasik kemoterapi sınırlamalarını aşmak için umut verici bir alternatiftir. Bu teknoloji çeşitli malzemelerin birleşimi sonucunda çok farklı özelliklerde nanoparçacıkların (nanopartiküllerin) üretilmesini mümkün kılar. Bu nanoparçacıklar arasında; kuantum noktaları (QDs), polimerik, altın manyetik, ve dendrimerik nanoparçacıklar yer almaktadırlar.

Çalışmanın ilk bölümünde, süperparamanyetik demir oksit nanoparçacıklar, birlikte çöktürme yöntemi ile sentezlenmiştir. Önce aminosilan ile modifiye edilen nanoparçacıklar daha sonra farklı nesillerde (G_2, G_3, G_4, G_5, G_6, G_7) PAMAM dendrimeri ile kaplanmıştır. Sentezlenen parçacıkların detaylı karakterizasyonu X-ışını kırınımı (XRD), X-ışını fotoelektron spektroskopisi (XPS), Fourier transform infrared spektroskopisi (FTIR), elektron mikroskobu (TEM), dinamik ışık saçılması (DLS) ve titreşimli manyetometre (VSM) analiz yöntemleri ile yapılmıştır. TEM görüntüleri, dendrimer kaplı nanoparçacıkların düzgün boyut dağılımında ve 16 ± 5 nm civarı parçacık çapına sahip olduklarını göstermiştir. Dendrimer kaplı nanoparçacıkların süperparamanyetik olduğu saptanmıştır. Demir oksit nanoparçacıklarının sentezi, aminosilan modifikasyonu ve dendrimer kaplanması FTIR ve XPS analizi ile doğrulanmıştır. Nanoparçacıkların hücre içine alımı ters ışık saçılımlı mikroskop ile incelenmiş ve hücrelerdeki toksisiteleri XTT analizi ile belirlenmiştir. Elde edilen sonuçlar, sentezlenmiş olan dendrimer kaplı

nanoparçacıkların yüzeylerindeki fonksiyonel grupları, simetri mükemmellikleri, boyut dağılımları, manyetik özellikleri, ve toksik olmamaları nedeniyle çeşitli anti-kanser ajanların kanserli bölgeye hedefleme amacı için uygun olabileceğini göstermiştir.

Çalışmanın ikinci bölümünde, manyetik alan altında tümörlü bölgeye hedeflemek amacı ile, Poli (I:C) ilk kez olarak farklı nesillerdeki PAMAM dendrimer ile kaplanmış manyetik nanoparçacıkların (DcMNPs) yüzeyine bağlanmıştır. Çift sarmallı sentetik bir RNA olan Poli (I:C)'nin tümör hücreleri üzerinde önemli bir toksisiteye sahip olduğu bilinmektedir. Öncelikle EDC ve 1-Metilimidazol kullanarak, Poli (I:C) aktivasyonu gerçekleşmiş, Poli (I:C) moleküllerinin bağlanması, agaroz jel elektroforezi ile takip edilmiştir. Yüzeyinde daha fazla fonksiyonel gruba sahip olan yüksek nesil (G_7, G_6, G_5) nanoparçacıkların, Poli (I:C) için daha uygun taşıyıcılar olduğu gösterilmiştir. Farklı meme kanseri hücre hatları üzerindeki *in vitro* sitotoksisite çalışmaları, DcMNP-bağlı Poly (I:C) sisteminin serbest Poly (I:C) den daha etkili olduğunu göstermiştir. DcMNP' lere bağlı Poli (I:C)'nin sitotoksik etkisinin, doksorubisin dirençli MCF7 hücre hattında en yüksek olduğu gözlenmiştir. Bu nedenle, Poli (I:C) bağlı DcMNP'ler Doksorubisine dirençli kanserlerin tedavisi için daha uygun görünmektedirler.

Bu çalışmanın üçüncü bölümünde, Doksorubisin'in nanoparçacıklara yüklenmesi, salımı, ve dayanıklılığı incelenmiştir. Doksorubisin ilk olarak %97 verimle G_2, G_3 ve G_4 nanoparçacıklara yüklenmiş, bu düşük nesil nanoparçacıkların pH- duyarlı ilaç salım özelliğine sahip oldukları gösterilmiştir. G_4DcMNP, ilacın çoğunu düşük pH'da salmakta ve Doxorubisin hedeflemesi için en uygun nesil olarak görünmektedir. Doksorubisin dirençli MCF7 hücreleri üzerindeki *in vitro* sitotoksisite çalışmaları, Doxorubisin yüklü DcMNP lerin serbest doksorubisin'e göre beş kat daha fazla etkili olduğunu göstermiştir. Bu nedenle, Doksorubisin yüklü G_4DcMNP'ler, Doksorubisin dirençliliğini yenmek için yararlı olabilirler. G_2 ve G_3DcMNP'ler ise Vinka alkaloid veya Taksoid grubu ilaçların yüklenmesi için daha uygun olacaktır.

Araştırmanın son bölümünde, Poli (I:C)'nin, Doksorubisin yüklü G_4DcMNP'ler üzerine bağlanma özellikleri pH 6.0 ve pH 6.5 değerlerinde incelenmiştir. Doksorubisin G4DcMNP'lere yüklendiği zaman, Poli (I:C)'nin yüzeydeki fonksiyonel guruplara bağlanmasının on kat daha arttığı gözlenmiştir. Poli (I:C)'nin Doksorubisin yüklü DcMNP'lerin yüzeyindeki amin gruplarına bağlanması, bu nanoparçacıkların kandaki sitotoksik etkilerini azaltarak onları biyo-uyumlu hale getirmeye yardımcı olmaktadır. Çünki DcMNP'lerin amin grupları bu nanoparçacıkların asıl toksisite nedenleridir. Ayrıca, TEM sonuçlarına göre Poli (I:C) DcMNP'lere bağlandığında nanoparçacıkların birbirlerinden ayrılmasını da sağlamaktadır. Serbest Doksorubisin ve bu çalışmada hazırlanan diğer taşıyıcı sistemler kullanılarak yapılan sitotoksisite karşılaştırmaları, Poli (I:C) bağlı, Doksorubisin yüklü DcMNP'lerin Doksorubisin'e dirençli MCF7 hücrelerinde en yüksek toksik etkiye sahip olduğunu göstermiştir. Bu nedenle, geliştirilen Poli (I:C) bağlı, Doksorubisin yüklü DcMNP'ler, kanserli hücrelerdeki dirençliliği aşabilecek önemli bir ilaç hedefleme sistemi olma potansiyeli taşımaktadırlar.

Anahtar Kelimeler: DcMNPs, Poly (I:C), TLR3, Doksorubisin, Meme kanseri

To my beloved Wife Elham Malekifard

ACKNOWLEDGEMENTS

First, I would like to express my deepest gratitude to my supervisor Prof. Dr. Ufuk Gündüz for her great advises, support and guidance throughout this study. I would also thank to my co-supervisor Prof. Dr. Güngör Gündüz for his valuable contributions, support and encouragement in this research.

I feel great appreciation to Assoc. Prof. Dr. Bora Maviş for his valuable support for FTIR analysis throughout our research.

I would like to thank Examining committee members Assoc. Prof. Dr. Sreeparna Banerjee and Assoc. Prof. Dr. Ayşen Tezcaner for their participation and valuable comments.

I am grateful to Gözde Ünsoy, SerapYalçin and Pelin Kaya for their friendship and pleasant collaboration in this study.

Aktan Alpsoy, Murat Erdem, Esra Kaplan, Gülistan Tansık, Tuğba Keskin, Cağri Urfali, Negar Taghavi, other members of Lab 206 and also our special project students are greatly acknowledged for their friendship and contributions throughout this study.

I would like to express my great appreciation to my family members for their physical and moral support and encouragement in my life.

I am deeply indebted to my father Ismail and my mother for their endless love, trust and support in every step of my life.

Lastly, I am thankful to my wife Elham more than expressed in words for her endless love and physical help in my thesis.

This study was supported by the Research Fund of METU Grant No: BAP-07-02-2010-06 and TÜBİTAK Grant No: TBAG: 109T949.

In addition, PhD scholarship for foreign students-TÜBİTAK Grant No: 2215 is acknowledged.

TABLE OF CONTENTS

ABSTRACT v

ÖZ vii

ACKNOWLEDGEMENTS x

TABLE OF CONTENTS xi

LIST OF TABLES xvi

LIST OF FIGURES xvii

CHAPTERS

1. INTRODUCTION 1

1.1 Cancer 1

1.1.1 Breast Cancer 1

1.2 Nanoparticles and Cancer Therapy 1

1.2.1 Magnetic Nanoparticles 3

1.2.1.1 Synthesis of Magnetic Nanoparticles with Coprecipitation Method 4

1.2.1.1.1 Ferrous Salts Only 5

1.2.1.1.2 Ferrous and Ferric Salts 6

1.2.1.2 Superparamagnetism 6

1.2.2 Dendrimeric Nanoparticles 7

1.2.2.1 PAMAM Dendrimers 8

1.2.2.1.1 Structure of PAMAM Dendrimers 8

1.2.2.1.2 Divergent Synthesis of PAMAM Dendrimers 11

1.2.2.1.3 Surface Modification of PAMAM Dendrimers 13

1.2.2.1.3.1 Amine Acetylation 13

1.2.2.1.3.2 PEGylation 14

1.2.2.1.3.3 Folic Acid Modification 15

1.2.2.1.4 PAMAM Dendrimer, a Suitable Delivery System 16

1.2.2.1.4.1 Encapsulation of Drugs into the Cavities of PAMAM Dendrimer 17

1.2.2.1.4.2 Covalently Conjugation of Drug or Chemotherapeutic Reagents - PAMAM Dendrimer 18

1.2.2.1.4.3 Gene Therapy 19

1.3 Doxorubicin 20

1.3.1 Action Mechanism of Doxorubicin 21

1.3.2 Resistance Mechanism of Doxorubicin 22

1.4 Polyinosinic: Polycytidylic Acid (Poly (I:C)) 23

1.4.1 Poly (I:C) Endosomal Mechanism of Action 25

1.4.2 Poly (I:C) Cytosolic Mechanism of Action 26

2. MATERIALS AND METHODS 29

2.1 Materials 29

2.2 Cell Culture 29

2.2.1 Growth Conditions 29

2.2.2 Cell Harvesting (Passaging) 30

2.2.3 Freezing and Thawing of Cells 30

2.2.4 Cell Proliferation Assays (XTT Cell Proliferation Assay) 30

2.3 Synthesis of DcMNPs 31

2.3.1 Preparation of MNPs 31

2.3.2 Preparation of APTS Coated NPs 32

2.3.3 Surface Coating with PAMAM Dendrimer 33

2.3.4 Cellular internalization of dendrimer coated magnetic nanoparticles 33

2.3.5 Cytotoxicity Analysis of G_4DcMNPs and G_7DcMNPs 33

2.4 Poly (I:C) loading on DcMNPs 34

2.4.1 Poly (I:C) Activation 34

2.4.2 Poly (I:C) Loading Optimization on G_7DcMNPs at pH 7, and pH 7.5 34

2.4.3 Poly (I:C) Loading Optimization on G_7DcMNPs at pH 6 34

2.4.4 Stability of Poly (I:C)-bound DcMNPs..... 34

2.4.5 Cytotoxicity Analysis of Poly (I:C)-bound G_7DcMNPs 35

2.5 Doxorubicin Loading on DcMNPs 35

2.5.1 Doxorubicin Loading on Different Generation of DcMNPs..... 35

2.5.2 Stability of Doxorubicin on DcMNPs..... 35

2.5.3 Release of Doxorubicin from DcMNPs 35

2.5.4 Cellular Internalization of Doxorubicin-Loaded Dendrimer Coated Magnetic Nanoparticles 35

2.5.5 Cytotoxicity Analysis of Doxorubicin-Loaded G_4DcMNPs on Resistant MCF7 Cells 36

2.6 Poly (I:C)-bounding on Doxorubicin-Loaded DcMNPs..... 36

2.6.1 Poly (I:C) Binding on G_4DcMNPs..... 36

2.6.2 The Amount of Loaded Doxorubicin on G_4DcMNPs Affects the Efficiency of Poly (I:C) Binding..... 36

2.6.3 PH Effects on Poly (I:C) Binding on Doxorubicin-Loaded G_4DcMNPs..... 36

2.6.4 Cytotoxicity Analysis of Poly (I:C)-bound Doxorubicin-Loaded G_4DcMNPs. 36

3. RESULTS 37

3.1 Synthesis of DcMNPs 37

3.1.1 Synthesis of Magnetic Nanoparticles..... 37

3.1.2 Aminosilane Modification of Nanoparticles..... 37

3.1.3 X-ray Diffraction Analysis (XRD)..... 38

3.1.4 Fourier Transform-Infrared Spectroscopy (FT-IR)..... 39

3.1.5 Transmission Electron Microscopy Analysis (TEM) 40

3.1.6 Dynamic Light Scattering Analysis (DLS)..... 40

3.1.7 Zeta (ζ) Potential Analysis..... 41

3.1.8 Vibrating Sample Magnetometer Analysis (VSM)..... 41

3.1.9 Thermal Gravimetric Analysis (TGA-FTIR)..... 42

3.1.10 X-ray Photoelectron Spectroscopy (XPS) 43

3.1.11 Cellular Internalization of Dendrimer Coated Magnetic Nanoparticles 45

3.1.12 Cytotoxicity study of dendrimer-coated magnetic nanoparticles 47

3.2 Poly (I:C) Binding on DcMNP 49

3.2.1 Surface Functional Group 49

3.2.2 Poly (I:C) Activation in the Presence of EDC and 1-Methylimidazole 49

3.2.3 Poly (I:C) Loading Efficiency Studies 50

3.2.3.1 Poly (I:C) Loading Efficiency Studies on DcMNPs at pH 7 and pH 7.5 .. 51

3.2.3.2 Poly (I:C) Loading Efficiency Studies on DcMNPs at pH 6 53

3.2.4 Poly (I:C) Loaded DcMNPs Stability Studies 54

3.2.5 Cytotoxicity Study of Poly (I:C)-Bound DcMNPs 55

3.3 Doxorubicin Loading on DcMNPs 57

3.3.1 Doxorubicin Loading on DcMNPs Using Different Buffers 58

3.3.2 Doxorubicin Loading Efficiencies into DcMNPs at Different Concentrations . 59

3.3.3 Doxorubicin Loading, Encapsulation Efficiency, Doxorubicin Content and Process Yield on G_4DcMNPs 60

3.3.4 Doxorubicin Loading Efficiencies on Different Generation of DcMNPs 61

3.3.5 Doxorubicin Loading, Encapsulation Efficiency, Doxorubicin Content and Process Yield on Different Generation of DcMNPs 62

3.3.6 Stability Study of Doxorubicin-Loaded DcMNPs 65

3.3.6 Release study of Doxorubicin-Loaded DcMNPs 67

3.3.7 Cellular Internalization of Doxorubicin-Loaded Dendrimer Coated Magnetic Nanoparticles 68

3.3.8 Cytotoxicity Study of Doxorubicin-Loaded DcMNPs 69

3.4 Poly (I:C) Binding on Doxorubicin-Loaded DcMNPs 71

3.4.1 Poly (I:C) Binding on G_4DcMNPs 72

3.4.2 The Amount of Loaded Doxorubicin on G_4DcMNPs Affects the Efficiency of Poly (I:C) Binding 72

3.4.3 PH Affects the Poly (I:C) Binding on Doxorubicin-Loaded G_4DcMNPs..... 73

3.4.4 Doxorubicin Release from G_4DcMNPs and PIC-G_4DcMNPs 74

3.4.5 Cytotoxicity Analysis of Poly (I:C)-Bound Doxorubicin-Loaded G_4DcMNPs 75

4. DISCUSSION 77

5. CONCLUSIONS..... 87

REFERENCES 89

CURRICULUM VITAE 103

LIST OF TABLES

TABLES

Table1.1 Organisms with biogenic magnetite in their body (Landmark *et al.*, 2008)..... 4

Table1.2 Particle properties as produced by the listed techniques. (Landmark *et al.*, 2008)... 5

Table1.3 Approximate diameters of diferent generations of PAMAM dendrimers. Adapted from (Tomalia *et al.*, 2004). 10

Table 3.1 Atomic percentage changes in bare iron oxide, aminosilane-modified, G_5 and G_7DcMNPs. 45

Table 3.2 Doxorubicin loading, encapsulation efficiency, Doxorubicin content and process yield on G_4DcMNPs calculated from equations; 3.2, 3.3, 3.4 and 3.5. 61

Table 3.3 Drug loading, encapsulation efficiency, drug content and process yield of 400 µg/ml Doxorubicin concentrations on different generation of DcMNPs at room temperature. 63

Table 3.4 Drug loading, encapsulation efficiency, drug content and process yield of 500 µg/ml Doxorubicin concentrations on different generation of DcMNPs at room temperature. 63

Table 3.5 Drug loading, encapsulation efficiency, drug content and process yield of 400 µg/ml Doxorubicin concentrations on different generation of DcMNPs at 4 °C. 64

Table 3.6 Drug loading, encapsulation efficiency, drug content and process yield of 500 µg/ml Doxorubicin concentrations on different generation of DcMNPs at 4 °C. 65

Table 3.7 IC_{50} values related to free Poly (I:C), Doxorubicin, Doxorubicin-loaded DcMNPs Poly (I:C) linked DcMNPs, and Poly (I:C)-bound Doxorubicin-loaded DcMNPs. 76

LIST OF FIGURES

FIGURES

Figure 1.1 Naturally present nano and micro-molecules and synthesized nanoparticles comparison in size (Arruebo *et al.*, 2007)..... 2

Figure 1.2 Schematic Representation of the targeting of the Doxorubicin and Poly (I:C) with DcMNPs..... 3

Figure 1.3 The scheme illustrates two strategies to fabricate multifunctional magnetic nanoparticles and their potential applications (Gao *et al.*, 2009)..... 7

Figure 1.4 The core shell structure of PAMAM dendrimer..... 9

Figure 1.5 Periodic properties of PAMAM dendrimers as a function of their generations. Adapted from (Tomalia *et al.*, 2004) 11

Figure 1.6 Structure of dendritic macromolecules: A) structural elements, B) dendron, and C) Dendrimer. 12

Figure 1.7 Synthesis of PAMAM dendrimers with ethylenediamine core. 13

Figure 1.8 Acetylation of PAMAM dendrimers. Acetic anhydride reacts with primary amines of G_5PAMAM dendrimers to produce acetylated PAMAM..... 14

Figure 1.9 Synthesis of PEGylated PAMAM dendrimers. 15

Figure 1.10 Chemical structures of folic acid- PEG4000- G_4 PAMAM dendrimers..... 16

Figure 1.11 Drugs encapsulated inside the cavities of PAMAM dendrimer. 17

Figure 1.12 PAMAM dendrimer−drug conjugate where the drug molecules are either directly coupled to the surface groups of PAMAM dendrimer or via a pH-sensitive linkage. 18

Figure 1.13 Gene transfection of PAMAM dendrimer. 19

Figure 1.14 Chemical structure of Doxorubicin. 21

Figure 1.15 Doxorubicin mechanism of action (Thorn *et al.*, 2011) 22

Figure 1.16 Doxorubicin resistance mechanisms; P-gps inhibit Doxorubicin effect by drug efflux (a). When delivered through endosome by nanoparticles, Doxorubicin cannot be caught efflux P-glycoprotein (b) (Wu *et al.*, 2012)..... 23

Figure 1.17 Schematic representation of TLRs and their related ligands and adaptors (Okado. *et al.*, 2009)..... 24

Figure 1.18 Chemical structure of Polyinosinic: Polycytidylic acid. 24

Figure 1.19 Structure of TLR3 receptor protein and the way that dsRNA bind to it (Vercammen *et al.*, 2008)..... 25

Figure 1.20 TLR3 Mediated Signaling Pathways activated by dsRNA (Vercamman *et al.*, 2008)..... 26

Figure 1.21 RIG-1 and MDA-5 Signaling Pathways Activated By dsRNA (Vince *et al.*, 2010)..... 27

Figure 2.1 Schematic representation of 96-well plate 4 h after XTT reagent addition to drug treated MCF7 cells. 31

Figure 2.2 Schematic representation of the system for the synthesis of bare iron oxide nanoparticles..... 32

Figure 3.1 Stepwise modification of iron oxide nanoparticles with APTS and dendron. 38

Figure 3.2 XRD analysis of nanoparticles synthesized at different temperatures..... 38

Figure 3.3 X-Ray powder diffraction of Fe_3O_4 and Fe_3O_4-APTS nanoparticles..... 39

Figure 3.4 FT-IR results related to MNP, MNP-APTS, and different generations of dendrimer-modified magnetic nanoparticles..... 39

Figure 3.5 The sizes of obtained G_7DcMNPs were 16 ± 5 nm. The change of the size after dendrimer modification was around 8 nm..... 40

Figure 3.6 Dynamic light scattering graphs of bare MNPs (a) and G_7DcMNPs (b). 41

Figure 3.7 Magnetization curve of the MNPs, APTS-modified MNPs and DcMNPs at 37 °C. 41

Figure 3.8 Magnetization curve of the MNPs, APTS-modified MNPs and DcMNPs at 25 °C. 42

Figure 3.9 The TGA curve of bare, aminosilane modified and dendrimer coated MNPs..... 43

Figure 3.10 General XPS scanning spectrum belonging to the surfaces of bare MNP, G_0, G_5, and G_7 nanoparticles (a), the peaks obtained upon XPS analysis belonging to O 1s (b), Fe 2p (c), Si 2p (d), N 1s (e), and C 1s (f)..... 44

Figure 3.11 Cellular internalization of dendrimer-coated magnetic nanoparticles by inverted light scattering microscopy (40X)..... 46

Figure 3.12 Cellular internalization of FITC binding dendrimer coated magnetic nanoparticles by confocal microscopy (40 X). 47

Figure 3.13 Cytotoxicity of G_4DcMNPs (a), and G_7DcMNPs (b) on 1µM Doxorubicin resistant MCF7 cells. 48

Figure 3.14 Cytotoxicity of G_4DcMNPs (a), and G_7DcMNPs (b) on MCF7..... 48

Figure 3.15 Cytotoxicity of G_4DcMNPs (a), and G_7DcMNPs (b) on SkBr-3..... 48

Figure 3.16 The X-ray photoelectron spectroscopy (XPS) analysis of bare MNP, G_0DcMNPs, G_5DcMNPs and G_7DcMNPs..... 49

Figure 3.17 Activation of Poly (I:C) by EDC and formation of phosphoramidate bond between phosphate group of Poly (I:C) and surface amine groups of DcMNPs. 50

Figure 3.18 Dynamic Light Scattering graphs of Poly (I:C)-bounded G_7DcMNPs (a).TEM images of Poly (I:C)-bounded G_7DcMNPs in 200 nm (b), and 100 nm scale bars(c). 51

Figure 3.19 Agarose gel electrophoresis of loading optimization 4 µg Poly (I:C) on G7DcMNPs at pH 7.5. Well 1,2, 3, 4, 5 and 6 contain 1:10, 1:15, 1:20, 1:25, 1:30, 1:35 ratio of Poly (I:C) :G7DcMNPs. Well 7 contains control Poly (I:C) and wells 8,9,10,11, and 12 contain 1/2,1/4,1/8, 1/16, 1/32 dilution of control Poly (I:C) . 1 in the ratio represents 4 µg of Poly (I:C) or DcMNP..... 52

Figure 3.20 Agarose gel electrophoresis of loading optimization of 4 µg Poly (I:C) on G_7DcMNPs at pH 7. In first well 4 µg Poly (I:C) was loaded as control. Wells 2, 3 and 4 contain 40 µg , 80 µg, and 120 µg G_7DcMNPs, respectively. The wells 5-9 contain 1:2.5, 1:5, 1: 10, 1:20, and 1:30 ratio of Poly (I:C): G_7DcMNPs. 1 in the ratio represents 4 µg of Poly (I:C) or DcMNP..... 52

Figure 3.21 Agarose gel electrophoresis of loading optimization Poly (I:C) on G_7, G_4, G_3, and G_2DcMNPs at pH 7. Wells 1-16 show the Poly (I:C) loading on G_7, G_4, G_3, and G_2DcMNPs at four different ratio. Wells 17-20 show the control Poly (I:C) and different dilution. 1 in the ratio represents 4 µg of Poly (I:C) or DcMNP. 53

Figure 3.22 Agarose gel electrophoresis of loading optimization Poly (I:C) on G_7, G_6, and G_5DcMNPs at pH 6. The ratios of Poly (I:C) to G_7, G_6 and G_5DcMNP were changed from 1:10 to 1:15. Wells 16-20 show the Poly (I:C) control and different dilutions. 1 in the ratio represents 4 µg of Poly (I:C) or DcMNPs. 53

Figure 3.23 Agarose gel electrophoresis of loading optimization Poly (I:C) on G_7, G_6, G_5, G_4, G_3, and G_2DcMNPs at pH 6. Wells 1-5 demonstrate the control Poly (I:C) and different dilutions. Wells 6-11 show the PIC: DcMNPs ratios of G_7, G_6, G_5, G_4, G_3, and G_2DcMNPs. 1 in the ratio represents 4 µg of Poly (I:C) or DcMNP..... 54

Figure 3.24 Agarose gel electrophoresis of release study of Poly (I:C) on G_7, G_6, G_5, G_4, G_3, and G_2DcMNPs at pH 8.8, 9.0, and 9.2 for each generation respectively. 1 in the ratio represents 4 µg of Poly (I:C) or DcMNPs. 55

Figure 3.25 XTT cell proliferation assay of Poly (I:C)-bound DcMNPs on MCF7S cells. The IC50 values of Poly (I:C)-bound DcMNPs on MCF7 were calculated as 40 µg/ml. 55

Figure 3.26 XTT cell proliferation assay of Poly (I:C)-bound DcMNPs on SkBr-3 cells. The IC50 values of Poly (I:C)-bound DcMNPs on SkBr-3 were calculated as 44 µg/ml. 56

Figure 3.27 XTT cell proliferation assay of Poly (I:C)-bound DcMNPs on MCF7 Dox resistant cells. The IC50 values of Poly (I:C)-bound DcMNPs on MCF7 1µM Dox resistant cells were calculated as 28 µg/ml. 56

Figure 3.28 XTT cell proliferation assay of free Poly (I:C) and Poly (I:C)-bound DcMNPs on MCF7 Dox resistant cells. The IC50 values of free Poly (I:C) and Poly (I:C)-bound DcMNPs on MCF7 1µM Dox resistant cells were calculated as 450 µg/ml and 28 µg/ml. .. 57

Figure 3.29 Schematic representation of Doxorubicin loading into the cavities of DcMNPs. 57

Figure 3.30 Loading efficiencies of Doxorubicin to G_4DcMNPs in different buffers (PBS, TES, and acetate buffer) and in different drug concentrations. 58

Figure 3.31 FTIR analysis of Doxorubicin, G_4DcMNPs, and 400 µg/ml Doxorubicin-loaded G_4DcMNPs. 59

Figure 3.32 Doxorubicin loading efficiencies at different concentrations (90–600 µg/ml) on G_4DcMNPs (5 mg/ml). 60

Figure 3.33 Loading efficiencies of Doxorubicin (400 and 500 µg/ml) onto DcMNPs at room temperature (a) and at 4 °C (b). 62

Figure 3.34 The stability of 400 µg/ml Doxorubicin-loaded G_4DcMNPs (a) and 500 µg/ml Doxorubicin-loaded G_4DcMNPs (b) in PBS buffer (pH 7.2). 66

Figure 3.35 The stability of 400 µg/ml Doxorubicin-loaded G_4DcMNPs (a) and 500 µg/ml Doxorubicin-loaded G_4DcMNPs (b) in human blood serum. 66

Figure 3.36 Release of 400 µg/ml Doxorubicin from (G_2, G_3 and G_4) DcMNPs at pH 5.2 (a) and pH 4.2 (b). 67

Figure 3. 37 Release of 500 µg/ml Doxorubicin from (G_2, G_3 and G_4) DcMNPs at pH 5.2 (a) and pH 4.2 (b). 68

Figure 3.38 Bright field microscopy image of Doxorubicin Resistant MCF7 cells Treated with 30 µM (18 µg/ml) Doxorubicin which was loaded on G_4DcMNPs (a) fluorescent microscopy image of MCF7/ 1µM Doxorubicin Resistant cells Treated with 30 µM (18

µg/ml) Doxorubicin-loaded G_4DcMNPs (b). Bright field microscopy image of MCF7/ 1µM Doxorubicin Resistant cells Treated with 30 µM free Dox (c) and fluorescent microscopy image of MCF7/ 1µM Doxorubicin Resistant cells Treated with 30 µM free Doxorubicin (d) 69

Figure 3.39 Doxorubicin cytotoxicity effect on Dox-resistant MCF7 cells..... 70

Figure 3.40 Cytotoxic effects of Doxorubicin-loaded G_4DcMNPs on MCF7/ 1µM Doxorubicin resistant cells..... 71

Figure 3.41 Schematic representation of Poly (I:C) modification of Doxorubicin-loaded DcMNPs..... 72

Figure 3.42 Agarose gel electrophoresis of loading optimization of poly on G_4DcMNPs at pH 6 and pH 6.5. Wells 1-8 demonstrate the loading of Poly (I:C) at pH 6. Wells 9-16 demonstrate the loading of Poly (I:C) at pH 6.5. Wells 17-20 demonstrate the control Poly (I:C) and different dilutions. 1 in the ratio represents 4 µg of Poly (I:C) or DcMNP..... 72

Figure 3.43 Agarose gel electrophoresis of loading optimization Poly on 500 µg/ml and 400 µg/ml Doxorubicin-loaded G_4DcMNPs at pH 6. Wells 1-8 demonstrate the loading of Poly (I:C) on 500 µg/ml Doxorubicin-loaded G_4DcMNPs. Wells 9-16 demonstrate the loading of Poly (I:C) on 400 µg/ml Doxorubicin-loaded G_4DcMNPs. Wells 17-20 demonstrate the control Poly (I:C) and different dilutions. 1 in the ratio represents 4 µg of Poly (I:C) or DcMNP. 73

Figure 3.44 Agarose gel electrophoresis of binding optimization of poly on 500 µg/ml Doxorubicin-loaded G_4DcMNPs at pH 6 and pH 6.5. Wells 1-8 demonstrate the loading of Poly (I:C) on 500 µg/ml Doxorubicin-loaded G_4DcMNPs at pH 6. Wells 9-16 demonstrate the loading of Poly (I:C) on 500 µg/ml Doxorubicin-loaded G_4DcMNPs at pH 6.5. Wells 17-20 demonstrate the control Poly (I:C) and different dilutions. 1 in the ratio represents 4 µg of Poly (I:C) or DcMNP. 74

Figure 3.45 Release of 500 µg/ml Doxorubicin from G_4DcMNPs and G_4DcMNPs-PIC at pH 5.2 and pH 4.5..... 75

Figure 3.46 IC50 Value of Doxorubicin (a) and Poly (I:C) (b) in Poly (I:C) linked Doxorubicin-loaded DcMNPs were calculated as 12 µg/ml and 7 µg/ml. 75

CHAPTER 1

INTRODUCTION

1.1 Cancer

Cancer is a group of diseases characterized by uncontrolled growth and spread abnormal cells originated from normal body cells. The transformation from a normal body cell into an abnormal tumor cell is a multistage process. It typically starts from a precancerous lesion to malignant tumors. The localization of the progression can be any single cell of the body. Therefore, cancer can arise in various body sites and behave differently depending on its site of origin. According to World Health Organization (WHO), in 2008 around 13% of all deaths (7.6 million people) worldwide were because of cancer, making it a leading cause of death (www.who.int/mediacentre/factsheets/fs297/en/). It was also reported by WHO, in July 2008 that deaths from cancer worldwide continued rising, with an estimated 12 million deaths in 2030. The main types of cancer leading to overall cancer mortality each year are; lung (1.4 million deaths), stomach (866,000 deaths), liver (653,000 deaths), colon (677,000 deaths) and breast (548,000 deaths). It was reported as the most frequent cancer among women (23% of all cancers) worldwide (Parkin *et al.*, 2005). Breast cancer was by far the most common cancer diagnosed in women (Ferlay *et al.*, 2008).

1.1.1 Breast Cancer

Breast cancer begins in breast tissue, that is made up of glands for milk production, called lobules, and the ducts which connect lobules to the nipple. The remainder of the breast is made up of fatty, connective, and lymphatic tissue. Theoretically, any type of tissue in the breast can form cancer; however, origin of tumor is usually either the ducts (called ductal carcinoma) or the glands (called lobular carcinoma). Breast cancer usually begins with the formation of a small, confined tumor and then spreads through channels to the lymph nodes or through the blood stream to other organs. When abnormal cells of lobules or ducts break out into the surrounding breast tissue, invasive breast cancer develops. Metastasis occurs when these cancer cells break away from the site of primary tumor and spread to other organs of the body through either the blood stream or the lymphatic system.

1.2 Nanoparticles and Cancer Therapy

The systemic distribution of therapeutics in contemporary treatment methods is problematic. It represents a major flaw, which can make the difference between success and failure (Dobson *et al.*, 2006). Higher doses are often needed to accumulate adequate amounts of

therapeutic at the target site. However, the Larger the doses are the higher the risk of adverse side effects and elevated toxicity to non-target sites would be (Ritter *et al.,* 2004; Torchilin *et al.,* 2000). Nanotechnology holds significant promise to overcome these obstacles, by enabling large amounts of therapeutic drugs to be encapsulated into nanoparticles. This technology has enabled the development of particles with nano sizes that can be fabricated from a multitude of materials in a variety of compositions. These nanoparticles include; quantum dots (QDs), (Ferrari *et al.,* 2005) polymeric nanoparticles, (Li *et al.,* 2004) gold nanoparticles,(Lagaru *et al.,* 2007) magnetic nanoparticles (Kjaer *et al.,* 2006) and dendrimeric nanoparticles (Pan *et al.,* 2007; Gao *et al.,* 2005) (Figure 1.1).

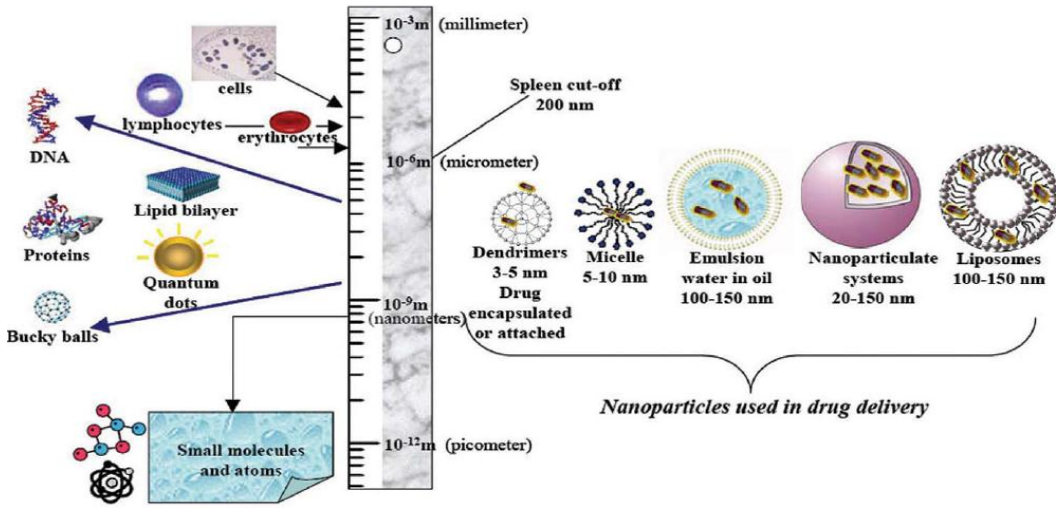

Figure 1.1 Naturally present nano and micro-molecules and synthesized nanoparticles comparison in size (Arruebo *et al.,* 2007).

The delivery of therapeutic drugs by nanoparticles simultaneously reduces toxic side effects and increases the half-life of drugs, which results in improvement of their pharmacokinetic profile and therapeutic efficacy (Shubayev *et al.,* 2009; Kim *et al.,* 2005; Pan *et al.,* 2007). Such therapeutic nanoparticles have been broadly applied in cancer drug delivery. They have been found to result in higher drug accumulation in tumors through passive targeting. They also resulted in enhanced permeability and retention (EPR) effect, which arises because of leaky vasculature and inefficient lymphatic drainage in the tumor (Gao *et al.,* 2005; Pan *et al.,* 2005). There are more than twenty therapeutic nanomaterials, which have been approved for clinical applications (Pan *et al.,* 2005). A strategy to overcome these obstacles studied by several researchers in the late 1970s, (Mosbach *et al.,* 1979; Senyei *et al.,* 1978; Widder *et al.,* 1979) is to label magnetically, therapeutic drugs so they can be targeted to a site of interest by the help of an external magnetic field. The magnetic field will also confine the drugs longer in the target region to boost efficacy (Alexiou *et al.,* 2000; Lübbe *et al.,* 2001; Lübbe *et al.,* 1999; Lübbe *et al.,* 1996; Lübbe *et al.,* 1996). Therefore, higher substantial therapeutic effects can be achieved at lower doses while minimizing the risk to body healthy tissues (Pankhurst *et al.,* 2003; Alexiou e *et al.,* 2000; Häfeli *et al.,* 2004) (Figure

1.2).

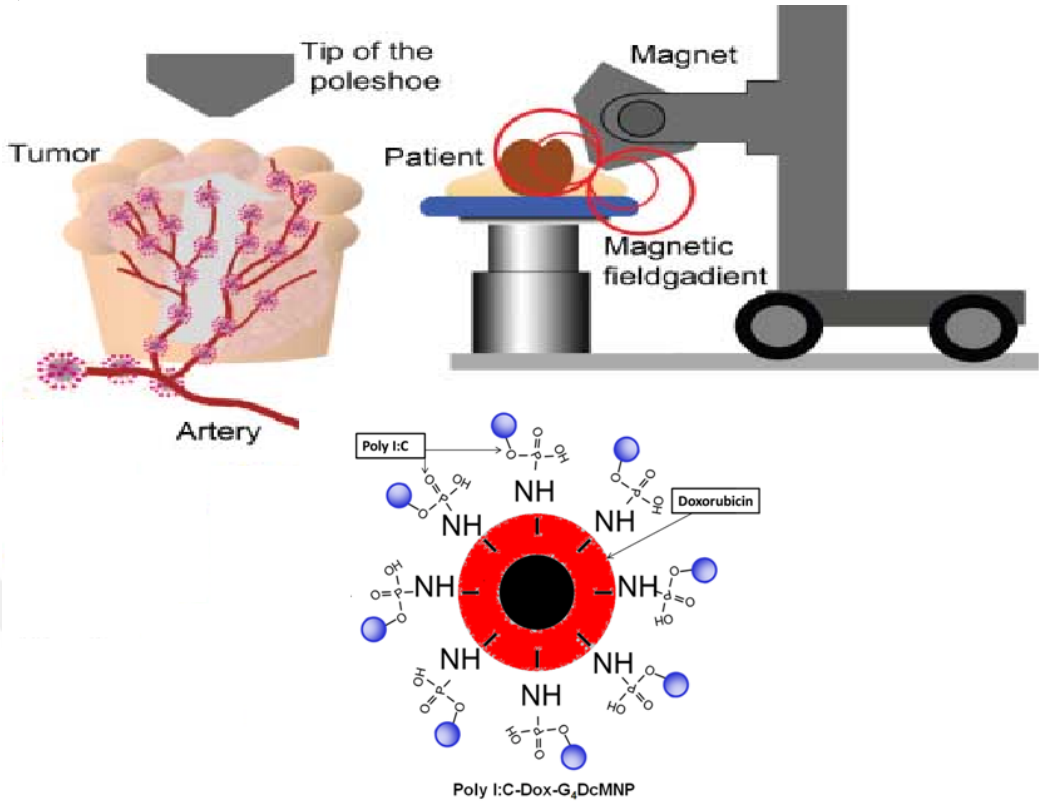

Figure 1.2 Schematic Representation of the targeting of the Doxorubicin and Poly (I:C) with DcMNPs.

1.2.1 Magnetic Nanoparticles

Endogenous uniform, crystalline magnetic nanoparticles (MNPs) have been produced by Biological entities for a very long time (Šafařík *et al.*, 2002). The advent of such biogenic MNPs was first done in 1962 by Lowenstam's group, who discovered magnetite (Fe_3O_4) nanoparticles in chitons and the confirmation of its biological origins (Lowenstam *et al.*, 1962). This finding was outstanding since it was against the traditional belief that magnetite could only form under geological conditions. Chitons, with bio-mineralization process, cover their radular denticles with an iron oxide precursor and convert some portion of the accumulated mineral into a layer of aggregated fine magnetite crystals (Mizota *et al.*, 1986). The magnetite crystals improve the stiffness of the teeth of the tongue plate. This enables the mollusks to scrape the rocks for their food requirements. Furthermore, some biological entities such as chitons use the magnetic property of their denticle caps for navigation purposes (Lowenstam *et al.*, 1962; Crozier *et al.*, 1921; Thorne *et al.*, 1968). This reaction to the Earth`s magnetic field is originated from the interactions between the magnetite nanocrystals of organisms and Earth`s magnetic field and the phenomena is called magnetotaxis.

Besides, to chitons there are many other biological entities, which display magnetotaxis.

Like chitons, these organisms also interact with the Earth`s magnetic fields through biogenic magnetite nanocrystals (Johnsen *et al.*, 2008). In Table 1.1 it can be seen various organisms with magnetite nanocrystals and their locations in the organism`s body. Although there exist significant amount of magnetic nanocrystals in human`s brains, spleens, levers and hearts they do not exhibit clear magnetotaxis (Schultheiss *et al.*, 1988). The abnormalities in the amounts of magnetite in the brains of human may be related to neurodegenerative diseases and epilepsy (Schultheiss *et al.*, 1988).

Table 1.1 Organisms with biogenic magnetite in their body (Landmark *et al.*, 2008).

Organism type	Organism name	Location of MNPs
Amphibians	Eastern red-spotted newts	throughout bodies
Birds	Bobolinks	upper beaks
	Homing pigeons	upper beaks
Fish	Atlantic salmon	along lateral lines
	Rainbow trout	olfactory lamellae
	Sockeye salmon	ethmoid cartilage of skulls
	Yellowfin tuna	dermethmoid bone of skulls
Insects	Honeybees	abdomens
	Migratory ants	thoraxes and abdomens
	Termites	thoraxes and abdomens
Mammals	Common Pacific dolphins	dura maters
	Humans	brains
		hearts, spleens, and livers
Micro-organisms	Magnetotactic bacteria	magnetosomes
	Algae	cells
Mollusks	Chitons	radular denticles

1.2.1.1 Synthesis of Magnetic Nanoparticles with Coprecipitation Method

Although uniform crystalline magnetic nanoparticles have been produced for a long time by various biological entities through biomineralization, the laboratory-based methods for the production of synthetic version of magnetic nanoparticls convenient for biomedical applications are relatively recent developments (Hyeon *et al.*, 2003; Neuberger *et al.*, 2005). There are physical and chemical methods for the laboratory-based production of MNPs. However, chemical methods are easier and more effective routes to produce MNPs with

desirable quality and quantity for biomedical applications (Hyeon *et al.*, 2003; Tartaj *et al.*, 2003; Willard *et al.*, 2004). In addition, magnetites synthesized with chemical methods will have well-defined size, shape, and will have more favorable magnetic properties (Kodama *et al.*, 1999; Krishnan *et al.*, 2006; Lu *et al.*, 2007; Tartaj *et al.*, 2003). The important chemical methods are coprecipitation, reverse micelles, and thermolysis of organometallic precursors in organic media (Willard *et al.*, 2004; Lu *et al.*, 2007; Gupta *et al.*, 2005; Xu *et al.*, 2007) (Table 1.2). Being related to thesis study only coprecipitation techniques was discussed.

Table 1.2 Particle properties as produced by the listed techniques. (Landmark *et al.*, 2008).

Technique	M_{sat} (emu/g Fe)	Size Range (nm)	Relative Size Distribution (σ/μ)	Yield (g)
Coprecipitation	20-50	10-50	~0.3	~10
Reverse Micelle	>30	4-15	0.10-0.15	~0.1
Thermal Decomposition	>50	3-50	0.05-0.10	~1

Coprecipitation method for the synthesizing of magnetite refers to the precipitation of ferric and ferrous iron ions in aqueous solution applying a base like ammonia (Gnanaprakash *et al.*, 2007). The Coprecipitation method can be classified with respect to the salts, which are used as precursors.

1.2.1.1.1 Ferrous Salts Only

Application of ferrous salts as precursors of iron ions will pave the way for the *in situ* production of ferric ions. It is possible to convert some Fe^{2+} to Fe^{3+} by the addition of a mild oxidant. This oxidative hydrolysis reaction, (Gnanaprakash *et al.*, 2007) occurs in three different stages (Bruce *et al.*, 2004; Lida *et al.*, 2007; Olowe *et al.*, 19991; Refait *et al.*, 1993). The ferrous salt is first hydrolyzed to ferrous hydroxide:

$$Fe^{2+} + 2OH^- \Longrightarrow Fe(OH)_2 \qquad \text{Equation 1.1}$$

Then Part of the $Fe(OH)_2$ is oxidized to a ferric hydroxide intermediate:

$$3Fe(OH)_2 + 1/2\ O_2 \Longrightarrow Fe(OH)_2 + 2FeOOH + H_2O \qquad \text{Equation 1.2}$$

At the end stage, magnetite nanoparticle is formed through the dehydration reaction between ferrous hydroxide and two equivalents of ferric hydroxide:

$$Fe(OH)_2 + 2FeOOH \Longrightarrow Fe_3O_4 + 2H_2O \qquad \text{Equation 1.3}$$

The characteristic method for the production of magnetite is to prepare ferrous salt`s aqueous solution and add it slowly into alkaline solution; (Ishikawa *et al.,* 2002; Kiyama *et al.,* 1974; Nedkov *et al.,* 2002). Magnetite nanoparticles can also be prepared, by titration of the metal together with the base solution (Sugimoto *et al.,* 1980).

1.2.1.1.2 Ferrous and Ferric Salts

The most successful method for the production of magnetic nanoparticles is the hydrolysis of a certain amount of Fe^{2+} and Fe^{3+} salts in alkaline solution. The ultimate equation for this reaction is similar to final equation of ferrous salt method and can be written as; (Gnanaprakash *et al.,* 2007; Lida *et al.,* 2003; Riu *et al.,* 2006; Kim *et al.,* 2003)

$$Fe^{2+} + 2Fe^{3+} + 8OH^- \Longrightarrow Fe(OH)_2 + 2FeOOH + 2H_2O \Longrightarrow Fe_3O_4 + 4H_2O \qquad \text{Equation 1.4}$$

1.2.1.2 Superparamagnetism

Magnetic nanoparticles themselves are divided into three main groups; ferromagnetic, paramagnetic and super paramagnetic nanoparticles. Considering ferromagnetic nanoparticles, the magnetic moments of neighboring atoms align resulting in a net magnetic moment and Paramagnetic materials randomly oriented due to Brownian motion, except in the presence of external magnetic field. However, superparamagnetic nanoparticles are materials with the Combination of paramagnetic and ferromagnetic properties and made of nano-sized (<50nm) ferrous magnetic particles such as Ni, Co, Fe, Fe3O4 and γ-Fe2O3, but affected by Brownian motion (Hergt *et al.,* 2006; Shubayev *et al.,* 2009). Superparamagnetic nanoparticles will align in the presence of an external magnetic field (Hergt *et al.,* 2006). Compared with cobalt and nickel, iron oxide nanoparticles are more suitable and safer for biomedical applications. Having these properties superparamagnetic iron oxide nanoparticles have been recognized as a promising tool for hyperthermia, (Kim *et al.,* 2005) and the site-specific delivery of drugs and diagnostics agents.

In order to be used in medical application and drug delivery, magnetic iron oxide nanoparticles need to be not only magnetically saturated and biocompatible but the surface should also be modified with different functional groups (Figure 1.3). To fabricate multifunctional magnetic nanoparticles and make them more biocompatible and suitable for biomolecules, drugs and signal molecules loading, the surface can be modified with different organic and inorganic polymers or dendrimers(Gao *et al.*, 2009) a novel class of polymers with a well-defined, three-dimensional structure.(Gao *et al.*, 2005; Pan *et al.*, 2005)

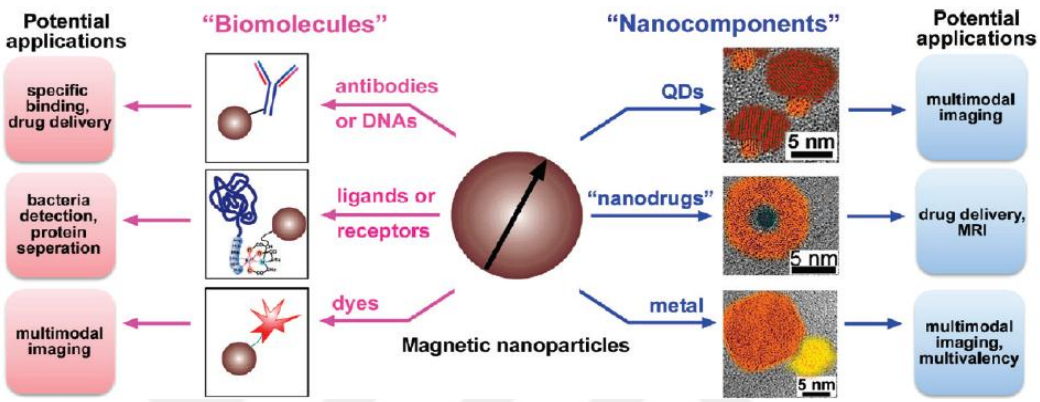

Figure 1.3 The scheme illustrates two strategies to fabricate multifunctional magnetic nanoparticles and their potential applications (Gao *et al.*, 2009).

1.2.2 Dendrimeric Nanoparticles

Dendrimers, polymers of the 21st century, are three-dimensionally symmetrical polymers characterized with a unique tree-like branching architecture and have a compact spherical geometry in solution (Contreras *et al.*, 2005; Schcharbin *et al.*, 2009; Yoo *et al.*, 1999). The word *"dendrimer"* originated from two words, the Greek word *dendron*, meaning tree, and *meros*, meaning part (Jana *et al.*, 2012). They simply consist of a core attached to peripheral branches (Figure1.1) with total size ranging between 2 to 10 nm (Brothers *et al.*, 1998; Eichman *et al.*, 2000; Labieniec *et al.*, 2008; Najlah *et al.*, 2006).

Fritz Vogtle and his co-workers introduced the first dendrimer in the 1970s. Then, in 1984, synthesizing the primary group of dendrimers was come up by Donald A. Tomalia (Cevc *et al.*, 2010; Medina *et al.*, 2009). Over the past three decades, generation of multiple dendrimer families was developed in different ways and since then, their use in research, treatment of disease, and even environmental (Shcharbin *et al.*, 2007) and industrial applications (Duan *et al.*, 2006; Joo *et al.*, 2006; Prasanna *et al.*, 2013; Raghu *et al.*, 2007; Sekowski *et al.*, 2009) are increasing progressively. They simply consist of a core attached to peripheral branches with total size ranging between 2 to 10 nm (Brothers et al. 1998; Eichman *et al.*, 2000; Labieniec *et al.*, 2008; Najlah *et al.*, 2006). There are various types of dendrimers; Poly(amidoamine-organosilicon) dendrimers (PAMAMOS)- Poly(amidoamine)

dendrimers (PAMAM)- Poly(propylene imine) dendrimers (PPI)- Chiral dendrimers- Liquid crystalline dendrimers- Tecto dendrimers- Hybrid dendrimers- Multilingual dendrimers- Micellar dendrimers (Eichman *et al.*, 2000; Labieniec *et al.*, 2009; Sadekar *et al.*, 2012; Zhou *et al.*, 2006).

1.2.2.1 PAMAM Dendrimers

Poly (amidoamine), or PAMAM, is the well-known dendrimer. PAMAM dendrimers possess various useful characteristics, which make them suitable carriers for drug and gene delivery applications (Chen *et al.*, 2000; Mukherjee *et al.*, 2013; Waite *et al.*, 2009). Some of the important ones are, great numbers of branches attached to the central core, their nanometer size and manageable molecular weight (Janaszewska *et al.*, 2013). Therefore, these spherical, biocompatible, safe, and non-immunogenic polymers can function as highly efficient cationic polymer vectors for delivering genetic material and different drugs into cells (Trivedi *et al.*, 2012). Additional advantages of PAMAM dendrimers include their acceptable biodegradation, their controlled drug release, and minimal nonspecific blood-protein binding properties (Esfand *et al.*, 2001).

1.2.2.1.1 Structure of PAMAM Dendrimers

In 1984, Tomalia and coworkers synthesized PAMAM dendrimers for the first time. These dendrimers are synthetic polymers, which have gained special significance as carrier system for specific genes and drugs into the various types of the cells such as primary cells, with minimum cytotoxicity (Shi *et al.*, 2005).

PAMAM dendrimer contains three architectural components: a core, an interior of shells (generations) consisting of repeating branch-cell units and terminal functional groups (the outer shell or periphery) (Prajapat *et al.*, 2011; Stojanovic *et al.*, 2010; Tajabadia *et al.*, 2013).

The synthesis of these highly organized and relatively mono-dispersed polymers starts from the central core (Tomalia *et al.*, 1994). The core selection is important, since it can affect the molecule and surface charge density. From this central core, “wedges” or dendrons radiate. Each layer of concentric branching units is considered as one generation and has special generation number (Figure 1.4).

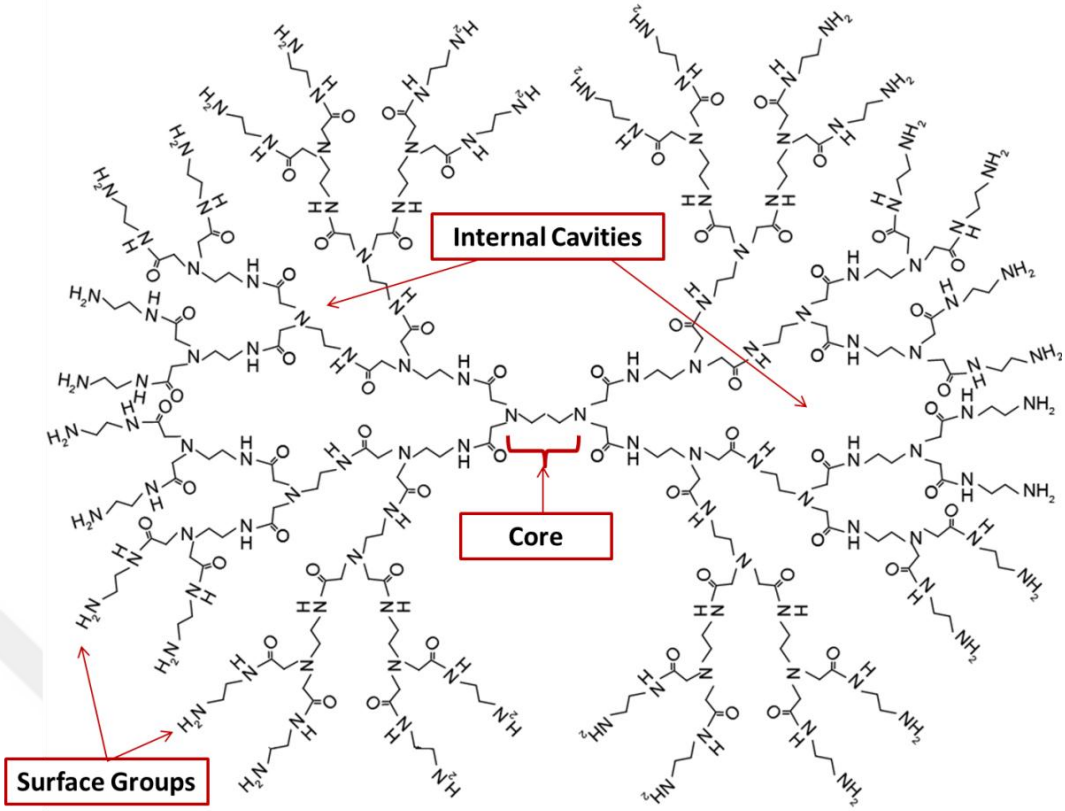

Figure 1.4 The core shell structure of PAMAM dendrimer.

The size of PAMAM dendrimers ranges from 10 ˚A to 130 ˚A in diameter for generation 0 (G_0) through generation 10 (G_{10}). It means that the molecule's diameter changes approximately 1 nm as each generation varies (Table 1.3). In detail, dendrimer diameter increases roughly linearly with generation, while the number of functional groups on the surface increases exponentially. An important consequence of this is that the distance between functional groups on the periphery of the dendrimer, and consequently the flexibility of peripheral groups, decreases with generation (Scott *et al.*, 2005).

Table1.3 Approximate diameters of diferent generations of PAMAM dendrimers. Adapted from (Tomalia *et al.*, 2004).

Generation	No. of NH_2 groups on the periphery	Molecular formula	MW	Hydrodynamic diameter (nm)
0	4	$C_{24}H_{52}N_{10}O_4S_2$	609	1.5
1	8	$C_{64}H_{132}N_{26}O_{12}S_2$	1,522	2.2
2	16	$C_{144}H_{292}N_{58}O_{28}S_2$	3,348	2.9
3	32	$C_{304}H_{612}N_{122}O_{60}S_2$	7,001	3.6
4	64	$C_{624}H_{1252}N_{250}O_{124}S_2$	14,307	4.5
5	128	$C_{1264}H_{2532}N_{506}O_{252}S_2$	28,918	5.4
6	256	$C_{2544}H_{5092}N_{1018}O_{508}S_2$	58,140	6.7
7	512	$C_{5104}H_{10212}N_{2042}O_{1020}S_2$	116,585	8.1

The numbers of generation affect the polymer's shape. Lower generation dendrimers (G_0 to G_4) have a planar, elliptical shape, whereas at the higher generations (G_5 to G_{10}), the densely packed branches induce the polymer to form a spherical conformation. Molecular weight, size, and number of surface groups are also affected by the number of generation (Table 1.3). "De Gennes dense packing effect", in which the steric crowding of the branches limits developing of the higher generations (G_7-G_{10}), can lead to the defective branching structures (Figure 1.5).

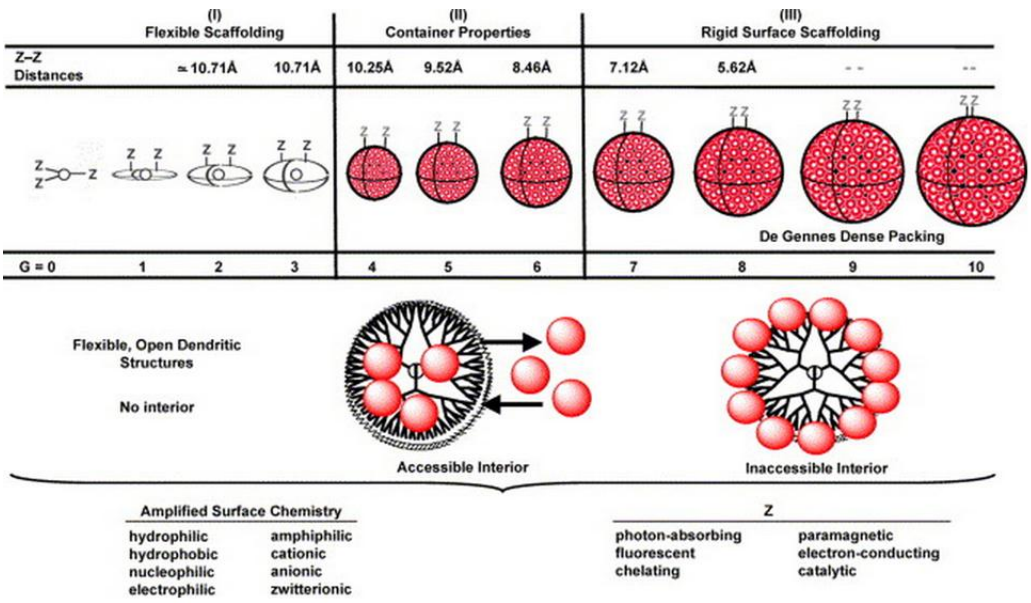

Figure 1.5 Periodic properties of PAMAM dendrimers as a function of their generations. Adapted from (Tomalia *et al.*, 2004)

In lower generations of PAMAM dendrimers, the polarity is higher while the toxicity is low. However, increase in the generation number has a direct relationship with in vitro toxicity, although this cannot be mentioned in terms of in vivo toxicity. Dobrovolskaia *et al.* indicated that only large cationic PAMAM dendrimers, but not anionic, neutral or small cationic dendrimers, induce aggregation of human platelets in plasma *in vitro*. The aggregation caused by large cationic dendrimers was proportional to the number of surface amines (Dobrovolskaia *et al.*, 2012).

1.2.2.1.2 Divergent Synthesis of PAMAM Dendrimers

Currently, there are four ways for synthesizing PAMAM dendrimers (Ina *et al.*, 2011; Tomalia *et al.*, 1990), namely; divergent synthesis, convergent synthesis, combined convergent-divergent synthesis, and Click synthesis Methods. However, it is only divergent synthesis method, which will be described here. This method was introduced by Tomalia and was used for synthesizing the first class of PAMAM dendrimers. In divergent synthesis, the growth of the PAMAM dendrimer starts from a multifunctional core molecule and the reaction takes place between the core and monomer molecules containing one reactive and two dormant groups. Because of this reaction, the first generation of PAMAM dendrimer was synthesized. Then the new periphery of the molecule activates for reactions with more monomers. Various layers of the dendrimer produce after repetition of these reactions (Bosman *et al.*, 1999; Medina *et al.*, 2009; Tomalia *et al.*, 2004).

The initiator core for PAMAM dendrimers is an ammonia or ethylenediamine (EDA) molecule. Ammonia has three and EDA has four possible binding sites for amidoamine

repeating units. The primary amino groups are on the surface of the molecule and two new branches may be conjugated to each of them (Peterson *et al.*, 2001) (Figure 1.6).

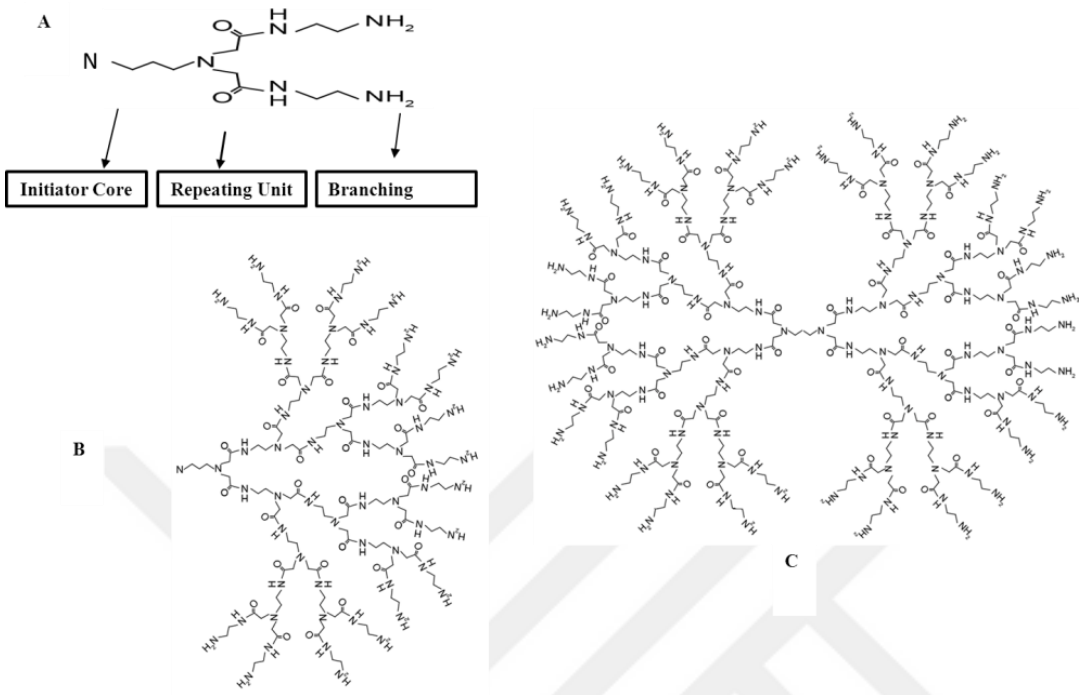

Figure 1.6 Structure of dendritic macromolecules: A) structural elements, B) dendron, and C) Dendrimer.

Synthesize a PAMAM dendrimer, a multistep reaction should be performed which is composed of a Michael addition of methyl acrylate and then, amidation with ethylenediamine (EDA). Each repetition results in a new generation that is indicated by consecutive integers. The outer surface of the PAMAM dendrimer has a high density of primary amino groups that confer positive charge to the dendrimer at physiological pH. These reactions can iterate up to ten layers (or generations) of polymer, where steric hindrance (i.e. de Gennes dense packing) prevents ideal growth because of high surface density of the polymer branches (Eichman *et al.*, 2000; Inoue *et al.*, 2000) (Figure 1.7).

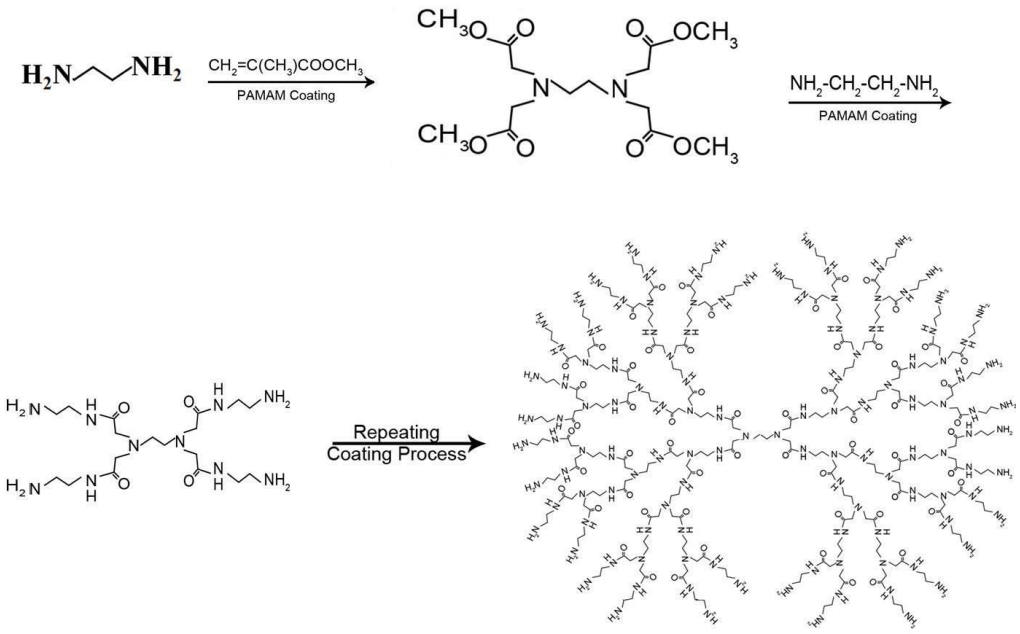

Figure 1.7 Synthesis of PAMAM dendrimers with ethylenediamine core.

The divergent method is ideal for the synthesis of large amounts of dendrimers, since in each generation-adding step, the molar mass of the dendrimer is doubled (Eichman *et al.*, 2000; Meldal *et al.*, 2008).

1.2.2.1.3 Surface Modification of PAMAM Dendrimers

In recent years, there have been an increasing number of studies on dendrimers application as drug carriers, transfection agents, or magnetic resonance imaging agents. A serious drawback of dendrimers is their toxicity, mainly due to the surface positive charge of the PAMAM dendrimers. One of the ways for reducing the toxicity of PAMAM dendrimers is modification of these surface groups (Hong *et al.*, 2004; Khodadust *et al.*, 2013). There is different modification performed on surface of PAMAM dendrimeric nanoparticles. Here Acetylation, PEGylation and folic acid modification were discussed in details.

1.2.2.1.3.1 Amine Acetylation

Amine acetylation is one of the mostly used modifications, which can decrease the cytotoxicity of PAMAM dendrimers. Amine acetylation of PAMAM dendrimers can lead to an increase in water-solubility, and this quality is essential for biomedical uses that need solubility in aqueous solutions (Majoros *et al.*, 2003). In a study done by Waite research group acetylation of the primary amines of generation 5 (G_5) PAMAM dendrimers was performed by reaction with distinct amounts of acetic anhydride as depicted in Figure 1.8 after acetylation, a decrease in cytotoxicity was observed. Results indicated that enhancing

the amine acetylation leads to a reduction in polymer cytotoxicity in U87 cells (Waite *et al.*, 2009).

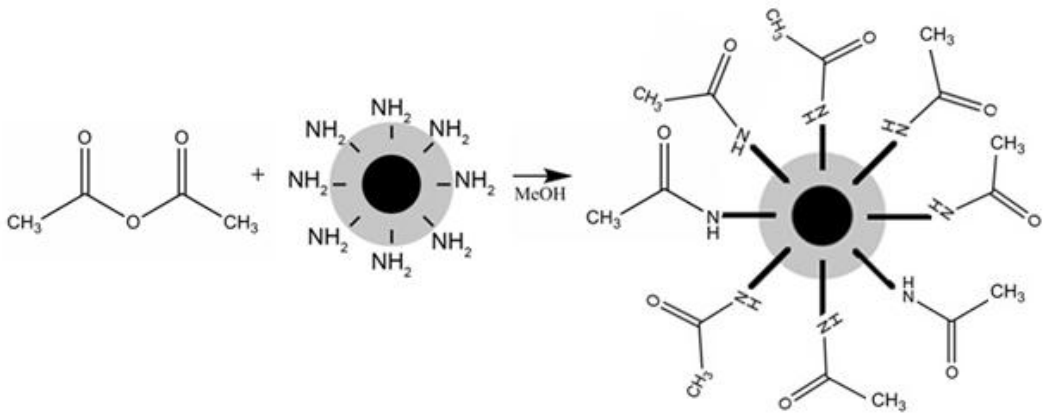

Figure 1.8 Acetylation of PAMAM dendrimers. Acetic anhydride reacts with primary amines of G_5PAMAM dendrimers to produce acetylated PAMAM.

1.2.2.1.3.2 PEGylation

Conjugation with poly (ethylene glycol) (PEG) chains has been considered as a method for reducing the toxicity and increasing the biocompatibility and the circulation time of dendrimers in the body, since PEG is nontoxic, non-immunogenic, and has favorable pharmacokinetics as well as tissue distribution (Figure 1.9). In earlier studies, PAMAM dendrimers with PEG grafts on the surface exhibited improved biocompatibility and efficiency in carrying genes or drugs. Luo *et al.* (Luo *et al.*, 2002) previously modified the generation 5 dendrimer with biocompatible PEG chains to use in basic research laboratories. The novel conjugate produced a 20-fold increase in transfection efficiency compared with partially degraded dendrimer controls. The cytotoxicity of PEGylated dendrimers was very low. This extremely efficient, highly biocompatible, low-cost DNA delivery system can be readily used in future clinical applications. Bhadra *et al.* (Bhadra *et al.*, 2003) evaluated uncoated and PEGylated G_4PAMAM dendrimers for the delivery of anti-cancer drug (5-fluorouracil). The results demonstrated PEGylation as a suitable way for modifying the PAMAM dendrimers for drug leakage and hemolytic toxicity reduction. This could improve drug-loading capacity and could help stabilizing such systems in body. The study suggested the use of such PEGylated dendrimeric systems for drug administration. In another experiment performed by Wang`s research group, it was demonstrated that conjugation of dendrimers with more PEG of higher molecular weight had much lower cytotoxicity (Wang *et al.*, 2009).

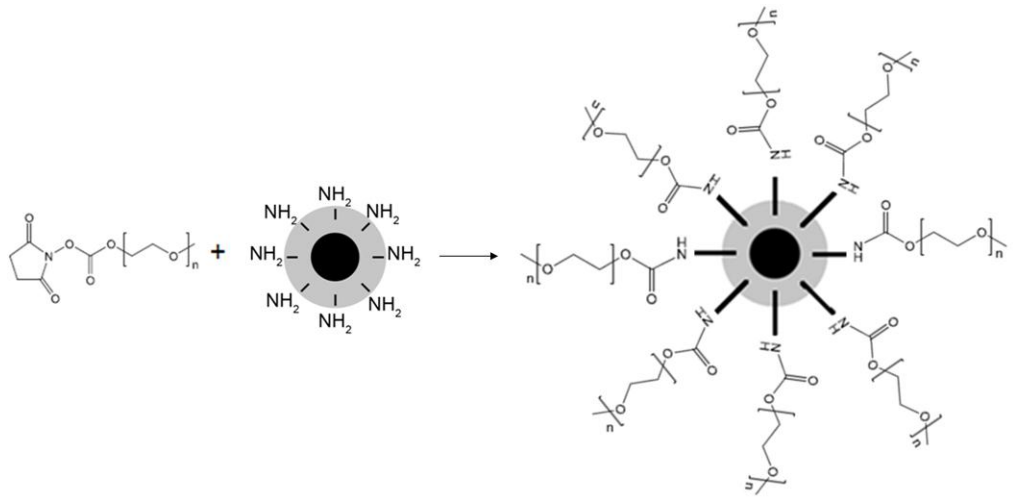

Figure 1.9 Synthesis of PEGylated PAMAM dendrimers.

1.2.2.1.3.3 Folic Acid Modification

In a different study PAMAM dendrimers up to fourth generation were produced, characterized, and attached to folic acid directly or indirectly through PEG4000 as spacer (Figure 1.10). Then prepared dendritic conjugates were evaluated for the anticancer drug delivery potential using 5-fluorouracil (5-FU) in tumor-bearing mice. Results indicated that folate-PEG-dendrimer conjugate was significantly safe and effective in tumor targeting compared to a non-PEGylated formulation. Tailoring of dendrimers via PEG-folic acid reduced hemolytic toxicity, which led to a sustained drug release pattern as well as highest accumulation in the tumor area. They suggested that because of the reduced toxicity and enhanced efficacy, FA-PEG-drug loaded G_4PAMAM dendrimers can be used most suitably as a controlled and targeted drug delivery system for the delivery of anticancer drugs like 5-FU (Singh *et al.*, 2008).

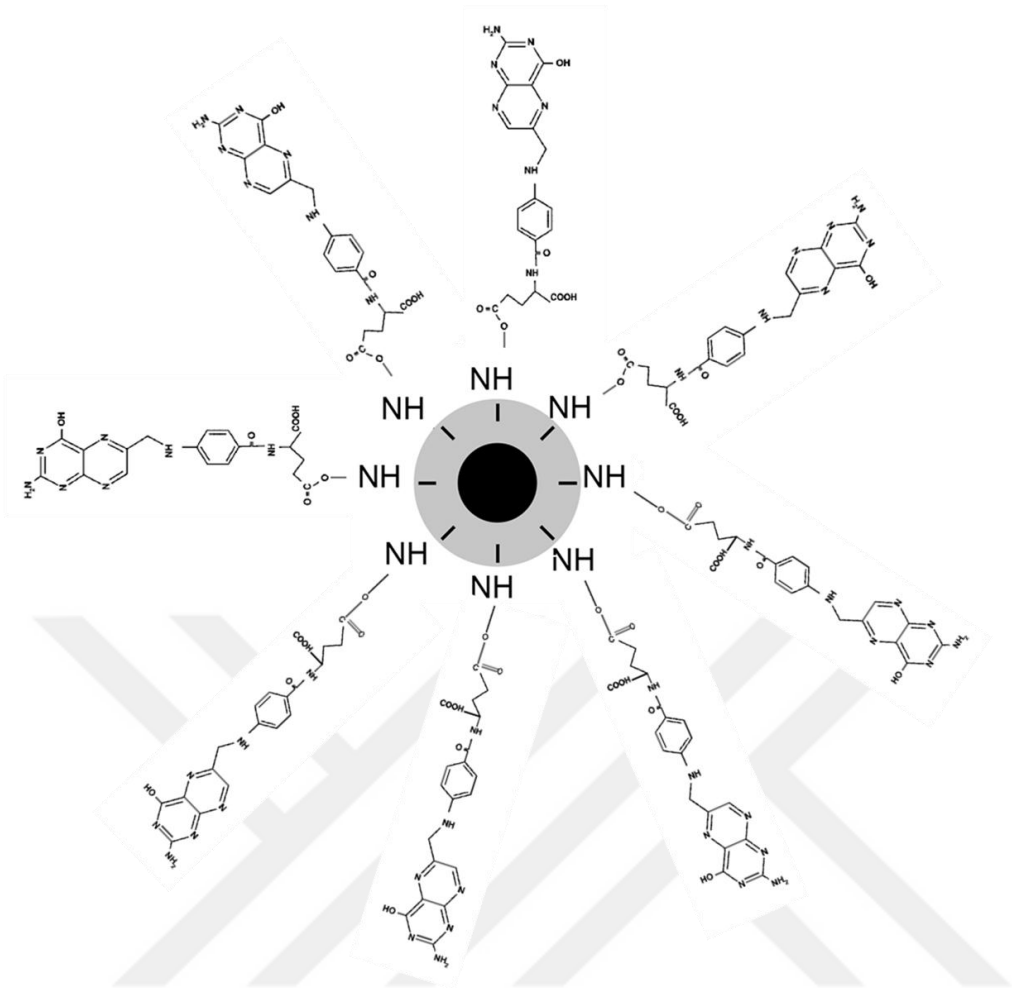

Figure 1.10 Chemical structures of folic acid- PEG4000- G_4 PAMAM dendrimers.

1.2.2.1.4 PAMAM Dendrimer, a Suitable Delivery System

Unparalleled molecular uniformity, multifunctional surface and presence of internal cavities, make PAMAM dendrimers particularly well suited to possible pharmaceutical applications (Medina *et al.*, 2009). Therefore, PAMAM dendrimers are selected as appropriate candidates in order to use in a variety of high technologies (Svenson *et al.*, 2005).

The unique properties of PAMAM dendrimers, namely their special three dimensional architecture, the large number of functional groups present on their surface, their great mono-dispersity and their high water solubility make them excellent candidates for evaluation as drug carriers. These characteristics also can facilitate and modulate the delivery process (Hu *et al.*, 2009; Markatou *et al.*, 2007; Zhao *et al.*, 2009). The literature indicated that in addition to drugs, vitamins such as vitamin B_6 and vitamin A readily form conjugates with third-generation PAMAM dendrimers (Filipowicz *et al.*, 2012). The host-guest interactions between PAMAM dendrimers and drugs are dependent on the protonation

ability (p*K*a), steric hindrance, size, hydrophobicity, and numbers of binding sites of the drug molecules (Hu *et al.*, 2009; Markatou *et al.*, 2007; Zhao *et al.*, 2009).

There are two possibilities for drug molecules or chemotherapeutic reagents to be carried by PAMAM dendrimers, either loading in the interior of the dendrimers, or attaching and interacting to the surface terminal functional groups via electrostatic or covalent bonds (Gillies *et al.*, 2005; Malik *et al.*, 2012; Medina *et al.*, 2009; Menjoge *et al.*, 2011).

1.2.2.1.4.1 Encapsulation of Drugs into the Cavities of PAMAM Dendrimer

Due to the ellipsoidal or spheroidal shape and presence of several branches and voids in the PAMAM dendrimer, encapsulation of drugs within these branches is applicable (Figure 1.11) (Cheng *et al.*, 2007; Trivedi *et al.*, 2012). The ability of PAMAM dendrimers to encapsulate the instable or poorly soluble drugs, enhances its aqueous solubility, bioavailability, and controls its release profile, but in turn depends on dendrimers generation number, internal composition, net surface charge, type and degree functionalization of surface groups (Eichman *et al.*, 2000; Patri *et al.*, 2002). The loaded drug may also make hydrogen bounds with the tertiary amines of PAMAM dendrimers.

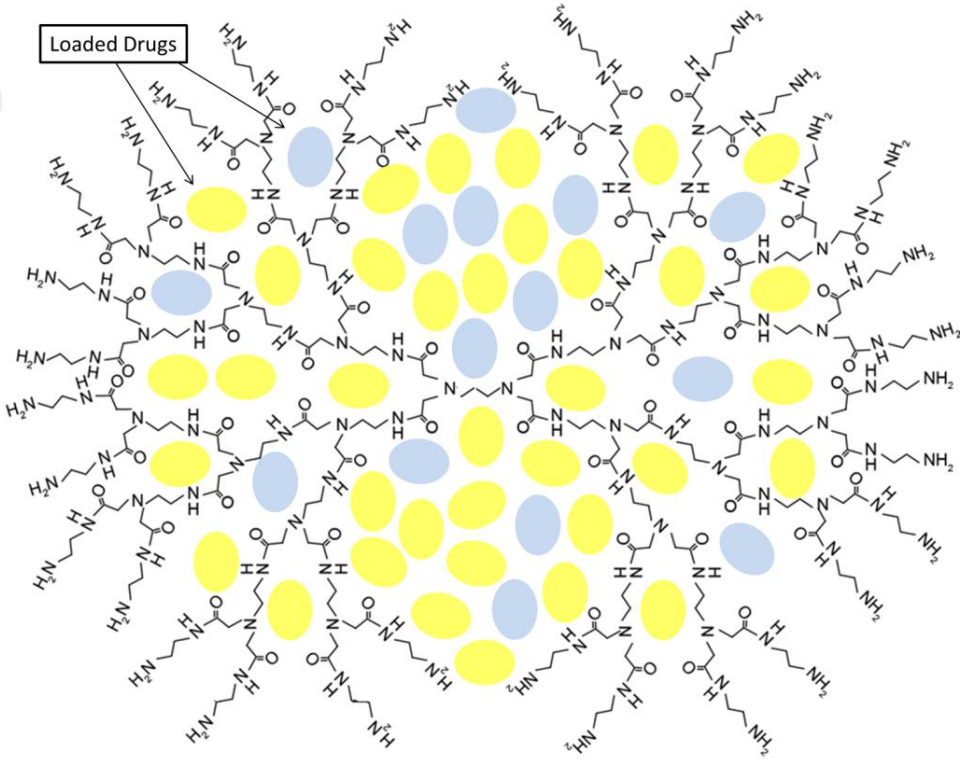

Figure 1.11 Drugs encapsulated inside the cavities of PAMAM dendrimer.

1.2.2.1.4.2 Covalently Conjugation of Drug or Chemotherapeutic Reagents -PAMAM Dendrimer

An alternative approach to the development of PAMAM dendrimer as anticancer drug carriers is to exploit their well-defined multivalency for the covalent attachment of drug molecules to the PAMAM dendrimer surface. The external surfaces of PAMAM dendrimers are useful sites to interact with drugs to control spatial and temporal release of the attached drugs. The interacting of the PAMAM dendrimer with drugs at their terminal functional groups occurs via electrostatic or covalent bonds (D'Emanuele *et al.*, 2005) (Figure 1.12). The binding capacity is directly proportional with the generation number of PAMAM dendrimers (Kim *et al.*, 1998). Methotrexate, folate, (Charles *et al.*, 2012; Gurdag *et al.*, 2006; Patel *et al.*, 2011) ibuprofen, (Devarakonda *et al.*, 2004; Papaioannou *et al.*, 2005) methylprednisolone, (Kolhe *et al.*, 2006) Doxorubicin, (Pan *et al.*, 2005) triamcinolone. (Khandare *et al.*, 2005) propranolol, (Koc *et al.*, 2013) 5-aminosalicylic acid, (Menjoge *et al.*, 2010) phosphorylcholine, (Ma *et al.*, 2009) folic acid, (Jia *et al.*, 2011) biotin, (Zhang *et al.*, 2011) and riboflavin (Yang *et al.*, 2009) are conjugated with PAMAM dendrimers and the *in vitro* examination performed.

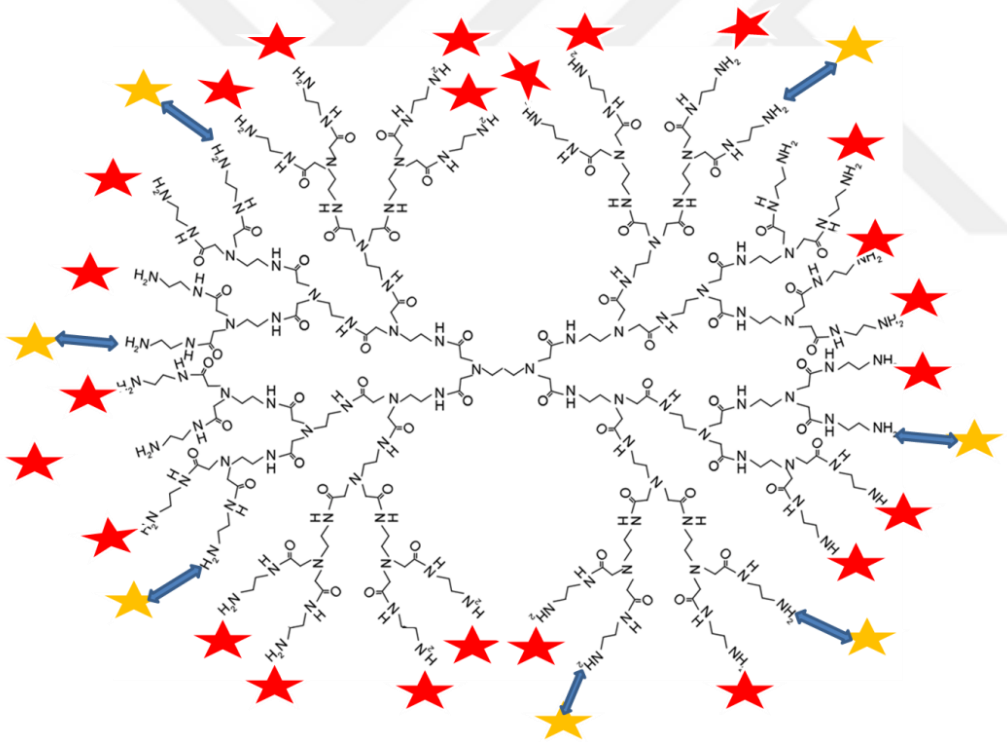

Figure 1.12 PAMAM dendrimer−drug conjugate where the drug molecules are either directly coupled to the surface groups of PAMAM dendrimer or via a pH-sensitive linkage.

Choi and his research group conjugated acetylated-G_5PAMAM dendrimers with fluorescein and folic acid. Then they linked 5'-phosphate-modified 34-base-long oligonucleotide to prepared fluorescein nanoparticle. In vitro studies of the DNA-linked dendrimer clusters

indicated specific binding to KB cells expressing the folate receptor and then, internalization of the dendrimer cluster (Choi *et al.*, 2005).

1.2.2.1.4.3 Gene Therapy

Gene therapy is a new technology providing a promising approach to eradicate genetic disease. The potential of dendrimers as gene delivery agents has been explored for several years (Ina *et al.*, 2011; Yu *et al.*, 2011). In 1993, Haensler and Szoka published the first report of the use of PAMAM dendrimers for gene transfection. They found that PAMAM dendrimers mediated the high-efficiency transfection of DNA into a variety of cultured mammalian cells, and that the transfection was a function of both the dendrimer–DNA ratio and the diameter of the dendrimers (Malik *et al.*, 2012; Svenson *et al.*, 2005). Various reports indicated that PAMAM dendrimer could successfully introduce a reporter gene in different cells both *in vitro* and *in vivo*. In other words, they can act as non-viral transfection agents in gene therapy. As their net charge is positive under physiological conditions, it is possible to form a complex with DNA (Bielinska *et al.*, 1999). Then, this complex can bind to negatively charged surface molecules on cell membrane. Followed by internalization into the cells via non-specific endocytosis, lysosomal degradation of the PAMAM dendrimer-DNA complexes takes place. After releasing the targeting gene, it enters into the nucleus to play a role in gene therapy (Wang *et al.*, 2011**)** (Figure 1.13).

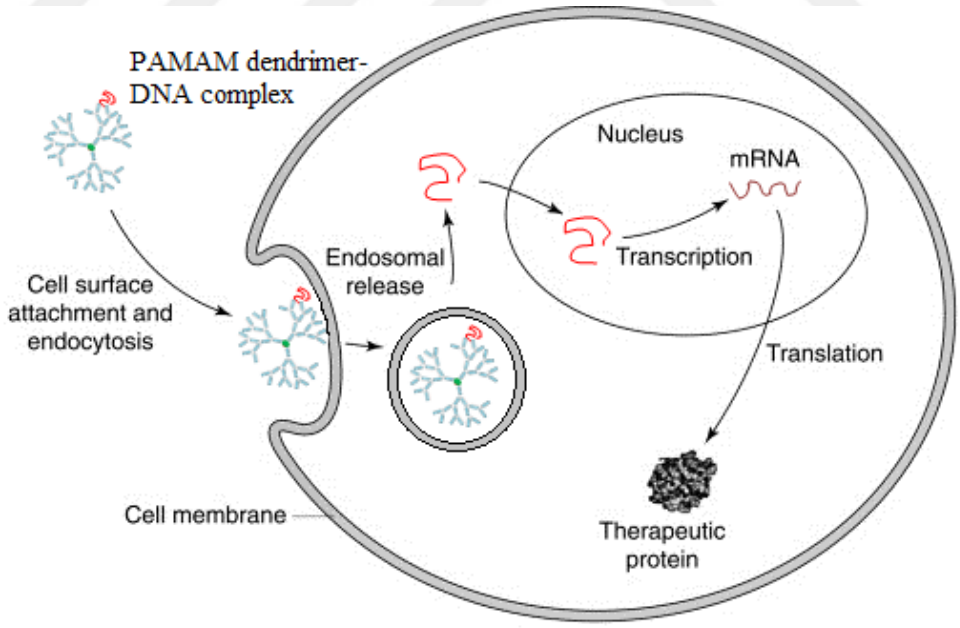

Figure 1.13 Gene transfection of PAMAM dendrimer.

Activated dendrimers called SuperFect™ are commercially available as transfection reagents. Activated dendrimers can carry a larger amount of genetic material than viruses. The unique characteristics of SuperFect DNA complexes are high stability and transportation of DNA into the nucleus more efficient than liposomes (Klajnert *et al.,* 2001; Wang *et al.*, 2011).

Zhou *et al.* introduced an effective siRNA delivery system based on structure flexible poly-cationic PAMAM dendrimers. These genuine, non-degraded dendrimers condense siRNA into nano-scale particles. They protect siRNA from enzymatic degradation and achieved substantial release of siRNA over an extended period of time, which resulted in efficient gene silencing. Taken together, these findings suggest that flexible PAMAM dendrimers may have great potential for in vitro (functional genomics) and possibly in vivo (therapeutic) applications (Zhou *et al.,* 2006).

PAMAM dendrimers can also be used, in photodynamic therapy, photo-thermal therapy, Diagnosis and imaging or they can be used as solubility enhancers (Yiyun *et al.,* 2005; Tao *et al.,* 2013; Wolinsky *et al.,* 2008; Barrett *et al.,* 2009).

It is possible to encapsulate the bioactive agents into the interior part of the dendrimers or they may be chemically attached or physically adsorbed onto the dendrimer surface. In this study Doxorubicin were successfully encapsulated in the cavities of newly synthesized PAMAM dendrimer coated magnetic nanoparticles. Then Polyinosinic:polycytidylic acid (Poly (I:C)), which is a synthetic analogue of double stranded RNA and exerts its immunostimulant function via TLR3, RIG-1 and MDA-5 receptors was bound to the surface amine functional groups. Finally, loading efficiencies and stabilities of the complex was discussed to evaluate the most effective delivery system in further cancer treatment studies.

1.3 Doxorubicin

Doxorubicin or hydroxydaunorubicin with the trade name Doxil is a drug used in cancer chemotherapy (Figure 1.14). Doxorubicin is an anthra-cycline antibiotic and works by intercalating DNA, inhibiting topoisomerase II activities, and the production of Reactive oxygen species (ROS). The most serious and life-threatening side effect of Doxorubicin is heart damage. This drug is usually used for the treatment of a various cancer types, including leukemia’s and Hodgkin's lymphoma, as well as cancers of the bladder, breast, stomach, lung, ovaries, thyroid, soft tissue sarcoma, multiple myeloma, and others.

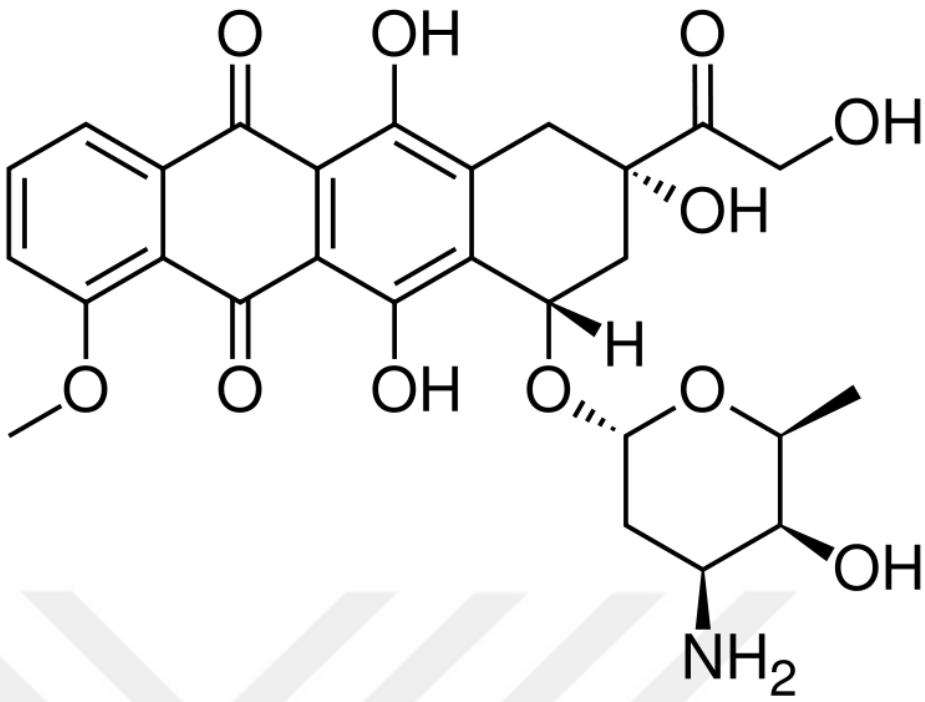

Figure 1.14 Chemical structure of Doxorubicin.

1.3.1 Action Mechanism of Doxorubicin

When delivered into cytoplasm Doxorubicin can be reduced to Doxorubicinol. This is a metabolite, that interferes with iron (by ACO1) and calcium regulations and the F0F1 proton pump of mitochondria (Mordente *et al.,* 2009; Minotti *et al.,* 1998; Olson *et al.,* 1998). The genes, which induce the formation of Doxorubicinol from Doxorubicin, are *AKR1C3*, *AKR1A1*, *CBR1*, and CBR3. On the other hand the genes which induce the production of reactive oxygen species (ROS) or reactive nitrogen species (RNS) from Doxorubicin metabolism include nitric oxide synthases and NAD(P)H oxidase complex genes *NCF4*, *CYBA*, and *RAC2* (Weinstein *et al.,* 2000; Wojnowski *et al.,* 2005). Doxorubicin is metabolized within the mitochondria, which results in the disruption of respiration and leads to the release of cytochrome-C initiating apoptosis (Clementi *et al.,* 2003) (Figure 1.15).

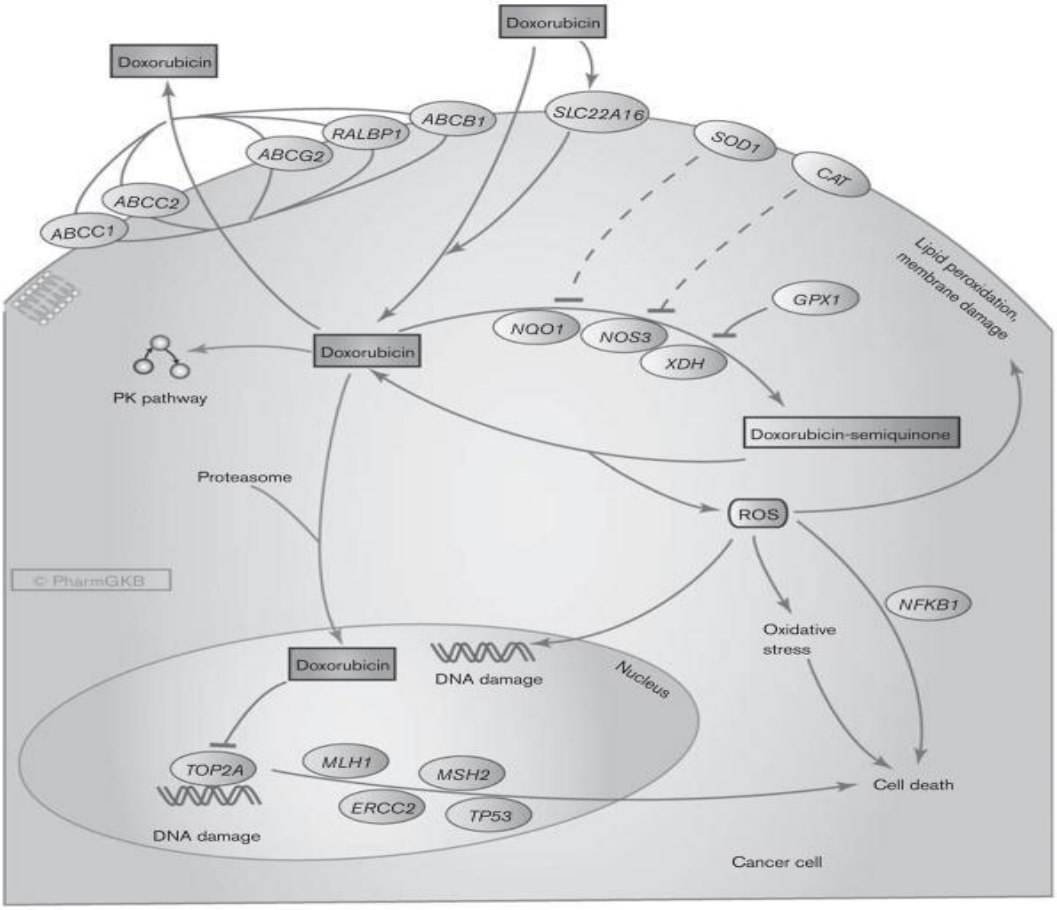

Figure 1.15 Doxorubicin mechanism of action (Thorn *et al.*, 2011)

1.3.2 Resistance Mechanism of Doxorubicin

Although Doxorubicin is a precious anticancer chemotherapeutic reagent, some obstacles prevent the wide range application of this drug. When applied in conventional method the main problem with this drug is the cardio-toxicity. The next and most important problem is resistance to Doxorubicin, which limits its application (Weis *et al.*, 1992). The mechanism of resistance involves different transporter proteins including; MDR1, P-gp (Genrmann *et al.*, 1996) and MRP1 (Cole *et al.*, 1992) and other ABC transporter proteins (Singhal *et al.*, 2003). It is possible to overcome the resistance mechanism by loading the Doxorubicin into suitable nanoparticles such as DcMNPs. This will result in the reduction of Doxorubicin concentration in blood stream and consequently will lower the cardio-toxicity. At the same time, loading of drug into nanoparticles will help the Doxorubicin to escape from efflux proteins (Figure 1.16).

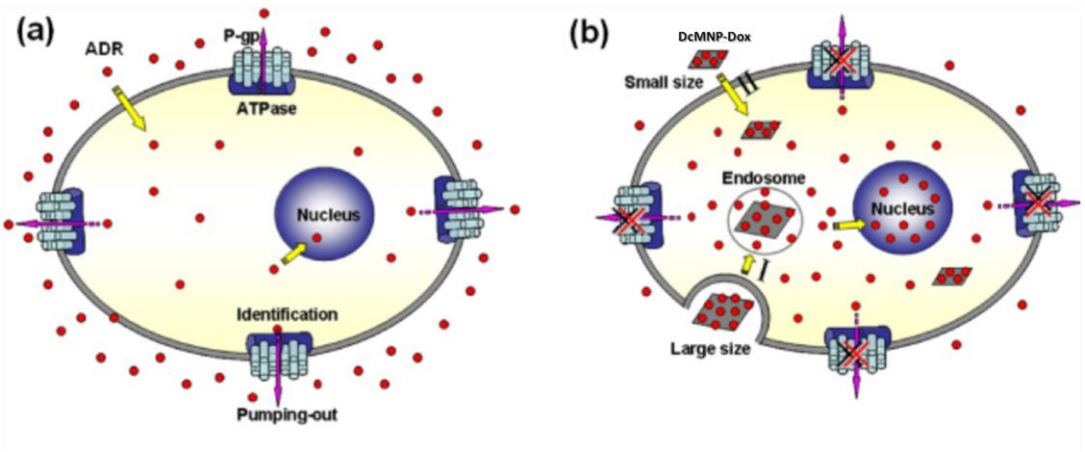

Figure 1.16 Doxorubicin resistance mechanisms; P-gps inhibit Doxorubicin effect by drug efflux (a). When delivered through endosome by nanoparticles, Doxorubicin cannot be caught efflux P-glycoprotein (b) (Wu *et al.*, 2012).

The amplification of TOP2A is the other mechanism of Doxorubicin resistance (Burgess *et al.*, 2008). TOP2A amplification has been shown to affect the treatment response (Pritchard *et al.*, 2008).

1.4 Polyinosinic: Polycytidylic Acid (Poly (I:C))

Successful immunization against pathogens or cancer cells results in the activation of adaptive immunity, in part, through stimulation of the Toll-like receptors (TLRs) (Kato *et al.*, 2006; Kawai *et al.*, 2010). Toll-like receptors (TLRs) are a class of proteins that play a key role in the innate immune system (Kawai *et al.*, 2005). It has been estimated that most mammalian species have between ten and fifteen types of Toll-like receptors (Khodadust *et al.*, 2013; Kohler *et al.*, 2004) (Figure 1.17).

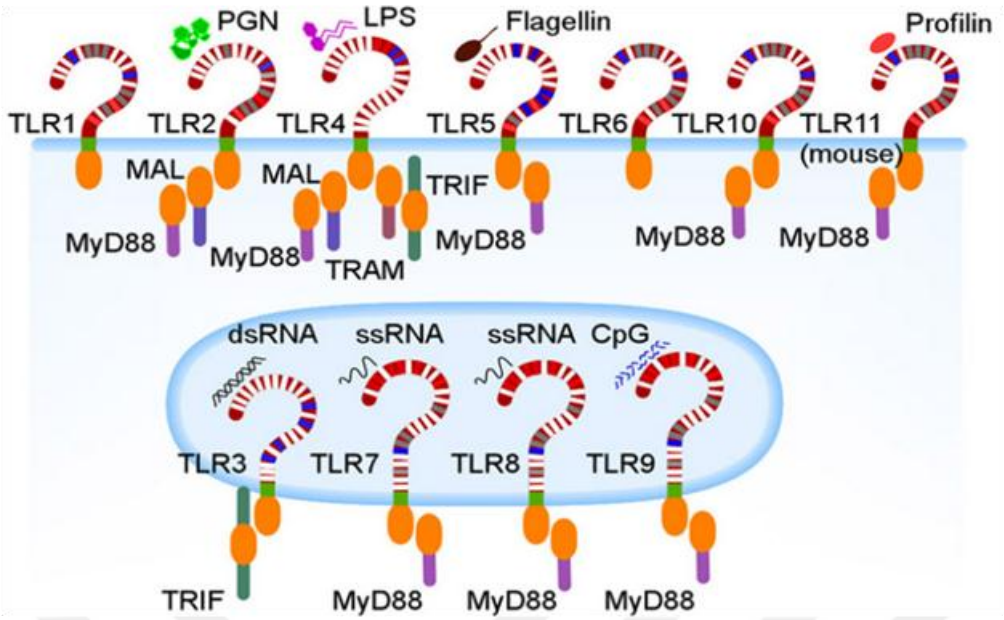

Figure 1.17 Schematic representation of TLRs and their related ligands and adaptors (Okado. *et al.*, 2009).

Well-conserved features in pathogens such as bacterial cell surface lipopolysaccharides, flagellin, double-stranded RNA of viruses and the unmethylated CpG islands of bacterial and viral DNA are the ligands of the TLRs (Khvalevsky *et al.*, 2007). Viral single- or double-stranded RNA is recognized by TLR3 receptor (Kawai *et al.*, 2010; Kumar *et al.*, 2006).

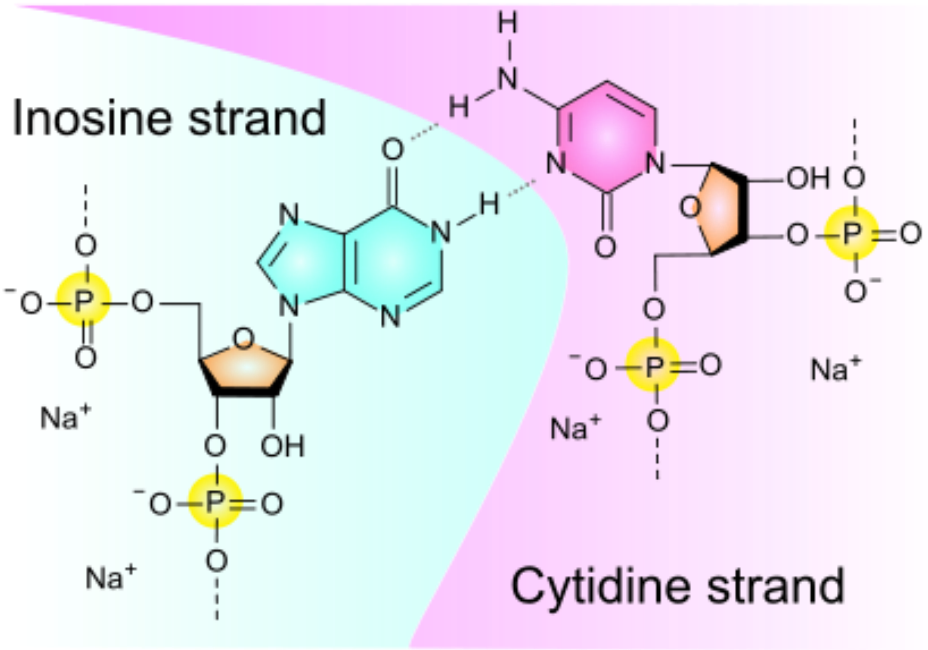

Figure 1.18 Chemical structure of Polyinosinic: Polycytidylic acid.

1.4.1 Poly (I:C) Endosomal Mechanism of Action

Polyinosinic: polycytidylic acid (Poly (I:C)) (Figure 1.18), being an immunostimulant, is a synthetic analogue of double stranded RNA which exerts its function via TLR3 (Liu *et al.*, 2009; Maiti *et al.*, 2005). It is a potent interferon inducer and can activate monocytes and natural killer cells to produce pro-inflammatory cytokines and chemokines (Maiti *et al.*, 2005; Matsumoto *et al.*, 2004). Poly (I:C) can directly trigger apoptosis in many types of human malignant cells including breast cancer, melanoma and hepatoma cells by activating TLR3 (McBain *et al.*, 2007; Milhaud *et al.*, 1992; Milhaud *et al.*, 1989). The TLR3 is primarily expressed in intracellular vesicles such as the endoplasmic reticulum, endosomes and lysosomes (Mornet *et al.*, 2004; Okada *et al.*, 2009).

Looking to the structure figure 1.19, TLR3 is a type I integral membrane protein comprises 904 amino acids. TLR3 protein consist three domain, extracellular domain (ECD), trans-membrane domain (TM), and cytoplasmic domain (CYT). The extracellular domain is a horseshoe-shaped solenoid in which Leucine-Rich Repeat (LRR) forms one turn of the solenoid. The LRRs are at the N-terminal and C-terminal regions, flanked by a cysteine-rich Cap domain. Ligand binds to TLR3 at the glycan-free surface involving LRR20. The trans-membrane domain (TM) is comprises one single helix. The cytoplasmic domain made up of the cytoplasmic linker region (CYT) (amino acid [Aa] 730 to Aa756) and the TIR domain, from which the adaptor-binding BB loop protrudes. Ala795 is a conserved residue is fitted at the top of the BB loop and involved in the binding of TRIF. There are three conserved boxes in the cytoplasmic domain of TLR3, which define the TIR domain. Two TLR3 ECDs associate on the dsRNA ligand bring the cytoplasmic TIR domains together to initiate downstream signaling (Vercammen *et al.*, 2008; Vince *et al.*, 2010).

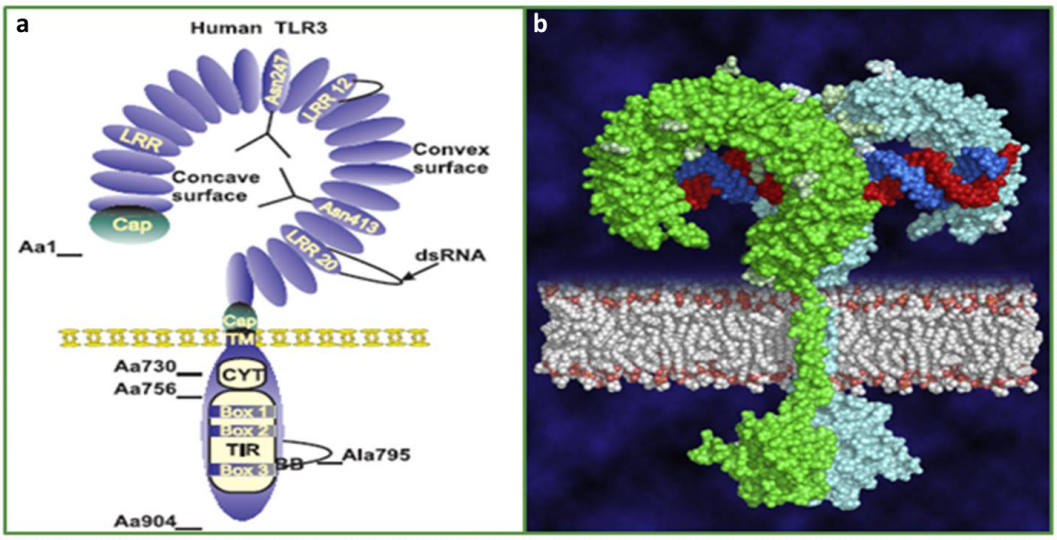

Figure 1.19 Structure of TLR3 receptor protein and the way that dsRNA bind to it (Vercammen *et al.*, 2008).

TLR3 signaling, which is induced by Poly (I:C), is mediated by the TIR domain-containing adaptor-inducing interferon-β (TRIF) adaptor molecule through the TRIF-dependent pathway. TRIF is responsible for the activation of interferon regulatory factor 3 (IRF-3) and NF-κB and the induction of type I IFN (Mornet *et al.*, 2004; Okada *et al.*, 2009) (Figure 1.20).

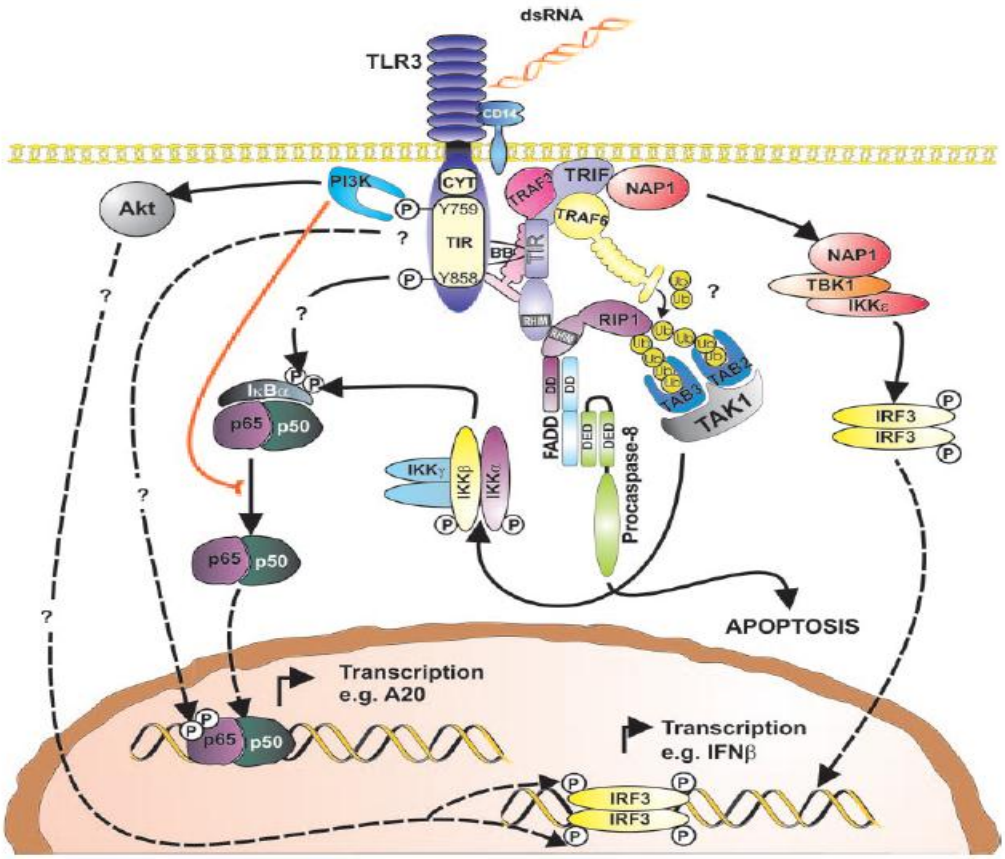

Figure 1.20 TLR3 Mediated Signaling Pathways activated by dsRNA (Vercamman *et al.*, 2008).

1.4.2 Poly (I:C) Cytosolic Mechanism of Action

On the other hand, retinoic acid inducible gene I (RIG-I) and melanoma differentiation-associated gene 5 (MDA-5) are potential cytosolic sensors of Poly (I:C) (Milhaud *et al.*, 1989; Pan *et al.*, 2007). After activation with dsRNAs, RIG-1 and MDA-5 bind with IFN-β promoter stimulator 1 (IPS-1) which is located in the outer mitochondrial membrane activates type I IFN and NF-κB (Parti *et al.*, 2002; Salaun *et al.*, 2009). Poly (I:C) shows antitumor and antiviral activity and recently entered into phase II clinical trials for patients with malignant gliomas (Salem *et al.*, 2006; Kawai *et al.*, 2010) (Figure 1.21).

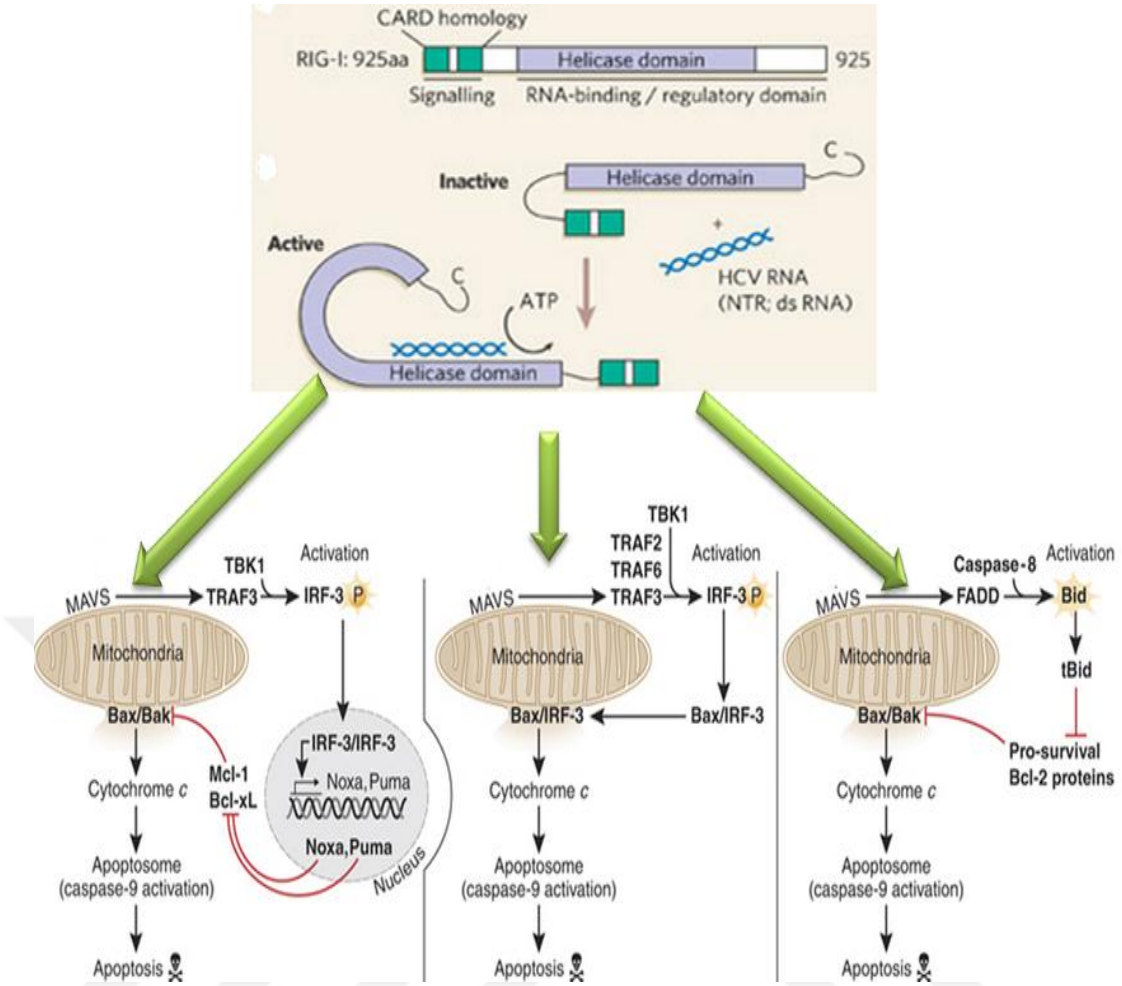

Figure 1.21 RIG-1 and MDA-5 Signaling Pathways Activated By dsRNA (Vince *et al.*, 2010).

When Poly (I:C) is given in vivo, they are rapidly cleared by nucleases so several strategies were proposed as carriers for these kind of nucleic acids attempting to increase their in vivo performances (Salvador *et al.*, 2012; Sanz *et al.*, 2012; Schlosser *et al.*, 2008). In cancer therapy, in order to increase the therapeutic efficacy, a triple effector strategy has been developed, combining targeted delivery, apoptosis induction and immunostimulatory properties of the artificial dsRNA Poly (I:C) (Schulz *et al.*, 2005). The immobilization of Poly (I:C) onto magnetic nanoparticles is an important tool for the fabrication of targeted delivery systems since they can contribute to precise delivery to an exact target site through the application of external magnetic fields (Kwai *et al.*, 2010; Shechan *et al.*, 1961; Shen *et al.*, 1993).

CHAPTER 2

MATERIALS AND METHODS

2.1 Materials

Ferric chloride hexahydrate ($FeCl_36 \cdot H_2O$), ferrous chloride tetrahydrate ($FeCl_24 \cdot H2O$), ammonia solu-tion (NH_3) (32%), 3-aminopropyl trimethoxysilane (APTS) [NH_2 $(CH_2)_3$-Si-$(OCH_3)_3$], methylacrylate, methanol, ethanol, ethylenediamine, phosphate buffer saline (PBS), ethylenediaminetetraacetic acid, trisaminomethane, EDC (1-ethyl-3-[3-dimethylaminopropyl]carbodiimide hydrochloride), 1-Methylimidazole, Polyinosinic-Polycytidylic acid (Poly (I:C)), sodium carbonate and acetic acid were purchased from Sigma–Aldrich (St. Louis, MO, USA) then were used in the synthesis of PAMAM-coated MNPs. The 2,3-bis(2-methoxy-4-nitro-5-sulfophenyl)-5-((phenylamino)carbonyl)-2H-tetrazolium hydroxide (XTT) reagent was purchased from Biological Industries (Kibbutz Beit-Haemek, Israel). Doxorubicin was kindly provided by Gulhane¨ Military Academy (School of Medicine, Ankara, Turkey). Human serum was donated by the authors of this manuscript (Rouhollah Khodadust and Pelin Mutlu) for physiological stability studies. MCF7 cell line was obtained from S¸ AP Institute (Ankara, Turkey), and Doxorubicin-resistant MCF7 cell line was developed by Kars et al.

2.2 Cell Culture

2.2.1 Growth Conditions

Three breast-cancer cell lines were used for in vitro studies. These cells are MCF7, MCF7 Doxorubicin resistant and SkBr-3 cells. Parental MCF7 cell line was donated by the ŞAP Institute, Ankara, Turkey. It is a model cell line for human mammary carcinoma, which exhibits some features of differentiated mammary epithelium (Bacus *et al.*, 1990). Doxorubicin-resistant MCF7 cell line was developed by Kars *et al.* (SkBr-3 is a cell line isolated by the Memorial Sloan–Kettering Cancer Center in 1970. It was derived from a pleural effusion due to an adenocarcinoma originating in the breast of a 43 year old, Caucasian female. The cell line over-expresses the HER2 gene product. MCF7, MCF7 1µM Doxorubicin resistant, and SKBR-3 cells were maintained as an attached type monolayer culture in commercially defined RPMI 1640 medium (Biochrom AG, Germany) (Appendix A) supplemented with 10% (v/v) heat-inactivated fetal bovine serum (FBS) (Biochrom AG) and 1% (v/v) gentamycin (Biological Industries, Israel). Incubation conditions at 37 °C in a 95% (v/v) humidified atmosphere of 5% (v/v) CO_2 were maintained in a Heraeus incubator (Hanau, Germany). The solutions used were cell culture

grade quality and the equipment used in cell culture were commercially pastoralized and disposable.

2.2.2 Cell Harvesting (Passaging)

Cells were grown in either 25 cm^2 or 75 cm^2 attached types, filter cap culture flasks (Greiner Bio-One Germany). When attached cell concentration on flask surface exceeded 80% confluency, the cells were trypsinated with trypsin-EDTA (Biochrom AG). Medium was poured out and cells attached to flask surface were washed out with FBS-free growth medium. Trypsin-EDTA was added (1 ml for 25 cm^2 and 3 ml for 75 cm^2 flasks) and discarded immediately leaving small amount of trypsin-EDTA (~0.5 ml in 25 cm^2 and ~1 mL in 75 cm^2 flasks). The flasks then incubated at 37 °C until detachment of cells was observed from outside of the flasks. Growth medium was added and detached cells were homogenized and passed into new culture flasks or separated for further experiments or they were frozen.

2.2.3 Freezing and Thawing of Cells

Trypsinated and detached cells (concentration no more than $5x10^6$ cells/mL) were centrifuged at 800 rpm for 5 min in 15ml falcon tubes (Greiner). Supernatant was discarded and pellet of cells were resuspended in 1 mL of cold freezing medium (90% (v/v) FBS and 10% (v/v) DMSO (Sigma-Aldrich, USA)). The freezing medium was transferred into the cryovials (Greiner) and maintained on ice for 30 min. The cryovials were then kept in -20 ºC freezer for 24 h and transferred to -80 ºC freezers. For long-term storage, they were immersed into liquid nitrogen container.

Cryovials were removed from -80 ºC freezer or liquid nitrogen container and immediately transferred to 37 ºC. When they were completely thawed, aliquots were transferred into the 15 ml falcon tubes and cells were pelleted at 800 rpm for 5 min. Supernatant was discarded and pellet was resuspended in a volume of complete media appropriate for type of culture flask. Cells were maintained in defined growth conditions.

2.2.4 Cell Proliferation Assays (XTT Cell Proliferation Assay)

Antiproliferative effects of DcMNPs, Poly (I:C)-bound DcMNPs, Doxorubicin-loaded DcMNPs and Doxorubicin-loaded Poly (I:C)-bound DcMNPs on different MCF7 cells, Doxorubicin-resistant MCF7 cells and SKBR-3 cells were evaluated by means of the Cell Proliferation Kit (Biological Industries) according to manufacturer's instructions. Assay was a colorimetric test based on the reduction tetrazolium salt, XTT to colored formazan products by mitochondria of live cells. In brief, cells were seeded to 96-well microliter plates (Greiner) at a concentration of $5.0x10^4$ cells/well and incubated for 72 h in medium

containing horizontal dilutions of drugs. In each plate assay was performed with a column of blank medium control and a cell control columns. Then, XTT reagent was added and soluble product was measured at 500 nm with a Spectromax 340 96-well plate reader (Molecular Devices, USA).

Figure 2.1 Schematic representation of 96-well plate 4 h after XTT reagent addition to drug treated MCF7 cells.

2.3 Synthesis of DcMNPs

2.3.1 Preparation of MNPs

Ferric chloride hexahydrate ($FeCl_3 6H_2O$), ferrous chloride tetrahydrate ($FeCl_2 4H_2O$), 32 % ammonia solution (NH_3), 3-aminopropyltrimethoxysilane (NH_2 $(CH2)_3$–Si–$(OCH_3)_3$, APTS), methyl acrylate, methanol, ethanol, and ethylenediamine were purchased from Sigma Aldrich. The MNPs (Fe_3O_4) were prepared by coprecipitation method (Khodadust *et al.*, 2013). $FeCl_2.4H_2O$ and $FeCl_3 6 \cdot H_2O$ (Fe^{+2}: Fe^{+3}= 1:2) were dissolved in distilled water under nitrogen environment. Ammonia solution was added slowly with vigorous mechanical stirring at 2000 rpm for 2 h. During the reaction, temperature was kept at 90 ◦C. The black precipitate was washed five times with distilled water and five times with ethanol using magnetic separation. The obtained iron oxide NPs were dispersed in ethanol (5 g/l) (Khodadust *et al.*, 2013; Pan *et al.*, 2007; Gao *et al.*, 2005; Esfand *et al.*, 2001; Lai *et al.*, 2007). The characterization of bare NPs were performed by transmission electron

microscopy (TEM), dynamic light scattering (DLS), X-ray diffraction (XRD), X-ray photoelectron spectroscopy (XPS), Fourier transform infrared spectroscopy (FTIR), thermal gravimetric analysis (TGA), and vibrating sample magnetometer (VSM) analyses (Khodadust *et al.*, 2013).

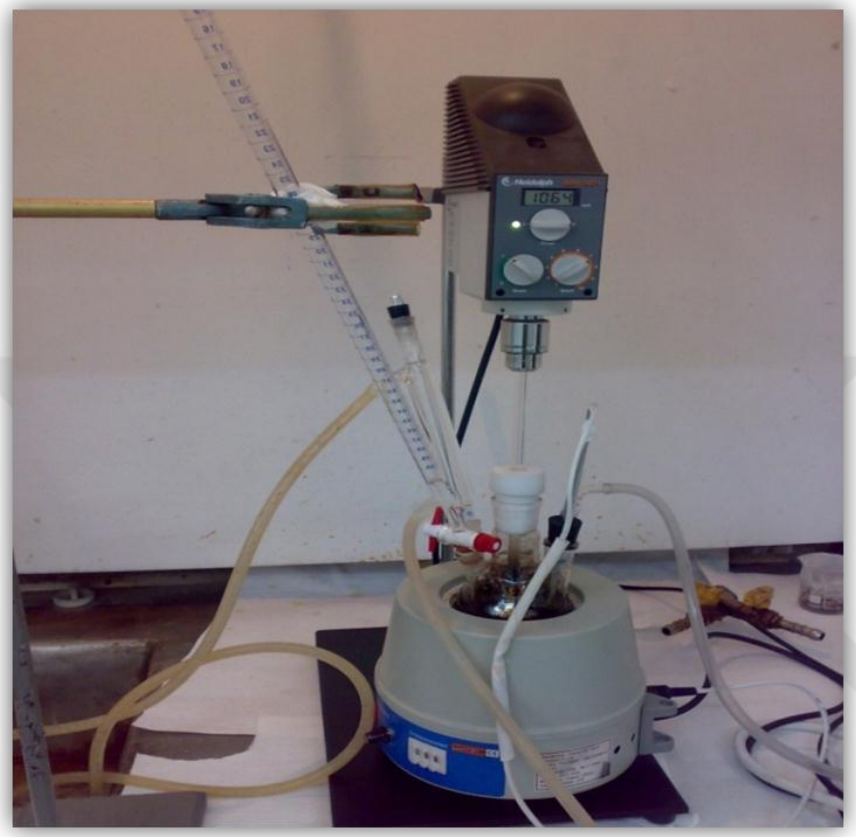

Figure 2.2 Schematic representation of the system for the synthesis of bare iron oxide nanoparticles.

2.3.2 Preparation of APTS Coated NPs

Surface modification of Fe_3O_4 was performed with APTS. Ethanol was added into the Fe_3O_4–ethanol solution and sonicated with ultrasonicator (Bandelin Sonopuls Ultrasonic Homogenizer HD 2200, Berlin, Germany) at 100% amplitude for 30 min at room temperature. APTS was added to the mixture at twentieth minute of sonication. Then, the mixture was stirred with mechanical stirrer at 2000 rpm and at room temperature for 15 h. The resulting black precipitate was separated by magnetic decantation and washed with methanol for several times. The obtained NPs modified with APTS are called G_0 generation (Khodadust *et al.*, 2013; Pan *et al.*, 2007; Gao *et al.*, 2005; Esfand *et al.*, 2001; Lai *et al.*, 2007). The characterization of APTS-modified MNPs was performed by XRD, TEM, VSM, FTIR, XPS, and TGA analyses (Khodadust *et al.*, 2013).

2.3.3 Surface Coating with PAMAM Dendrimer

Coating of G_0NPs was carried out with PAMAM dendrimer through Michael reaction. Methylacrylate methanol solutions (20%, v/v) were added to the G_0NPs, and the suspension was sonicated in an ultrasonic water bath at room temperature for 7 h. After ultrasonication, NPs were eluted by magnetic decantation and washed with methanol. Ethylenediamine–methanol solution (50%, v/v) was added and suspension was sonicated for 3 h. The particles were washed with methanol. The stepwise growth of dendrimers was repeated until the desired number of generations (G_1–G_7) of DcMNPs (G_1DcMNPs–G_7DcMNPs) were achieved using the methylacrylate and ethylenediamine steps. The obtained DcMNPs were then washed three times with methanol and five times with distilled water by magnetic decantation (Khodadust *et al.,* 2013; Pan *et al.,* 2007; Gao *et al.,* 2005; Esfand *et al.,* 2001; Lai *et al.,* 2007). The characterization of PAMAM DcMNPs was performed by TEM, VSM, FTIR, XPS, TGA, and DLS analyses (Khodadust *et al.,* 2013).

2.3.4 Cellular internalization of dendrimer coated magnetic nanoparticles

The internalization of dendrimer-coated iron oxide nanoparticles were shown by light and confocal microscopy. The nanoparticles were incubated with breast cancer MCF7 cell lines in 6 well plates. After 24 h incubation, the medium was removed from the plates and the plates were washed with PBS for several times so that all free DcMNPs were removed from the environment. Their photographs were taken under an inverted optical microscope to determine cellular internalizations of DcMNPs (Wuang *et al.,* 2007; Mahmoudi *et al.,* 2009). In addition, G_4DcMNPs were conjugated with fluorescein isothiocyanate (FITC) in EDC/NHS solution, which was applied onto the MCF7 cells. The conjugation process was carried out using the surface activation method by EDC–NHS chemistry (Acharya *et al.,* 2009). 20 mg EDC and 4.6 mg NHS were dissolved in 2 ml of PBS (pH 5.8) followed by the addition of 100 ml of FITC in the suspension. After 2 h, 5 mg ml-1 of G_4DcMNPs was added to the above solution and left to remain at 4 ^{o}C under continuous magnetic stirring for overnight. Then, product was washed three times with PBS by magnetic decantation. The resultant FITC-conjugated MNPs were visualized by confocal microscopy.

2.3.5 Cytotoxicity Analysis of G_4DcMNPs and G_7DcMNPs

The cytotoxicity study of synthesized G_4DcMNPs and G_7DcMNPs were performed on three breast-cancer cell lines namely; MCF7, MCF7/ 1μM Doxorubicin resistant, and SKBR-3 cells.

2.4 Poly (I:C) loading on DcMNPs

2.4.1 Poly (I:C) Activation

The Poly (I:C) products were dissolved in nuclease free water to a final concentration of 10 mg/ml as stock, yielding a very faint hazy to clear, colorless solution. In order to make bound between 5'-phosphate group of Poly (I:C) and NH_2 groups at the surface of DcMNPs, first Poly (I:C) was heated to 55 °C and then cooled to room temperature to make ds-Poly (I:C) according to manufacturer's procedure (Sigma-Aldrich). Then the activation procedure was continued in the presence of EDC and 1-methylimidazole (Shukoor *et al.*, 2007; Shukoor *et al.*, 2008).

2.4.2 Poly (I:C) Loading Optimization on G_7DcMNPs at pH 7, and pH 7.5

G_7DcMNPs were dissolved in 0.1 M 1-methyl-imidazole buffer (pH 7) to a final concentration of 10 mg/ml. The EDC solution of 0.013 M was prepared using 0.1 M 1-methyl-imidazole buffer (pH 7) and used fresh. Poly (I:C) was diluted as 200 µg/ml in 0.1 M 1-methyl-imidazole buffer (pH 7) and 4 µg of Poly (I:C) was put into microcentrifuge tubes. Freshly prepared EDC solution was added immediately and incubated for 15 min at room temperature. Then G_7DcMNPs/1-methylimidazole solution was added to the reaction with final volume as 100 µl and rotated for 2 h at room temperature. The applied PIC: G_7DcMNPs ratios were as 1:10, 1:15, 1:20, 1:30, and 1:35. Poly (I:C) loaded G_7DcMNPs were washed with distilled water by using magnetic separation in order to remove EDC from the solution. The loading procedure of Poly (I:C) also performed on other generations at pH 7, and pH 7.5.

2.4.3 Poly (I:C) Loading Optimization on G_7DcMNPs at pH 6

Poly (I:C) loading optimization on G_7DcMNPs at pH 6 was done by following the similar steps in the section 2.4. In contradiction, 0.1 M 1-methyl-imidazole buffer with pH 6 was used. In addition the applied PIC: G_7DcMNPs ratios were as 1:10, 1:11, 1:12, 1:13, and 1:15. After optimization with G_7DcMNPs, the loading efficiencies on G_2, G_3, G_4, G_5 and G_6DcMNPs were also done.

2.4.4 Stability of Poly (I:C)-bound DcMNPs

The stabilities of Poly (I:C) on different generations of DcMNPs were studied at different acidic (acetate buffer),basic (carbonate buffer) and neutral (injection buffer and PBS) pH conditions.

2.4.5 Cytotoxicity Analysis of Poly (I:C)-bound G_7DcMNPs

The cytotoxicity analysis of Poly (I:C)-bound G_7DcMNPs on different cell lines performed.

2.5 Doxorubicin Loading on DcMNPs

2.5.1 Doxorubicin Loading on Different Generation of DcMNPs

Loading studies of Doxorubicin was carried out in PBS (pH 7.2), TES (pH 7.3), and acetate (pH 5.0) buffers, in different drug concentrations. Maximum drug-loading studies on DcMNPs were carried out with different drug to DcMNPs concentration ratios (1:50–1:5) at two different temperatures (25 °C and 4 °C). The mixture of buffer, drug, and DcMNPs were rotated at 10 rpm with five-second vibration intervals for 24 h while being protected from light. After the incubation period, Doxorubicin-loaded DcMNPs were separated by magnetic separation and the Doxorubicin loading efficiency was quantified by measuring the absorbance values at 481 nm by a Shimadzu UV spectrophotometer (Columbia, USA). The loading of maximum Doxorubicin to DcMNPs was confirmed by FTIR analysis (data not shown).

2.5.2 Stability of Doxorubicin on DcMNPs

Stabilities of DcMNPs loaded with maximum amounts of Doxorubicin (400 and 500 µg/mL) were studied in PBS buffer (pH 7.2) up to 8 weeks and in human serum up to 4 days at 37◦C. The release of Doxorubicin from the NPs in PBS buffer was measured as the absorbance values at 481 nm by a UV spectrophotometer. Doxorubicin release in human serum was measured by Varian Cary Eclipse fluorescence spectrophotometer (CA, USA) (excitation at 480 nm, emission maximum at 560–590 nm).

2.5.3 Release of Doxorubicin from DcMNPs

The release of Doxorubicin from DcMNPs loaded with 400 and 500 µg/ml was analyzed in acetate buffer at two different pH values (5.2 and 4.2) up to 90 h. The amount of released Doxorubicin was determined by measuring the absorbance of the solution at 481 nm.

2.5.4 Cellular Internalization of Doxorubicin-Loaded Dendrimer Coated Magnetic Nanoparticles

MCF7/ 1µM Doxorubicin resistant cells were treated with free Doxorubicin and Doxorubicin-loaded DcMNPs and visualized with fluorescent microscopy.

2.5.5 Cytotoxicity Analysis of Doxorubicin-Loaded G_4DcMNPs on Resistant MCF7 Cells

Doxorubicin resistant MCF7 cells were grown in 96-well tissue culture plate and free Doxorubicin, free G_4DcMNPs, and Doxorubicin-loaded G_4DcMNPs were added after 24 h. The cells were incubated for 72 h at 37 ◦C in 5% CO_2 incubator, and XTT reagent was added. After 4 h incubation period, the cytotoxicity was quantified spectrophotometrically using enzyme-linked immune-sorbent assay reader.

2.6 Poly (I:C)-bounding on Doxorubicin-Loaded DcMNPs

2.6.1 Poly (I:C) Binding on G_4DcMNPs

Poly (I:C) were bound onto the surface of G_4DcMNPs at pH 6 and pH 6.5 . Polyacrylamide gel electrophoresis (PAGE) applied to analyze the binding efficiency and the stability of the Poly (I:C) functionalized dendrimer coated magnetic nanoparticles.

2.6.2 The Amount of Loaded Doxorubicin on G_4DcMNPs Affects the Efficiency of Poly (I:C) Binding

Doxorubicin was loaded on G_4DcMNPs at 400 µg/ml and 500 µg/ml concentrations. The Doxorubicin-loaded G_4DcMNPs were washed with 0.1 M MeIm (pH 6) to remove the PBS buffer and make the Doxorubicin-loaded G_4DcMNPs ready for Poly (I:C) binding. The percentage of released Doxorubicin was calculated through washing steps. Then Poly (I:C) binding procedure was performed on Doxorubicin-loaded G_4DcMNPs. as in section 2.3.3.

2.6.3 PH Effects on Poly (I:C) Binding on Doxorubicin-Loaded G_4DcMNPs

The Doxorubicin-loaded G_4DcMNPs were very sensitive to acidic pH. Therefore, to determine the most efficient pH, binding of Poly (I:C) on Doxorubicin-loaded G_4DcMNPs were performed at pH 6 and pH 6.5 which are slightly acidic. This will results not only in efficient Poly (I:C) binding and but also will prevent significant Doxorubicin release during the Poly (I:C) binding process.

2.6.4 Cytotoxicity Analysis of Poly (I:C)-bound Doxorubicin-Loaded G_4DcMNPs

Cytotoxicity analysis of Poly (I:C)-bound Doxorubicin-loaded G_4DcMNPs was performed on 1µM Doxorubicin resistant MCF7 cells via cell proliferation assays.

CHAPTER 3

RESULTS

3.1 Synthesis of DcMNPs

3.1.1 Synthesis of Magnetic Nanoparticles

Temperatures of the reaction system and ammonia addition rate are two important factors that influence the synthesis of MNPs. In order to synthesize nano-sized, crystalline, bare iron oxide particles, these two parameters were tested. Iron oxide nanoparticles synthesized at different temperatures between 20 and 90 °C. XRD results demonstrated that the nanoparticles with preferred crystalline structure were obtained at 90 °C. The time of ammonia addition was also optimized. When the ammonia was added very slowly, smaller nanocrystals were synthesized, so that the size can be adjusted.

3.1.2 Aminosilane Modification of Nanoparticles

Optimizing sonication time during aminosilane modification improves magnetic properties and size distribution. Bare nanoparticles were modified with APTS to prepare them for dendrimer coating. The sonication time was optimized to obtain DcMNPs with desired size and shape. The magnetic properties of APTS-modified nanoparticles were improved when the time of sonication was increased from 10 to 30 min, and APTS was added to the reaction at the 20th min of sonication. Optimizations in aminosilane modification method decreased the agglomeration of nanoparticles, resulted in the synthesis of DcMNPs with desired size distribution, and improved magnetic properties.

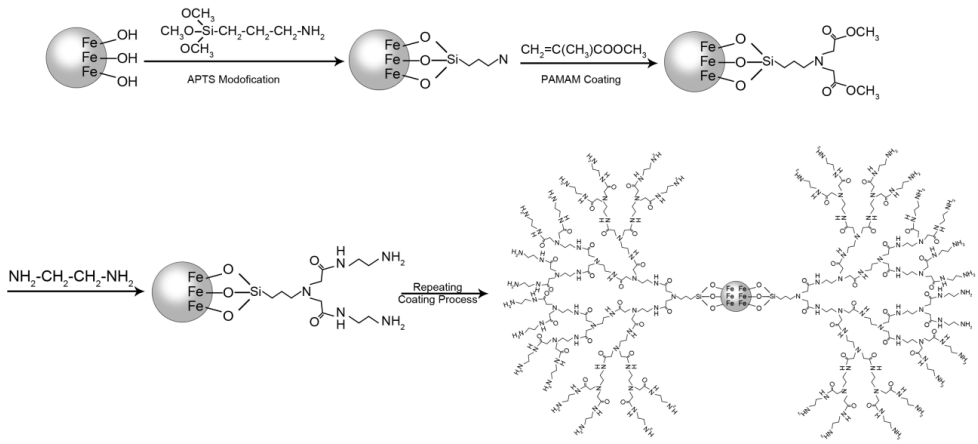

Figure 3.1 Stepwise modification of iron oxide nanoparticles with APTS and dendron.

3.1.3 X-ray Diffraction Analysis (XRD)

Bare iron oxide nanoparticles synthesized at different temperatures between 20 and 90 °C, and X-ray powder diffraction analyses of synthesized nanoparticles were performed to identify the crystal structure. It was observed that the highest crystalline was achieved at 90 °C. Up to 50 °C, the synthesized iron oxide nanoparticles show amorphous or non-crystalline solid characteristics. At temperatures greater than 50 °C, the nanoparticles started to show crystal-line characteristics.

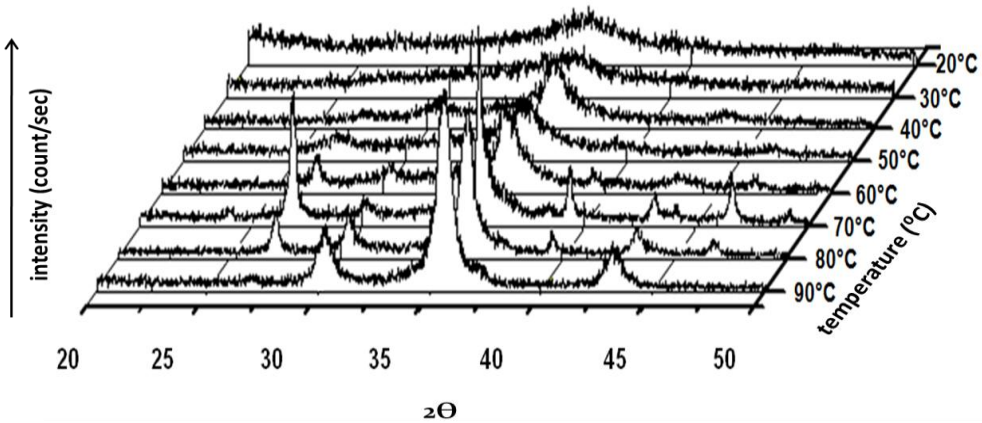

Figure 3.2 XRD analysis of nanoparticles synthesized at different temperatures.

XRD pattern of Fe_3O_4 nanoparticles synthesized at 90 °C appeared with diffraction peaks of (220), (311), (400), (422), (511), (440), and (533), which are the characteristic peaks of the magnetite crystal having a cubic spinal structure. Coating of nanoparticles with PAMAM dendrimers did not change the characteristic XRD pattern (Figure 3.3).

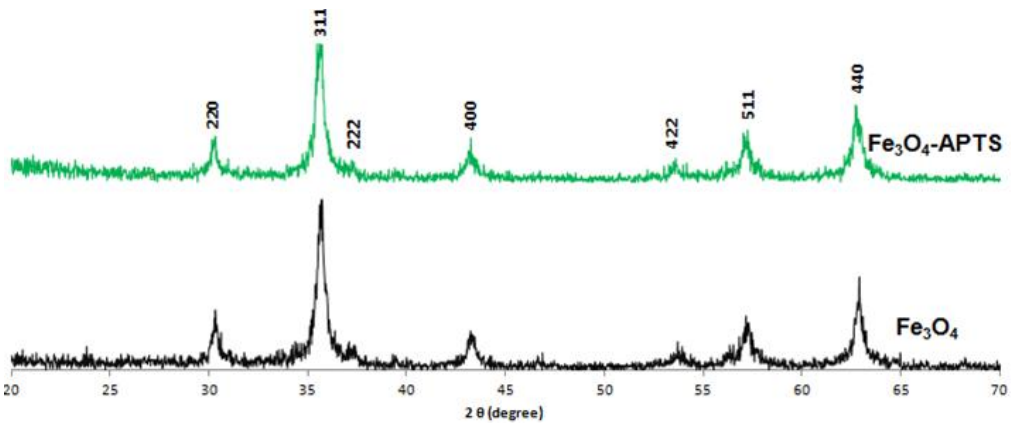

Figure 3.3 X-Ray powder diffraction of Fe_3O_4 and Fe_3O_4-APTS nanoparticles.

3.1.4 Fourier Transform-Infrared Spectroscopy (FT-IR)

FTIR results related to bare MNP, MNP-APTS, and different generation of dendrimer-modified MNPs are given in Figure 3.4.

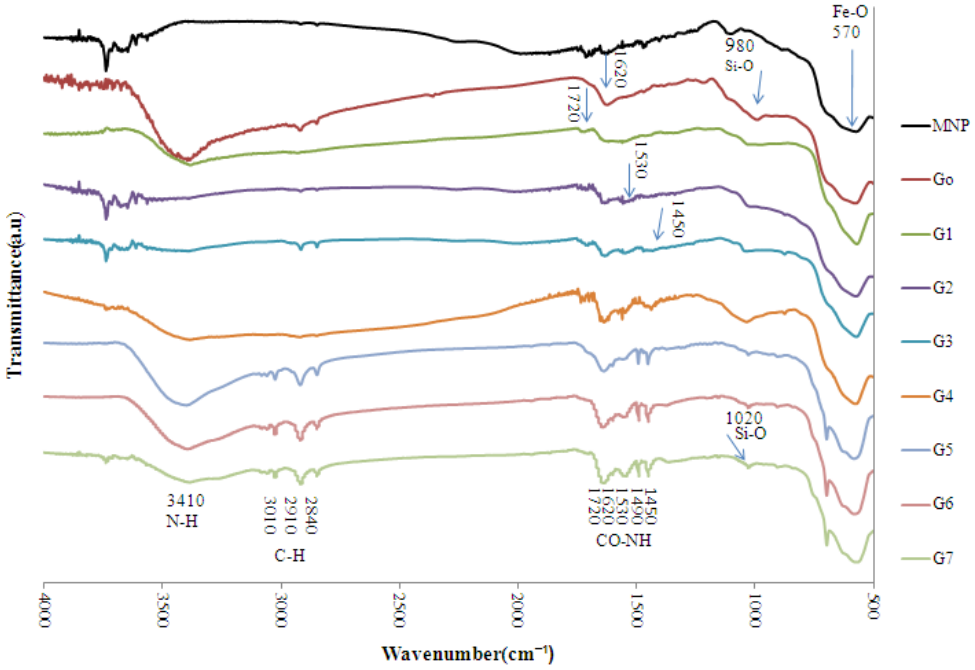

Figure 3.4 FT-IR results related to MNP, MNP-APTS, and different generations of dendrimer-modified magnetic nanoparticles.

The presence of Fe_3O_4 core could be identified by the strong stretching absorption band between 408 and 673 cm^{-1}, which correspond to the Fe–O bond of nanoparticles (Julian *et al.*, 1991).

IR analysis of aminosilane, methanol, and methyl-acrylate were separately performed (data not shown). Considering magnetite (Fe_3O_4) Fe–O group bond observed at 570 cm^{-1}, which corresponds to intrinsic stretching vibration of the metal at tetrahedral site (Fetetra–O). The vibration of NH_2 group is at around 3410 cm^{-1}. The stretching vibration of Si–O–Fe is at 950 cm^{-1}, which shifts to about 1050 cm^{-1} for G_7DcMNPs because of the presence of highly electronegative –CO–NH_2 groups. C–H bonds present in methylacrylate, aminosilanes, methanol, and the related bonds, can be seen at 2840, 3910 and 3010 cm^{-1}, respectively. Vibration of –CO–NH– bonds were observed at 1450, 1490, 1530, and 1620 cm^{-1}. O–H bonds related to alcohols were at 3200–3600 cm^{-1}. FT-IR spectra are compatible with the stepwise dendrimer modification process.

3.1.5 Transmission Electron Microscopy Analysis (TEM)

It is known that the size distribution smaller than 30 nm is the characteristics of superparamagnetic iron oxide nanoparticles. On analyzing the TEM results (Figure 3. 5), it was understood that the sizes of obtained bare iron oxide MNPs were 8 ± 5 nm. This shows that the synthesized MNPs are potentially superparamagnetic. However, in order to confirm this, vibrating sample magnetometer analysis was done.

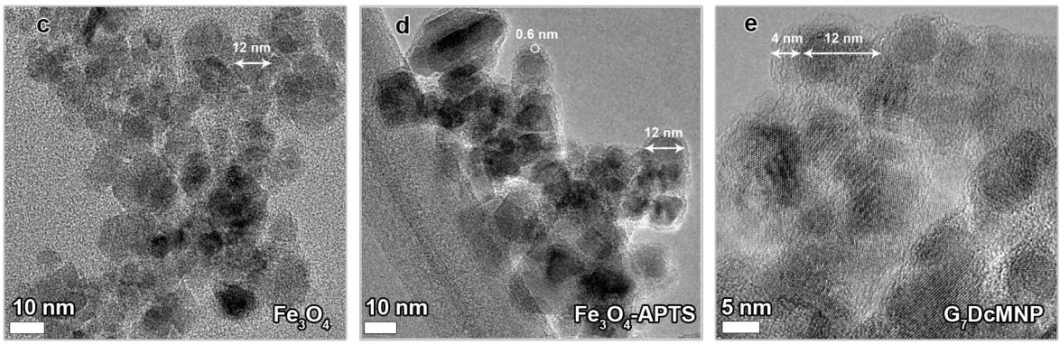

Figure 3.5 The sizes of obtained G_7DcMNPs were 16 ± 5 nm. The change of the size after dendrimer modification was around 8 nm.

TEM image of aminosilane-modified nanoparticles demonstrated that the size distribution of aminosilane-modified MNPs were more uniform. The size change was around one nm after modification with aminosilane that was observable on the surface of nanoparticles.

3.1.6 Dynamic Light Scattering Analysis (DLS)

The average diameters of bare MNPs were found as 55 ± 15 nm in DLS measurements (Figure 3.6 a). The average diameters of the dendrimer-coated MNPs (G_7DcMNPs) were 45 ± 10 nm in DLS measurements (Figure 3.6 b).

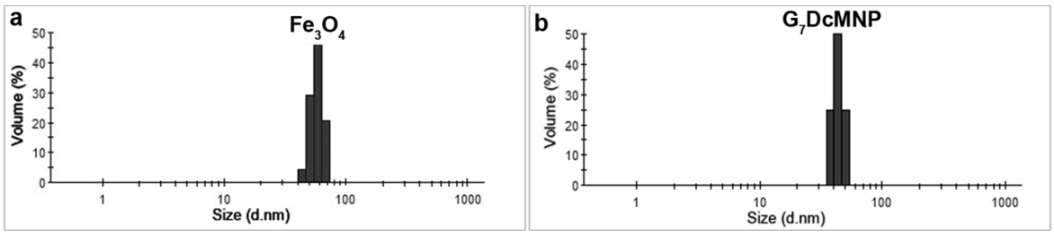

Figure 3.6 Dynamic light scattering graphs of bare MNPs (a) and G_7DcMNPs (b).

3.1.7 Zeta (ζ) Potential Analysis

The ζ potential values of bare MNPs were calculated as -23.2 mV in PBS buffer pH 7.2. The ζ potentials of G_4DcMNPs and G_7DcMNPs were observed at 15.1 mV and 20.9 mV, respectively.

3.1.8 Vibrating Sample Magnetometer Analysis (VSM)

The applied magnetic field was changed and magnetization properties of synthesized Fe_3O_4, aminosilane-modified MNPs, and DcMNPs were measured at 25 °C and 37 °C. Magnetization curves of the MNPs, APTS-modified MNPs, and DcMNPs at 37 °C are given in Figure 3.7. Magnetic materials showing a superparamagnetic behavior have zero value of remanence and coercivity. The remanence and coercivity observed in the hysteresis loops of MNPs, APTS-coated MNPs, and DcMNPs at both 25 °C and 37 °C were negligible. VSM results of bare MNPs analyzed at 25 °C (Figure 3. 7) and 37 °C (Figure 3.8) were obtained as 54.5 and 48.8 emu g^{-1} respectively.

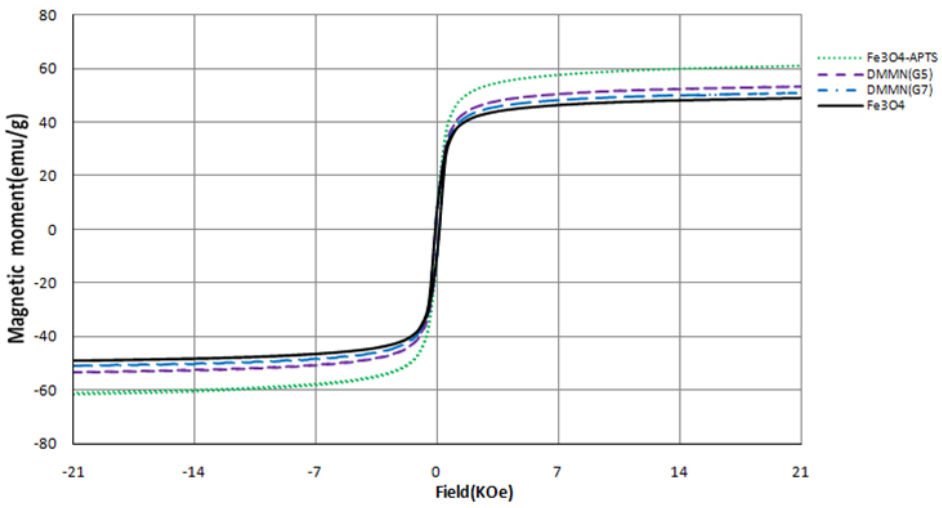

Figure 3.7 Magnetization curve of the MNPs, APTS-modified MNPs and DcMNPs at 37 °C.

In order to determine the magnetic characteristics of synthesized nanoparticles, VSM analysis was done at body temperature and room temperature. The maximum magnetization were found to be 48.8, 61.4, 53.4, and 51.1 emu g^{-1} for MNP, APTS-coated MNP, G_5DcMNPs, and G_7DcMNPs, respectively, at 37 °C. The maximum magnetizations at room temperature were found to be 54.5, 56.5 and 49.5 emu g^{-1} for MNP, APTS-coated MNP and G_5DcMNPs, respectively.

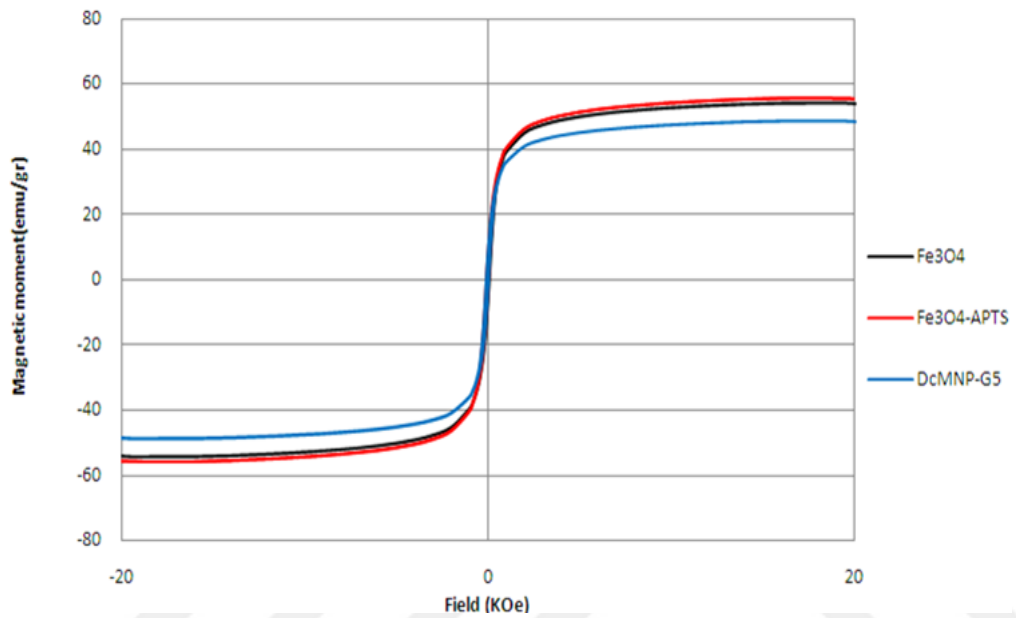

Figure 3.8 Magnetization curve of the MNPs, APTS-modified MNPs and DcMNPs at 25 °C.

3.1.9 Thermal Gravimetric Analysis (TGA-FTIR)

The TGA curve of bare, aminosilane modified and dendrimer coated MNPs (Figure 3.9) shows that the weight loss of bare MNPs over the temperature range from 30 to 850 LC is about 3.5 %, which might be because of the loss of residual water in the sample. In aminosilane-modified MNPs, the weight loss is about 5 %, which reflects the amount of APTS at the surface of nanoparticles (1.5 % aminosilane and 3.5 % water loss in the sample). The fifth (G_5DcMNPs) and seventh (G_7DcMNPs) generations of dendrimer-coated MNPs had 22 % and 27 % weight losses, respectively, indicating the amount of PAMAM dendrimer layers on the surfaces of nanoparticles.

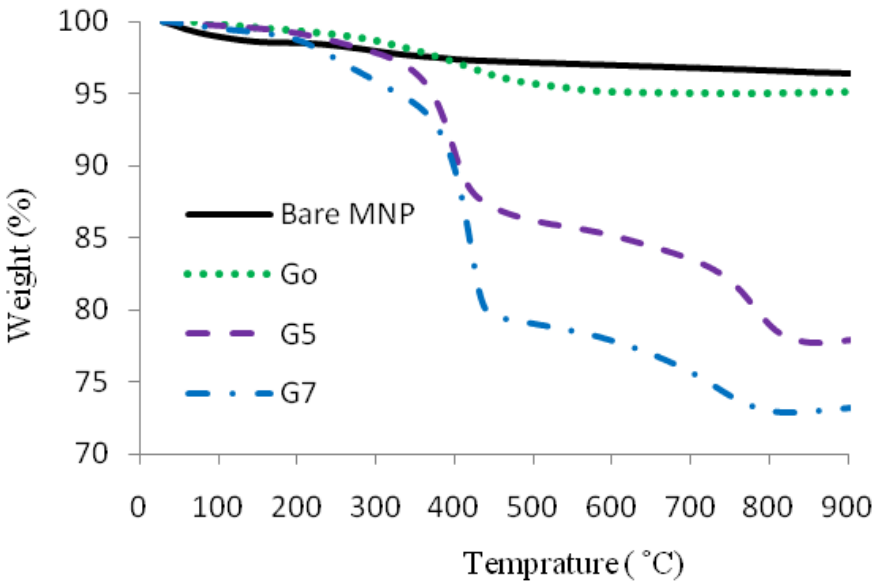

Figure 3.9 The TGA curve of bare, aminosilane modified and dendrimer coated MNPs.

TGA analysis shows that there was an increase in the organic content of MNPs when the growth of the PAMAM dendrimer was increased to higher generations.

3.1.10 X-ray Photoelectron Spectroscopy (XPS)

Qualitative and quantitative surface characterizations of synthesized bare MNPs, G_0, G_5, and G_7DcMNPs have been done by X-ray photoelectron spectroscopy (XPS). Figure 3.10 shows the general XPS scanning spectra of bare MNPs, G_0, G_5 and G_7DcMNPs. The peaks obtained upon XPS analysis were belonging to Si 2p (100.3 eV), C 1s (284.2 eV), N 1s (398.2 eV), O 1s (528.5 eV), and Fe 2p (710.3 eV). N 1s and Si 2p peaks belonging to nitrogen and silane were not present in the spectrum of bare MNPs as expected.

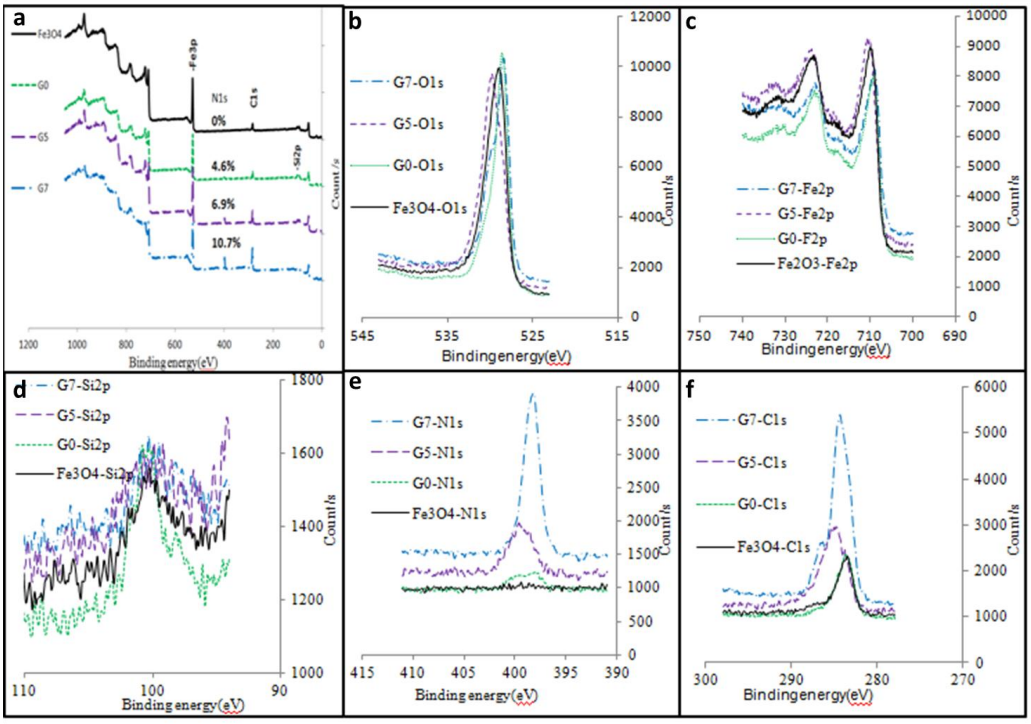

Figure 3.10 General XPS scanning spectrum belonging to the surfaces of bare MNP, G_0, G_5, and G_7 nanoparticles (a), the peaks obtained upon XPS analysis belonging to O 1s (b), Fe 2p (c), Si 2p (d), N 1s (e), and C 1s (f).

The regional XPS scans were also performed for the quantitative analyses of various atoms (Si, N, C, O, and Fe) found in nanoparticles. As seen in figure 3.10, there was a decrease in the oxygen (O 1s) and iron (Fe 2p) contents in (G_0, G_5, and G_7) DcMNPs due to the increase in the thicknesses of PAMAM layers at the surfaces of nanoparticles. The peaks of Si 2p (100.3 eV) and Fe 2p (398.2 eV) were observed in the nanoparticles after the aminosilane modification. During the synthesis of each generation of dendrimer at the surface of the nanoparticles, ramifying occurs, which results in an exponential increase on the amount of free surface atoms. The exponential increase of nitrogen and carbon atoms was observed in XPS spectra of (G_0, G_5, and G_7) DcMNPs.

The amount of nitrogen and carbon at the surface of (G_0, G_5, and G_7) DcMNPs were counted as 4.6, 6.9, and 10.7 % for nitrogen; and 18.6, 27.6, and 42.8 % for carbon, respectively (Table 3.1). These results demonstrate that the PAMAM dendrimer coating was achieved successfully.

Table 3.1 Atomic percentage changes in bare iron oxide, aminosilane-modified, G_5 and G_7DcMNPs.

MNP	Fe_3O_4 (%)	G_0DcMNP (%)	G_5DcMNP (%)	G_7DcMNP (%)
N ls (% of nitrogen atom)	0	4.6	6.9	10.7
C ls (% of carbon atom)	18.2	18.6	27.6	42.8
Fe 2p3 (% of iron atom)	21.6	21.5	18.7	11.8
Ol s (% of oxygen atom)	60.2	54.2	46.0	34.2
Si 2p	0	1.1	0.8	0.5

3.1.11 Cellular Internalization of Dendrimer Coated Magnetic Nanoparticles

It was demonstrated by inverted light microscopy that while none of the bare MNPs was taken up by the cells, most of the DcMNPs were internalized (at 37 LC, 2 h). G_4DcMNPs containing MCF7 cells are shown in Figure 3.11. Moreover, G_4DcMNPs were conjugated with FITC (fluorescein isothiocyanate). The resultant FITC-conjugated MNPs were visualized by confocal microscopy (Figure 3.12).

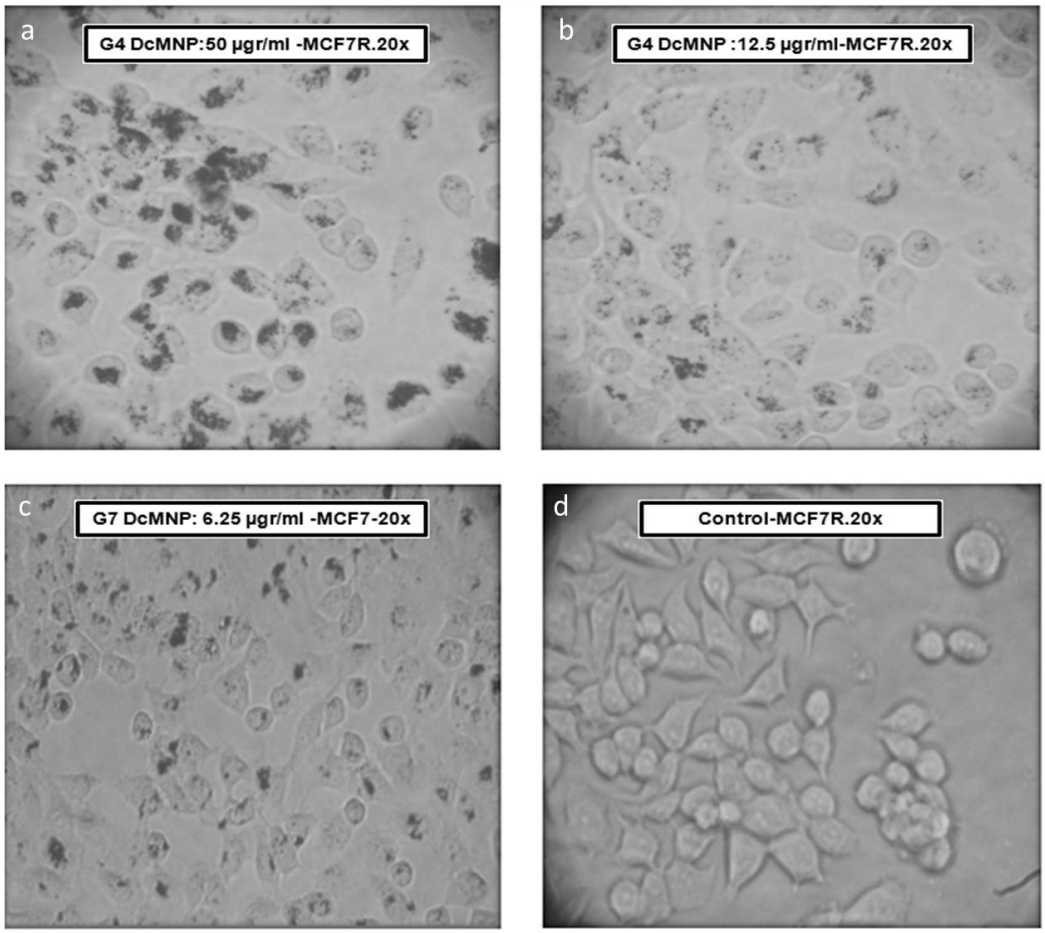

Figure 3.11 Cellular internalization of dendrimer-coated magnetic nanoparticles by inverted light scattering microscopy (40X).

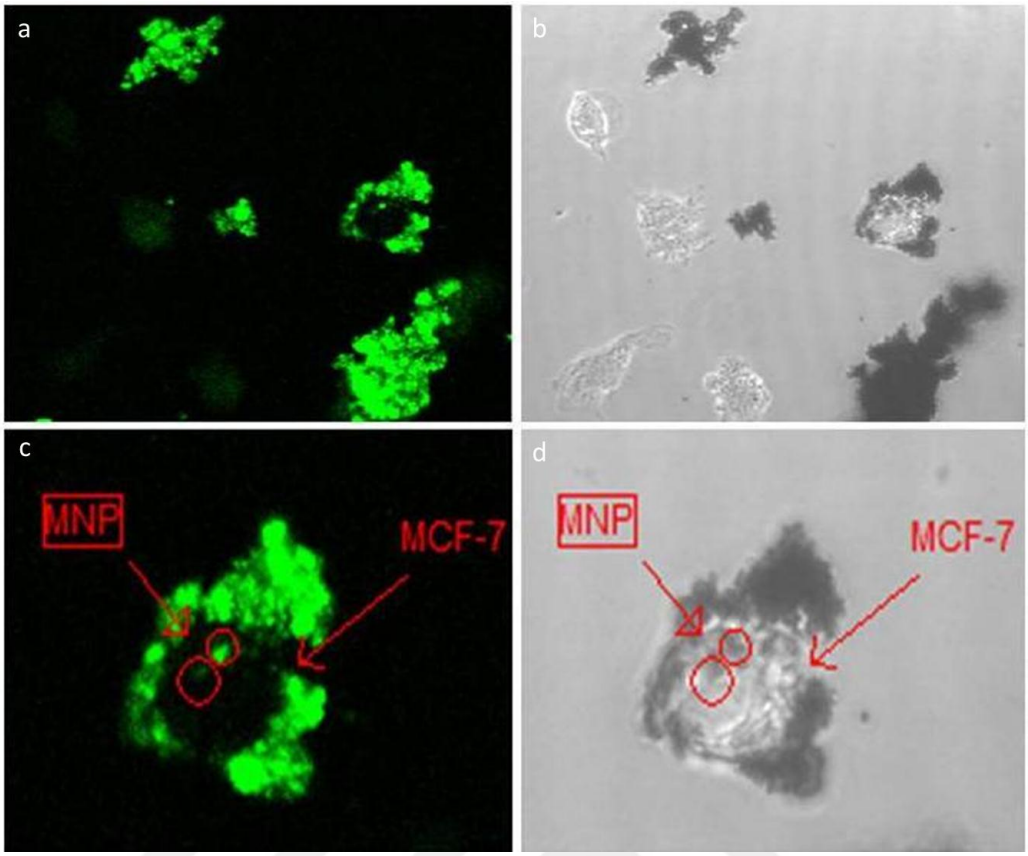

Figure 3.12 Cellular internalization of FITC binding dendrimer coated magnetic nanoparticles by confocal microscopy (40 X).

The results are promising because nanoparticles can be internalized into the cells even if they are applied at low concentrations and cell viability was not affected. Cellular internalization was carried out at five different concentrations of DcMNPs.

3.1.12 Cytotoxicity study of dendrimer-coated magnetic nanoparticles

Cytotoxicity of DcMNPs was investigated by XTT cell proliferation assay. Survival rates indicated that there is no significant cytotoxic effect of the nanoparticles on MCF7 cells (figures 3.13, 3.14, 3.15).

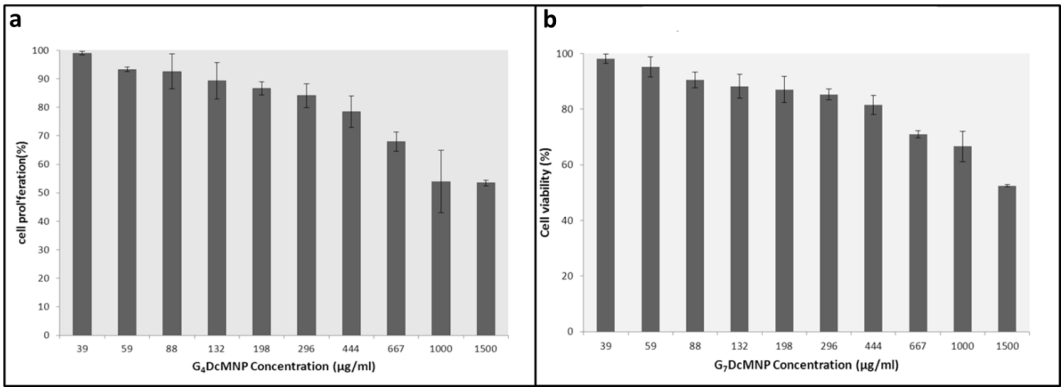

Figure 3.13 Cytotoxicity of G_4DcMNPs (a), and G_7DcMNPs (b) on 1µM Doxorubicin resistant MCF7 cells.

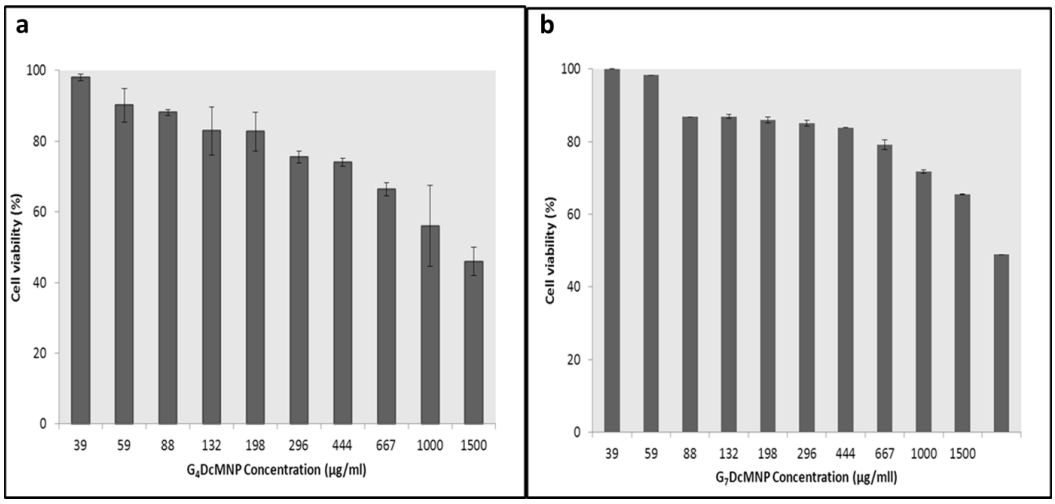

Figure 3.14 Cytotoxicity of G_4DcMNPs (a), and G_7DcMNPs (b) on MCF7.

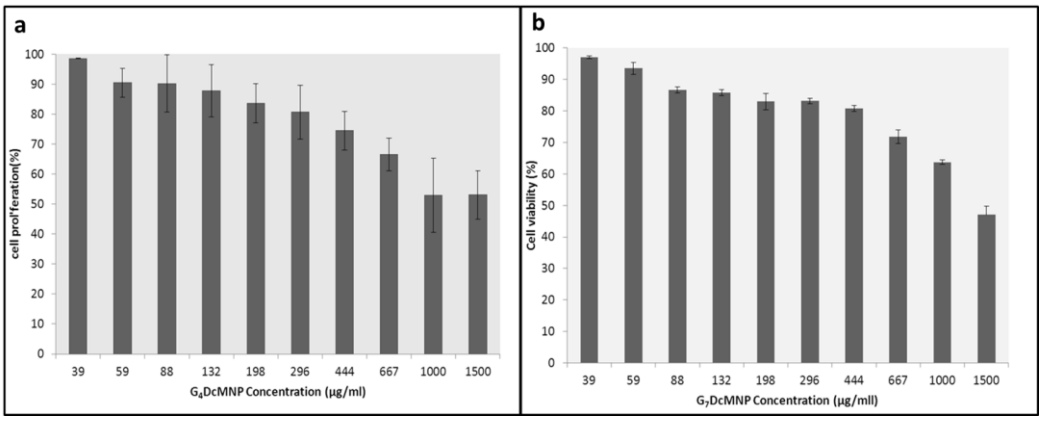

Figure 3.15 Cytotoxicity of G_4DcMNPs (a), and G_7DcMNPs (b) on SkBr-3.

3.2 Poly (I:C) Binding on DcMNP

3.2.1 Surface Functional Group

X-ray photoelectron spectroscopy (XPS) analysis demonstrated that the surface nitrogen atoms appear after aminosilane modification. The percentage of nitrogen atoms exponentially increases by increasing the generation numbers of DcMNPs as amine functional groups at the surface of DcMNPs increases exponentially (Figure 3. 16).

MNP	Fe_3O_4	G_0DcMNP	G_5DcMNP	G_7DcMNP
N1s(% of Nitrogen Atom)	0%	4.6%	6.9%	10.7%

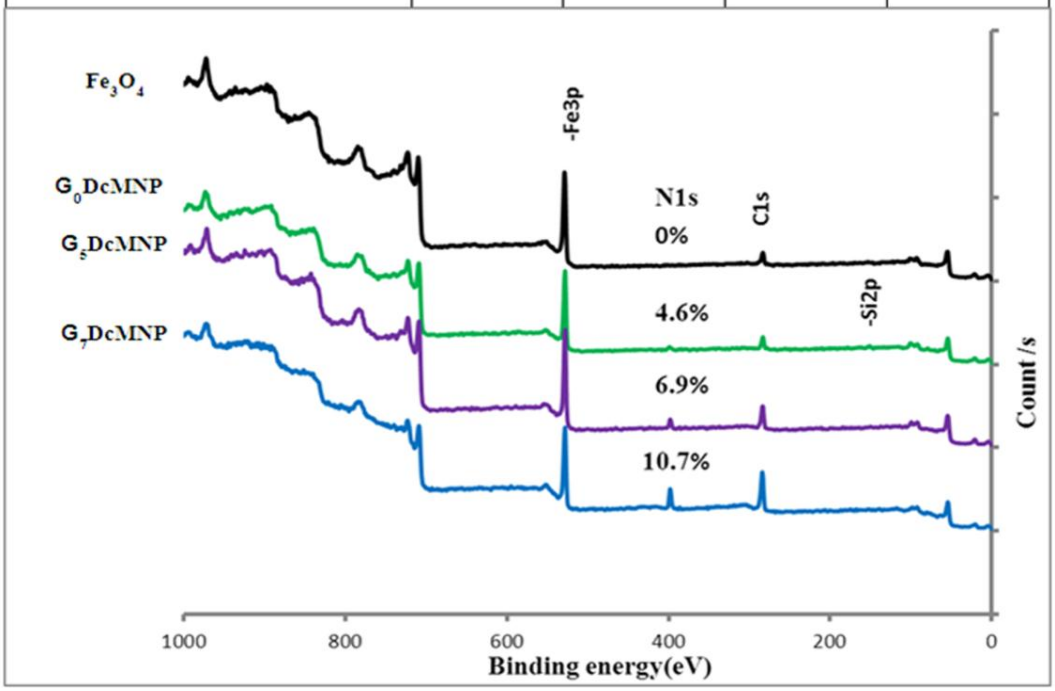

Figure 3.16 The X-ray photoelectron spectroscopy (XPS) analysis of bare MNP, G_0DcMNPs, G_5DcMNPs and G_7DcMNPs.

3.2.2 Poly (I:C) Activation in the Presence of EDC and 1-Methylimidazole

By the application of carbodiimides/1-methylimidazole the phosphoramidate linkages were formed between primary amines on the surface of DcMNP and 5'-phosphate of Poly (I:C) molecules. Poly (I:C) first activated by EDC (1-ethyl-3-[3-dimethylaminopropyl] carbodiimide hydrochloride). The immediate addition of 1-Methylimidazole causes the release of isourea by-product and formation of reactive phosphorylimidazolide bond between Poly (I:C) and imidazol molecules. In the presence of DcMNPs the reactive phosphorylimidazolide bond was hydrolyzed and replaced with phosphoramidate bond,

which was formed between the phosphate groups of Poly (I:C) and surface amine groups of DcMNPs. EDC and imidazole did not become part of the final crosslink between the molecules and they did not add any additional chemical structure to the resulting products, as a result the reaction by-products could be easily removed by magnetic separation (Figure 3.17).

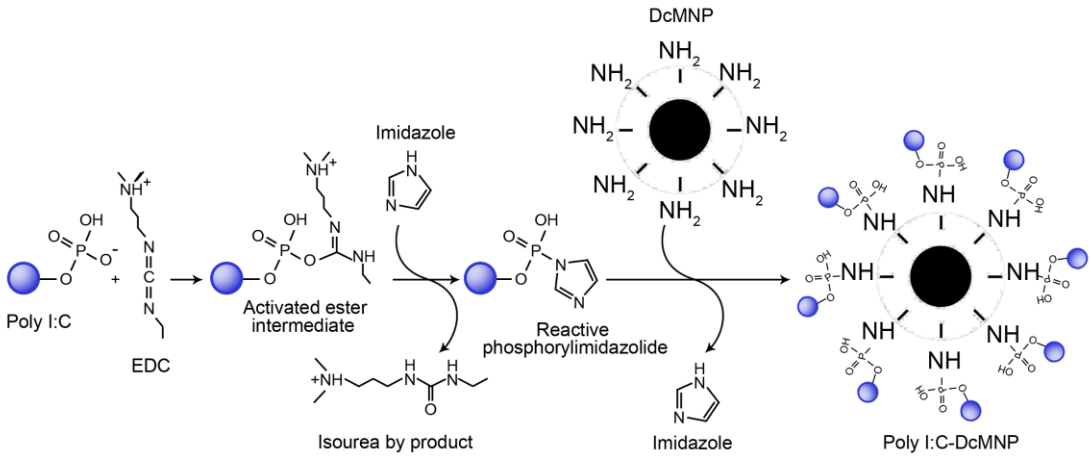

Figure 3.17 Activation of Poly (I:C) by EDC and formation of phosphoramidate bond between phosphate group of Poly (I:C) and surface amine groups of DcMNPs.

3.2.3 Poly (I:C) Loading Efficiency Studies

Poly (I:C) was bound to the surface of DcMNPs in 1-Methylimidazole (pH 7.5, pH 7 and pH 6) buffer. Transmission electron microscopy (TEM) and dynamic light scattering (DLS) analyses of G_7DcMNPs previously were shown in figures (3.5 and 3.6). DLS and TEM results of Poly (I:C)-bound G_7DcMNPs were shown in Figure 3.18. TEM analysis of G_7DcMNPs showed that the nanoparticle size was in the range of 20 ± 5 nm. However, DLS measurement showed the sizes of nanoparticles in the range of 45 ± 10 nm. The higher value of average size of DcMNP in DLS originates from the fact that DLS measures the hydrodynamic radii of the particles, which include the solvent layer at the interface (Tomalia el al. 1986). DLS results in figure 3.18 a demonstrated the size of Poly (I:C)-bound G_7DcMNPs as 75± 25. In figures 3.18 b and 3 .18 c, TEM results show that the sizes of Poly (I:C)-bound G_7DcMNPs were in the range of 50 ± 20 nm. In addition, the nanoparticles were more dispersed after Poly (I:C) binding.

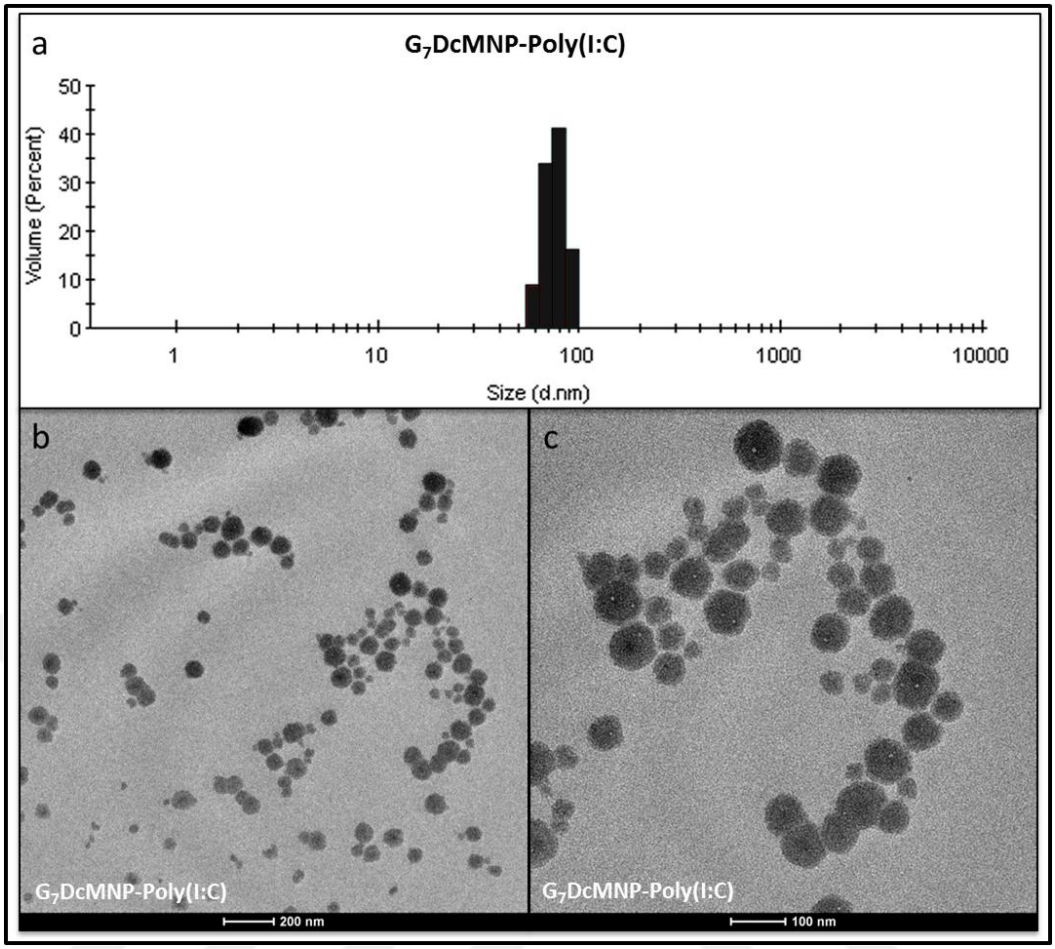

Figure 3.18 Dynamic Light Scattering graphs of Poly (I:C)-bounded G_7DcMNPs (a).TEM images of Poly (I:C)-bounded G_7DcMNPs in 200 nm (b), and 100 nm scale bars(c).

3.2.3.1 Poly (I:C) Loading Efficiency Studies on DcMNPs at pH 7 and pH 7.5

The loading efficiency was characterized by agarose gel electrophoresis. Figure 3.19 and Figure 3.20 show the loading optimization on G_7DcMNPs at pH 7.5 and pH 7. The results show that, to achieve 100% loading efficiency in 1-methylimidazole buffer at pH 7.5 and pH 7, the PIC: G_7DcMNPs ratios needed to be as 1:35 and 1:30 in the reaction respectively.

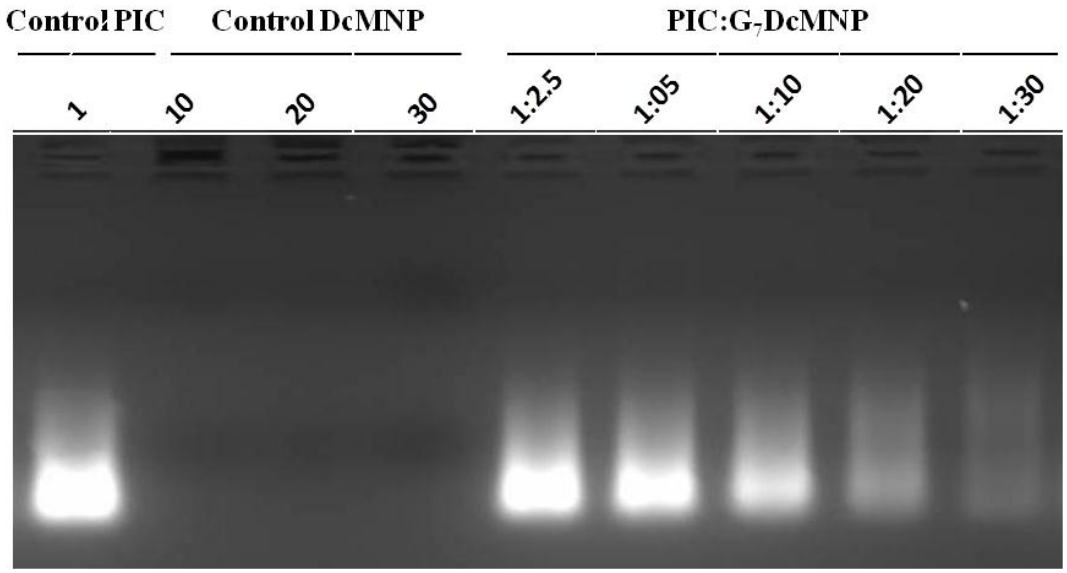

Figure 3.19 Agarose gel electrophoresis of loading optimization 4 µg Poly (I:C) on G7DcMNPs at pH 7.5. Well 1,2, 3, 4, 5 and 6 contain 1:10, 1:15, 1:20, 1:25, 1:30, 1:35 ratio of Poly (I:C) :G7DcMNPs. Well 7 contains control Poly (I:C) and wells 8,9,10,11, and 12 contain 1/2,1/4,1/8, 1/16, 1/32 dilution of control Poly (I:C) . 1 in the ratio represents 4 µg of Poly (I:C) or DcMNP.

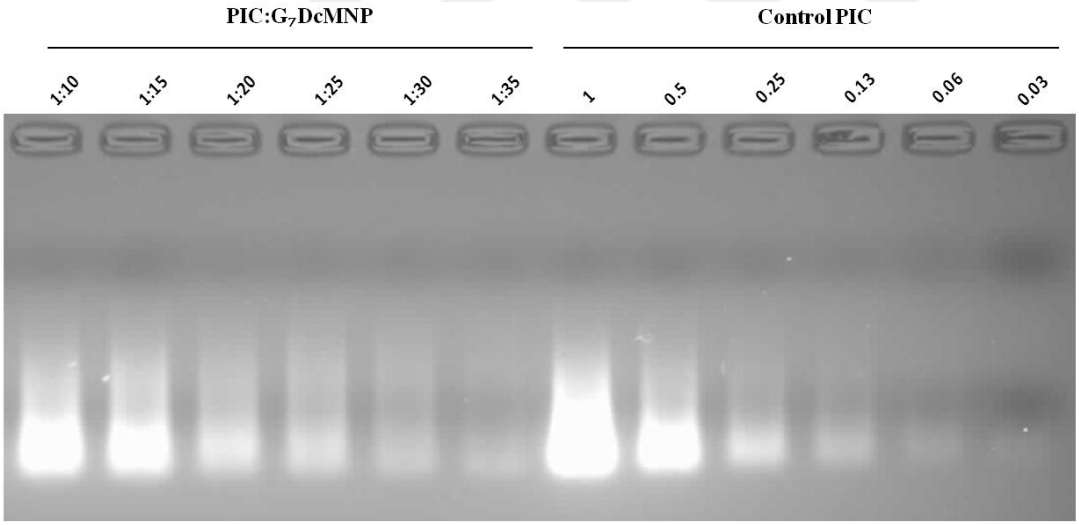

Figure 3.20 Agarose gel electrophoresis of loading optimization of 4 µg Poly (I:C) on G_7DcMNPs at pH 7. In first well 4 µg Poly (I:C) was loaded as control. Wells 2, 3 and 4 contain 40 µg , 80 µg, and 120 µg G_7DcMNPs, respectively. The wells 5-9 contain 1:2.5, 1:5, 1: 10, 1:20, and 1:30 ratio of Poly (I:C): G_7DcMNPs. 1 in the ratio represents 4 µg of Poly (I:C) or DcMNP.

The loading efficiencies on (G_2, G_3 and G_4) DcMNPs were also studied at pH 7. When the same ratio of DcMNPs were used for other generations (G2-G4) it was observed that the loading efficiency of Poly (I:C) on (G_2, G_3 and G_4) DcMNPs was very low (Figure 3.21).

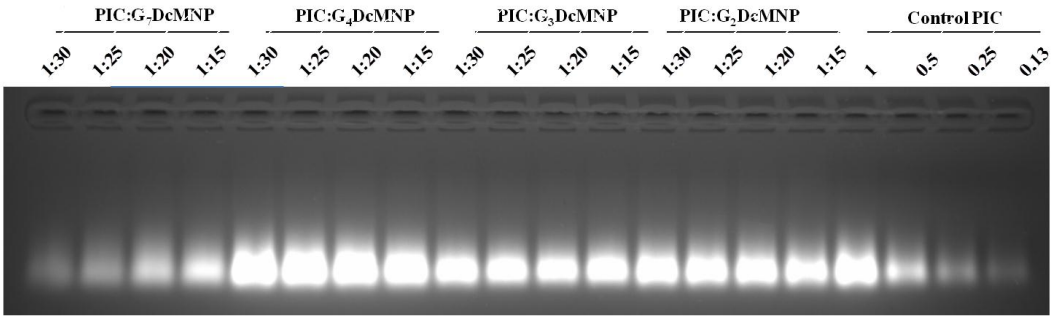

Figure 3.21 Agarose gel electrophoresis of loading optimization Poly (I:C) on G_7, G_4, G_3, and G_2DcMNPs at pH 7. Wells 1-16 show the Poly (I:C) loading on G_7, G_4, G_3, and G_2DcMNPs at four different ratio. Wells 17-20 show the control Poly (I:C) and different dilution. 1 in the ratio represents 4 µg of Poly (I:C) or DcMNP.

3.2.3.2 Poly (I:C) Loading Efficiency Studies on DcMNPs at pH 6

When Poly (I:C)-bounding was performed in 1-methylimidazole buffer at pH=6, 100% loading efficiency of Poly (I:C) was obtained when the PIC:DcMNPs ratios were 1:11, and 1:15 for G_7DcMNPs and G_6DcMNPs respectively (Figure 3.30). However for 100 % loading of Poly (I:C) on G_5DcMNPs it was needed to increase the PIC:DcMNPs ratios to 1:18 (Figure 3.22). When Poly (I:C) loading was performed in pH 6 the loading efficiency increased 3.5 fold compared to pH 7 and 8.

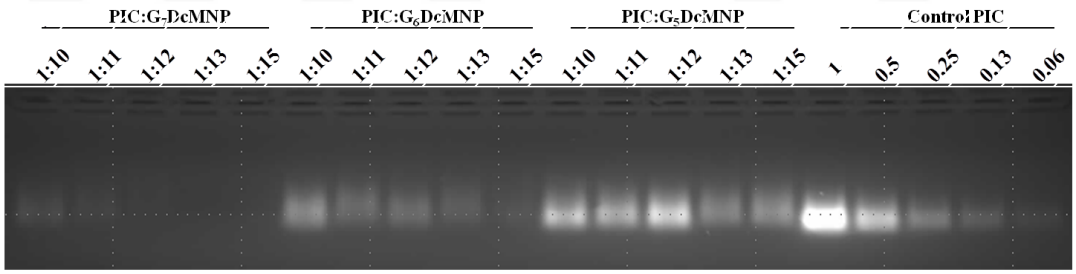

Figure 3.22 Agarose gel electrophoresis of loading optimization Poly (I:C) on G_7, G_6, and G_5DcMNPs at pH 6. The ratios of Poly (I:C) to G_7, G_6 and G_5DcMNP were changed from 1:10 to 1:15. Wells 16-20 show the Poly (I:C) control and different dilutions. 1 in the ratio represents 4 µg of Poly (I:C) or DcMNPs.

To obtain the loading efficiency of Poly (I:C) on other generations (G_2-G_6) of DcMNPs the amount of DcMNP was tried to be kept proportional to the generation numbers. In order to achieve 100% loading efficiency of Poly (I:C) for generation 7, 6, and 5, it was needed to keep the ratios of PIC:DcMNPs as 1:11, 1:15, and 1:18 for G_7, G_6 and G_5DcMNPs respectively. Loading efficiency of Poly (I:C) on G_4DcMNPs were about 80% when the PIC:DcMNPs ratios were applied as 1:22 at pH 6, while even at 1:38 ratio for the same

generation of DcMNPs the loading was almost zero when loading performed at pH 7 MeIm buffer. Due to the lower functional groups at the surface of G_3 and G_2DcMNPs the loading efficiency were very low in these generations at pH 6 (Figure 3.23).

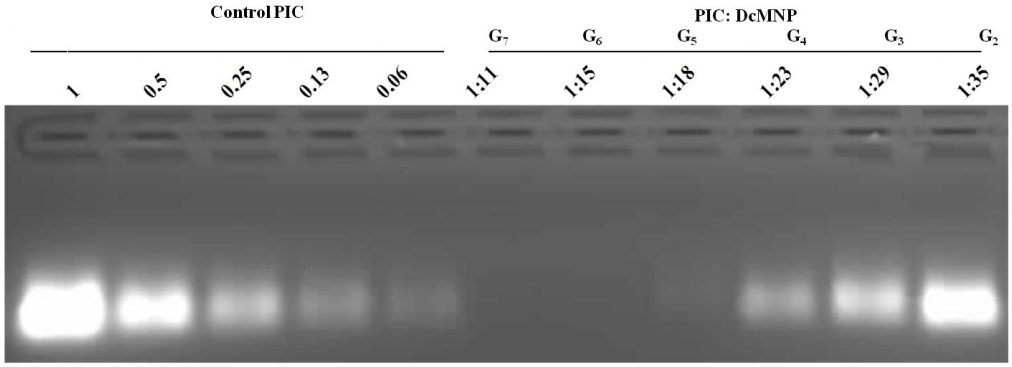

Figure 3.23 Agarose gel electrophoresis of loading optimization Poly (I:C) on G_7, G_6, G_5, G_4, G_3, and G_2DcMNPs at pH 6. Wells 1-5 demonstrate the control Poly (I:C) and different dilutions. Wells 6-11 show the PIC: DcMNPs ratios of G_7, G_6, G_5, G_4, G_3, and G_2DcMNPs. 1 in the ratio represents 4 µg of Poly (I:C) or DcMNP.

3.2.4 Poly (I:C) Loaded DcMNPs Stability Studies

The stability studies at different acidic pH (3, 4, 4.2, 4.4, 4.7, 6) conditions demonstrated that the bounding of Poly (I:C) to DcMNP surface functional groups were very stable at acidic pH. Poly (I:C) DcMNPs complex were very stable at lyophilized or aqueous forms in both injection water and 1-Methylimidazole buffer when stored at -20 ^{o}C up to 4 weeks. In addition, the complex was stable at high temperature (75 ^{o}C, 5 min) (data not shown).

The phosphoramide bound between Poly (I:C) and amine functional groups at the surface of DcMNPs were very sensitive to basic pH. The bond hydrolysis starts at pH 8.5 and the maximal hydrolysis was achieved at pH 9.4 for all generations. At pH 9.4 the half-life of the bound between Poly (I:C) and amine functional groups at the surface of DcMNPs was obtained as 15 min(data not shown). At pH 9±0.2 after 1 h, the release amount was around 25 % and the half-life was 1 h. At generation 2 due to the low Poly (I:C) loading efficiency, the release amount was also low with respect to the other generations (Figure 3.24).

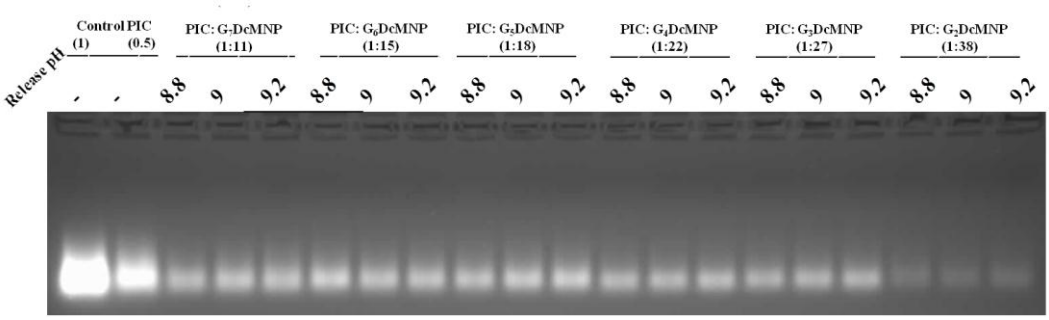

Figure 3.24 Agarose gel electrophoresis of release study of Poly (I:C) on G_7, G_6, G_5, G_4, G_3, and G_2DcMNPs at pH 8.8, 9.0, and 9.2 for each generation respectively. 1 in the ratio represents 4 µg of Poly (I:C) or DcMNPs.

3.2.5 Cytotoxicity Study of Poly (I:C)-Bound DcMNPs

Empty G_7DcMNPs did not show significant toxicity if up to 200 µg/ml. However, if used at higher concentration they would have toxic effect on cells (Figure 3.25, 3.26 and 3.27). It was found that The IC50 values of Poly (I:C)-bound DcMNPs on MCF7, MCF7 Dox, and SkBr-3 cells were found as 40 µg/ml, 28 µg/ml and 44 µg/ml (Figure 3.25, Figure 3.26, Figure 3.27). The cell proliferation assay demonstrated that Poly (I:C)-bound DcMNPs were most effective on MCF7- Dox. Therefore, Poly (I:C)-bound DcMNPs can be a replacement for Doxorubicin as a chemotherapeutic reagent.

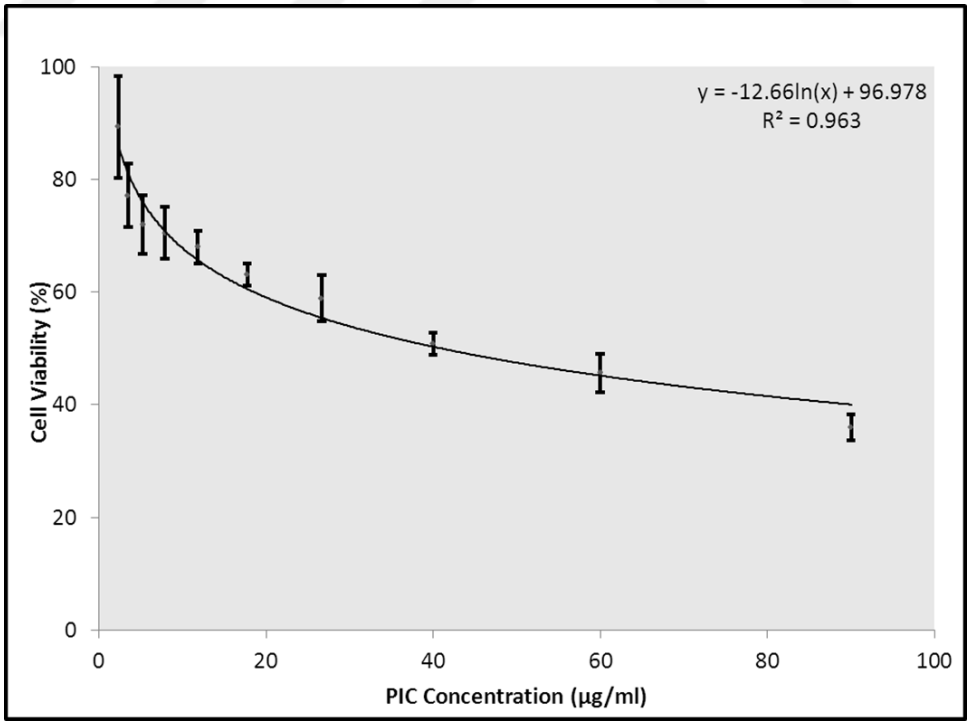

Figure 3.25 XTT cell proliferation assay of Poly (I:C)-bound DcMNPs on MCF7S cells. The IC50 values of Poly (I:C)-bound DcMNPs on MCF7 were calculated as 40 µg/ml.

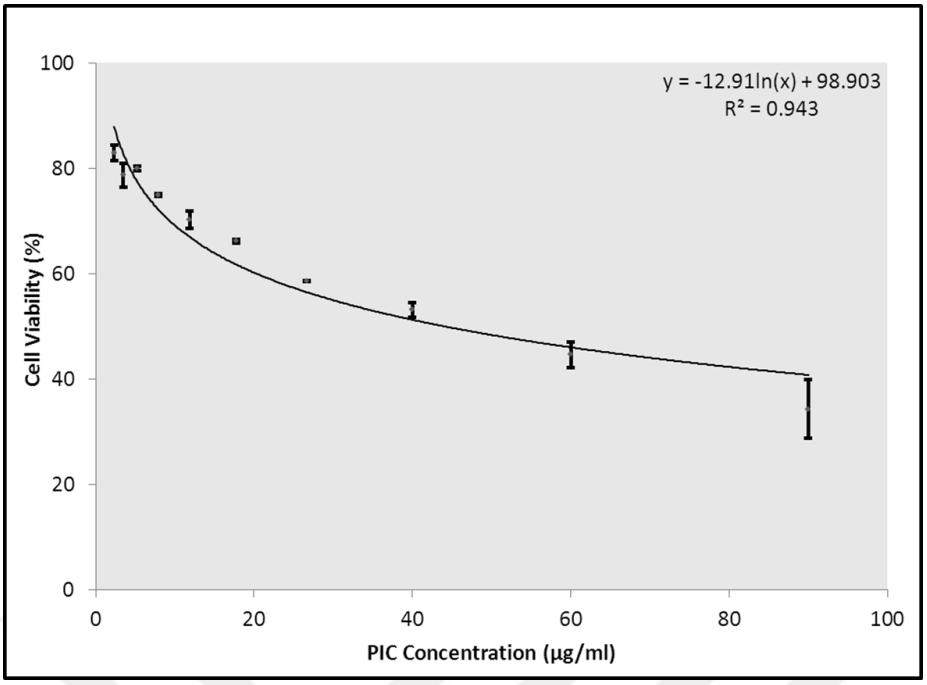

Figure 3.26 XTT cell proliferation assay of Poly (I:C)-bound DcMNPs on SkBr-3 cells. The IC50 values of Poly (I:C)-bound DcMNPs on SkBr-3 were calculated as 44 µg/ml.

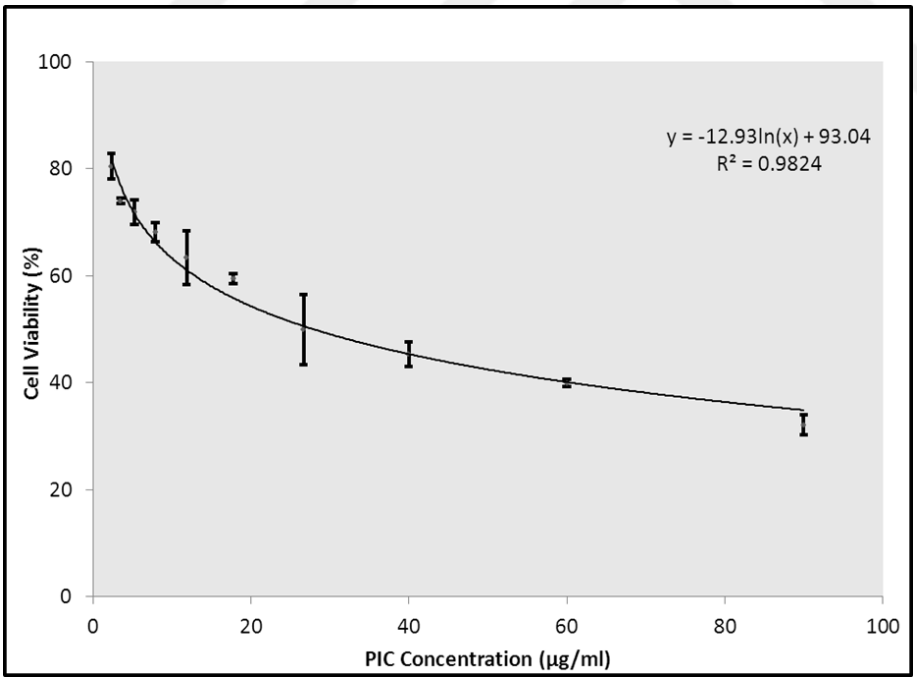

Figure 3.27 XTT cell proliferation assay of Poly (I:C)-bound DcMNPs on MCF7 Dox resistant cells. The IC50 values of Poly (I:C)-bound DcMNPs on MCF7 1µM Dox resistant cells were calculated as 28 µg/ml.

The cytotoxicity effect of free Poly (I:C) and Poly (I:C)-bound DcMNPs on MCF7 1µM Dox resistant cells were calculated as 450 µg/ml and 28 µg/ml (Figure 3.28). These results demonstrated that binding of Poly (I:C) on DcMNPs 16 fold increased its cytotoxicity effect.

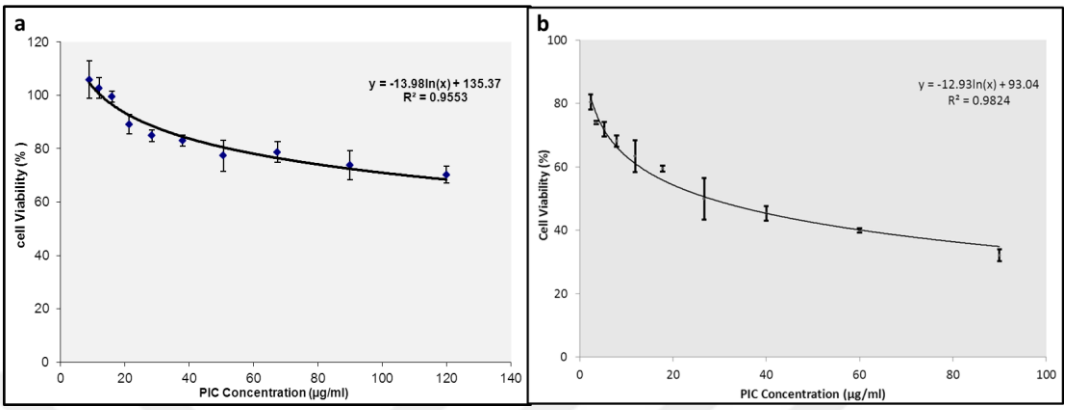

Figure 3.28 XTT cell proliferation assay of free Poly (I:C) and Poly (I:C)-bound DcMNPs on MCF7 Dox resistant cells. The IC50 values of free Poly (I:C) and Poly (I:C)-bound DcMNPs on MCF7 1µM Dox resistant cells were calculated as 450 µg/ml and 28 µg/ml.

3.3 Doxorubicin Loading on DcMNPs

Doxorubicin was loaded on DcMNPs at two temperatures (25 °C and 4 °C) and within different buffers, using Rotator for overnight. Figure 3.29 shows the schematic representation of Doxorubicin loading on DcMNPs.

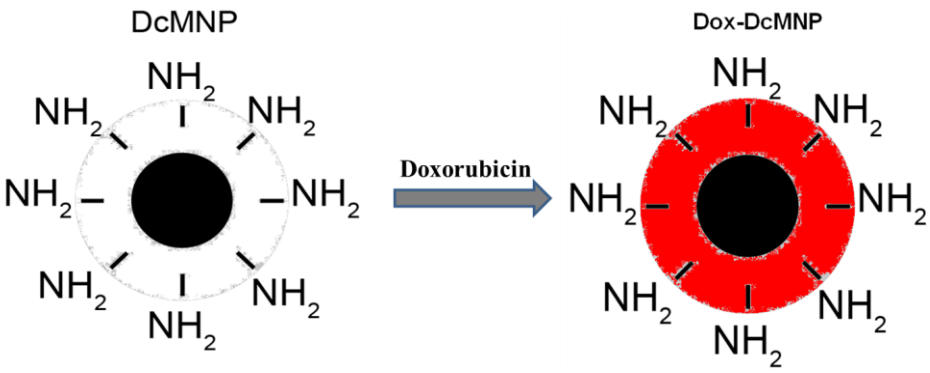

Figure 3.29 Schematic representation of Doxorubicin loading into the cavities of DcMNPs.

Throughout the thesis two formulas used for loading efficiencies calculation, however; to prevent complication results from equation 3.1 were discussed in detail (Desai *et al.*, 2005).

$$\text{Loading efficiency}(\%) = \frac{\text{Calculated drug concentration}}{\text{Theoretical drug concentration}} \times 100 \qquad \text{Equation 3.1}$$

3.3.1 Doxorubicin Loading on DcMNPs Using Different Buffers

Doxorubicin was loaded to DcMNPs in PBS (pH 7.2), TES (pH 7.3), and acetate (pH 5. 0) buffers. Doxorubicin loading efficiency of G_4DcMNPs was measured by spectrophotometric analysis and calculated from Equation 3.1.

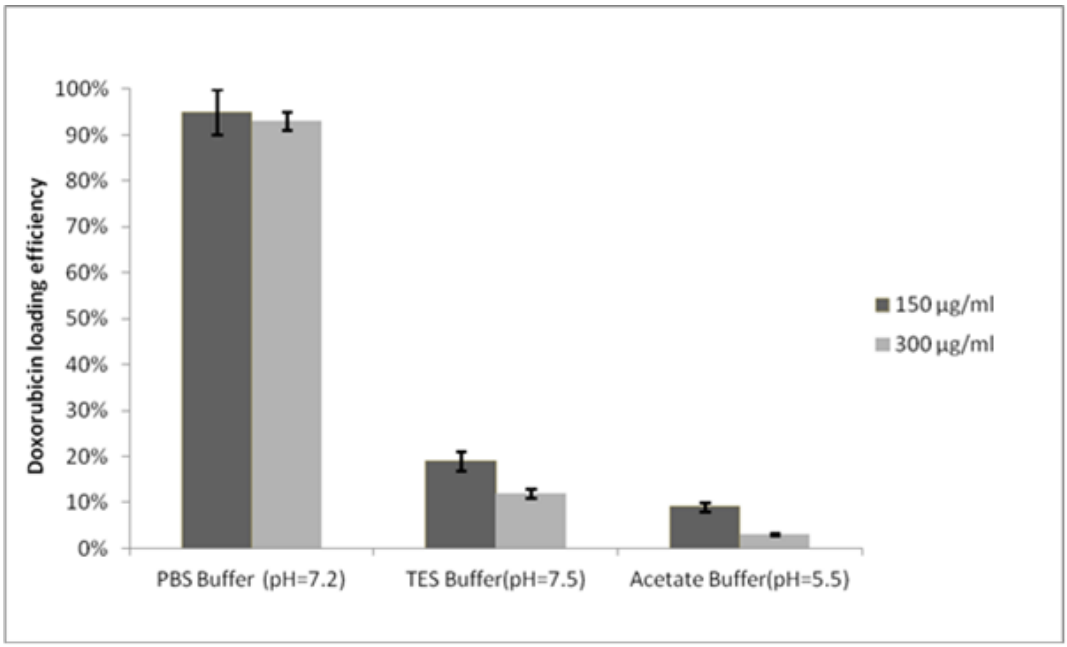

Figure 3.30 Loading efficiencies of Doxorubicin to G_4DcMNPs in different buffers (PBS, TES, and acetate buffer) and in different drug concentrations.

In the literature, most of the drug-loading studies were carried out using fourth generation of PAMAM dendrimer. In this study, Doxorubicin-loading studies were initially performed by using G_4PAMAM dendrimer with targetable magnetic core. Loading efficiencies were tested in PBS (pH 7.2), TES (pH 7.3), and acetate (pH 5.0) buffers with two different drug concentrations (150 and 300 µg/mL). The loading efficiencies of 150 µg/ml Doxorubicin were 94% 19%, and 9% in PBS, TES, and acetate buffers, respectively. These results were 96%, 12%, and 3% for 300 µg/ml Doxorubicin. The most efficient drug loading was obtained in PBS buffer (Figure 3.30).

To confirm the loading of Doxorubicin on DcMNPs, FTIR analysis of Doxorubicin, G_4DcMNPs, and 400 µg/ml Doxorubicin-loaded G_4DcMNPs were done (Figure 3.31).

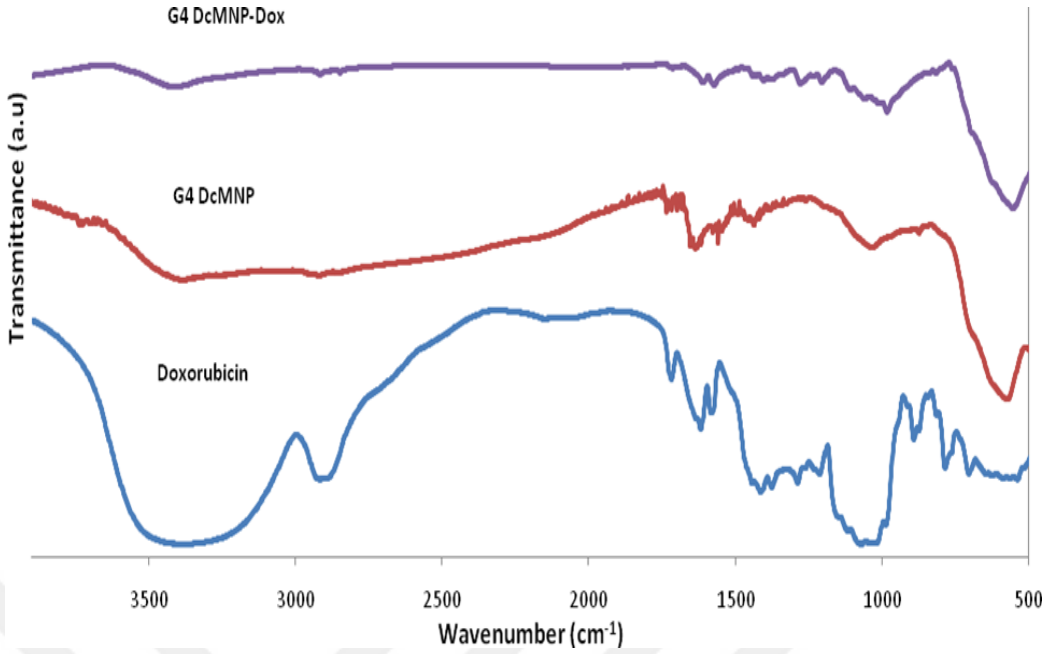

Figure 3.31 FTIR analysis of Doxorubicin, G_4DcMNPs, and 400 µg/ml Doxorubicin-loaded G_4DcMNPs.

3.3.2 Doxorubicin Loading Efficiencies into DcMNPs at Different Concentrations

To find maximum drug loading capacity on G_4DcMNPs, Doxorubicin concentration gradually increased up to 600 µg/ml, where the loading efficiency started to decrease. The loading efficiencies were calculated from the Equation 3.1. The highest and most efficient drug loading concentrations were obtained as 500 and 400 µg/ml (Figure 3.32).

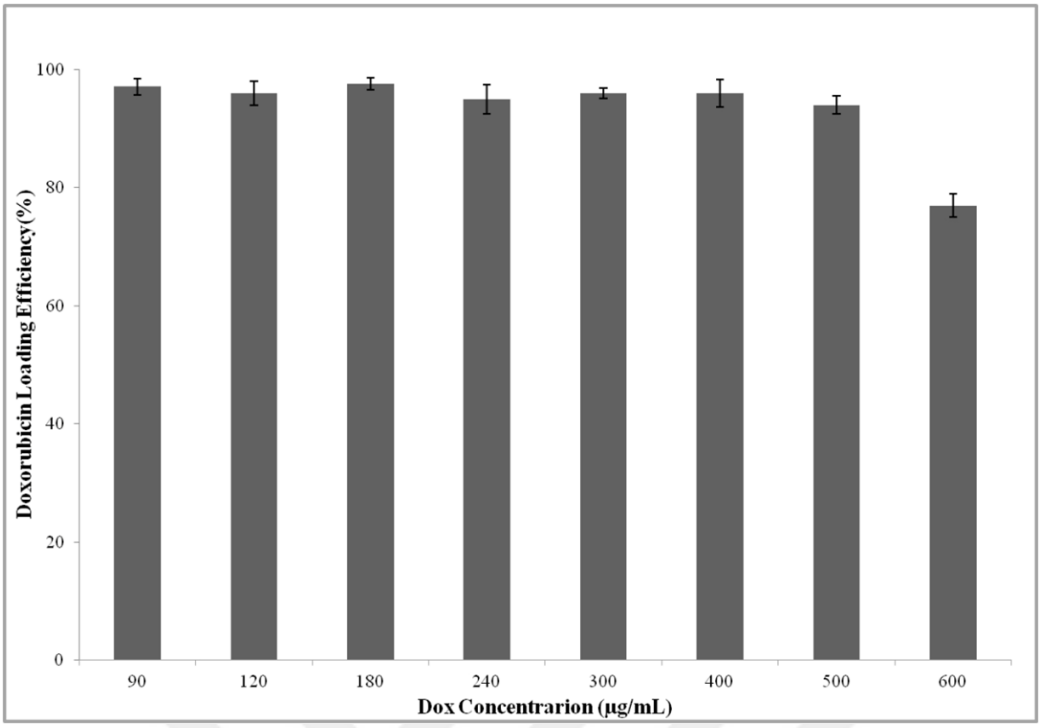

Figure 3.32 Doxorubicin loading efficiencies at different concentrations (90–600 µg/ml) on G_4DcMNPs (5 mg/ml).

3.3.3 Doxorubicin Loading, Encapsulation Efficiency, Doxorubicin Content and Process Yield on G_4DcMNPs

There are different equations for the calculation of drug loading in the literature. In addition, it is also possible to calculate drug content, drug entrapment, and process yield percentages from following equations (Tripathi *et al.*, 2010).

$$\text{Drug content (\% w/w)} = \frac{(\text{Mass of the total drug} - \text{Mass of free drug}) \times 100}{\text{Mass of nanoparticles}} \qquad \text{Equation 3.2}$$

$$\text{Drug entrapment (\%, w/w)} = \frac{(\text{Mass of the total drug} - \text{Mass of free drug}) \times 100}{\text{Mass of total drug}} \qquad \text{Equation 3.3}$$

$$\text{Drug loading (\%, w/ w)} = \frac{(\text{Mass of the total drug} - \text{Mass of free drug}) \times 100}{\text{Mass of total polymer}} \qquad \text{Equation 3.4}$$

$$\text{Process Yield (\%)} = \frac{(\text{Mass of nanoparticles}) \times 100}{\text{Total mass of drug + polymer}} \qquad \text{Equation 3.5}$$

From the equations 3.2, 3.3, 3.4 and 3.5 the Doxorubicin loading, encapsulation efficiency, Doxorubicin content and process yield on G_4DcMNPs were calculated (Table 3.2). The optimum drug entrapment was obtained when the applied Doxorubicin concentration was about 500 µg/ml. In addition, 400 µg/ml and 500 µg/ml Doxorubicin concentrations with 80% and 107% loading efficiencies were two most suitable concentrations to be used in drug loading processes.

Table 3.2 Doxorubicin loading, encapsulation efficiency, Doxorubicin content and process yield on G_4DcMNPs calculated from equations; 3.2, 3.3, 3.4 and 3.5.

	90 µg/ml	120 µg/ml	180 µg/ml	240 µg/ml	300 µg/ml	400 µg/ml	500 µg/ml	600 µg/ml
Drug Content (w/w)%	1.85%	2.5%	3.84%	5.3%	6.9%	9.6%	12.8%	13.4%
Drug Entrapment (w/w)%	98%	97%	97%	97%	97%	96%	96%	78%
Drug Loading (w/w)%	15.4%	21%	32%	44.1%	57%	80%	107%	110%
Process Yield %	722%	721%	631%	578%	530%	463%	403%	394%

3.3.4 Doxorubicin Loading Efficiencies on Different Generation of DcMNPs

Maximum amounts of Doxorubicin (400 and 500 µg/ mL) were loaded on other generations of NPs obtained (G_2–G_7) at room temperature. Although the loading efficiencies were around 96% in lower generations (G_2, G_3 and G_4) of DcMNPs, it was about 30% for higher generations (G_5, G_6 and G_7) of DcMNPs (Figure 3.33 a). Results demonstrated that the optimum generation for Doxorubicin loading is G_4DcMNPs. To see the temperature effect on loading efficiencies, the loading procedure was also performed at 4 °C (cold room). Loading efficiencies were generally lower at 4 °C. However, the loading percentages were higher at 400 µg/ml Doxorubicin. Loading efficiencies of 400 µg/ml Doxorubicin were found as 76%, 83%, 89%, for G_2, G_3, G_4, and around 27% for higher generations (G_5, G_6 and G_7) of DcMNPs, respectively (Figure 3.33 b). Higher generations (G_5, G_6 and G_7) of DcMNPs were not included in the rest of the study because of the low drug-loading efficiency and lower stability of the drug.

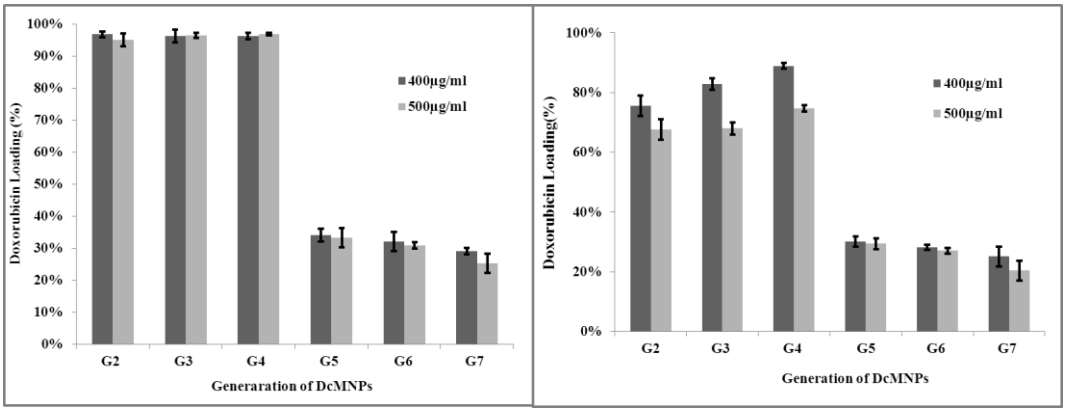

Figure 3.33 Loading efficiencies of Doxorubicin (400 and 500 µg/ml) onto DcMNPs at room temperature (a) and at 4 °C (b).

3.3.5 Doxorubicin Loading, Encapsulation Efficiency, Doxorubicin Content and Process Yield on Different Generation of DcMNPs

Drug content, drug entrapment, drug loading and process yield of 400 µg/ml and 500 µg/ml Doxorubicin on G_2, G_3, G_4, G_5, G_6 DcMNPs at room temperature and 4 °C were also calculated from the equations; 3.2, 3.3, 3.4 and 3.5. Tables 3.3 and 3.4 shows Doxorubicin loading, encapsulation efficiency, Doxorubicin content and process yield of 400 µg/ml and 500 µg/ml Doxorubicin at room temperature. Tables 3.5 and 3.6 demonstrate the Doxorubicin loading, encapsulation efficiency, Doxorubicin content and process yield at 4 °C.

Table 3.3 Drug loading, encapsulation efficiency, drug content and process yield of 400 µg/ml Doxorubicin concentrations on different generation of DcMNPs at room temperature.

	G_2	G_3	G_4	G_5	G_6	G_7
Drug Content (w/w)%	9.6%	9.6%	3.84%	3.4%	3.2%	2.9%
Drug Entrapment (w/w)%	96%	96%	96%	34%	32%	29%
Drug Loading (w/w)%	160%	107%	80%	23%	18%	14%
Process Yield %	641%	538%	463%	543%	472%	418%

Table 3.4 Drug loading, encapsulation efficiency, drug content and process yield of 500 µg/ml Doxorubicin concentrations on different generation of DcMNPs at room temperature.

	G_2	G_3	G_4	G_5	G_6	G_7
Drug Content (w/w)%	12.8%	12.8%	12.8%	3.4%	3.2%	2.9%
Drug Entrapment (w/w)%	96%	96%	96%	33%	31%	25%
Drug Loading (w/w)%	213%	142%	107%	29%	23%	16%
Process Yield %	556%	458%	403%	515%	452%	410%

Results of table 3.3 and 3.4 demonstrated that lower (G_2, G_3 and G_4) DcMNPs are suitable for Doxorubicin loading at room temperature. The drug entrapment efficiency in (G_2, G_3 and G_4) DcMNPs were the same as 96%. From equation 3.4 the highest Doxorubicin loading efficiency was obtained in G_2DcMNPs and the lowest was achieved in G_7DcMNPs.

Table 3.5 Drug loading, encapsulation efficiency, drug content and process yield of 400 µg/ml Doxorubicin concentrations on different generation of DcMNPs at 4 °C.

	G_2	**G_3**	**G_4**	**G_5**	**G_6**	**G_7**
Drug Content (w/w)%	7.6%	8.3%	8.9%	3%	3%	2.5%
Drug Entrapment (w/w)%	76%	83%	89%	30%	28%	25%
Drug Loading (w/w)%	127%	92%	75%	20%	16%	12%
Process Yield %	735%	578%	478%	556%	480%	425%

Table 3.6 Drug loading, encapsulation efficiency, drug content and process yield of 500 µg/ml Doxorubicin concentrations on different generation of DcMNPs at 4 °C.

	G_2	G_3	G_4	G_5	G_6	G_7
Drug Content (w/w)%	9%	9%	10%	4%	3.6%	2.7%
Drug Entrapment (w/w)%	67%	68%	75%	29%	27%	20%
Drug Loading (w/w)%	150%	100%	83%	26%	20%	13%
Process Yield %	664%	553%	455%	530%	463%	422%

Results of table 3.5 and 3.6 also shown that lower (G_2, G_3 and G_4) DcMNPs will be suitable for Doxorubicin loading at cold temperature. The maximum entrapment occurred in G_4DcMNPs. From the equation 3.4, the highest Doxorubicin loading efficiency was obtained in G_2DcMNPs and the lowest loading efficiency was achieved in G_7DcMNPs.

3.3.6 Stability Study of Doxorubicin-Loaded DcMNPs

The stability of Doxorubicin-loaded (G_2, G_3, G_4) DcMNPs was studied up to 8 weeks in PBS buffer (pH 7.2) at 37◦ C and also in human serum up to 4 days to mimic the physiological conditions. The results show that in all generations examined only about 5% of the drug was released in PBS buffer in about 2 months (Figure 3. 34).

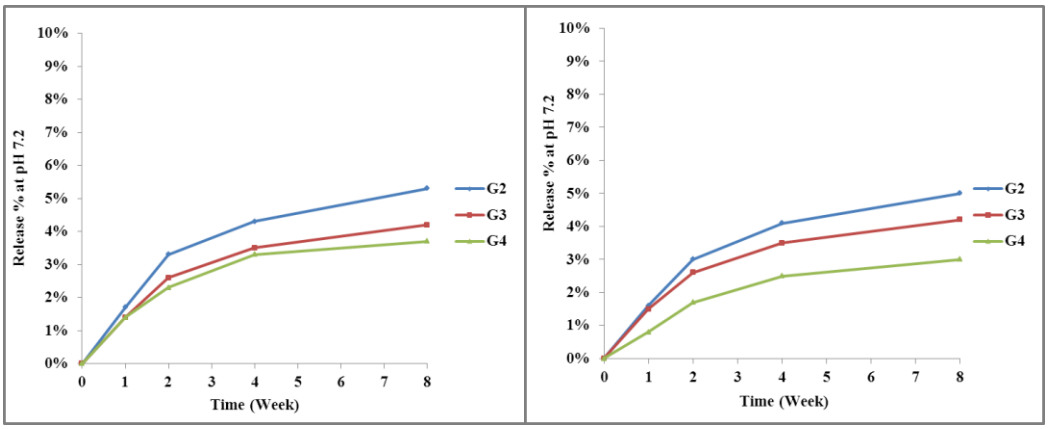

Figure 3.34 The stability of 400 µg/ml Doxorubicin-loaded G_4DcMNPs (a) and 500 µg/ml Doxorubicin-loaded G_4DcMNPs (b) in PBS buffer (pH 7.2).

In human serum, the results were similar with those in PBS buffer for 400 µg/ mL Doxorubicin-loaded NPs, indicating a significant stability under physiological conditions. However, for 500 µg/ml Doxorubicin-loaded NPs, about 30% of the drug was released within first 15 h (Figure 3. 35). Then, the drug release was almost stopped as in the case of PBS buffer.

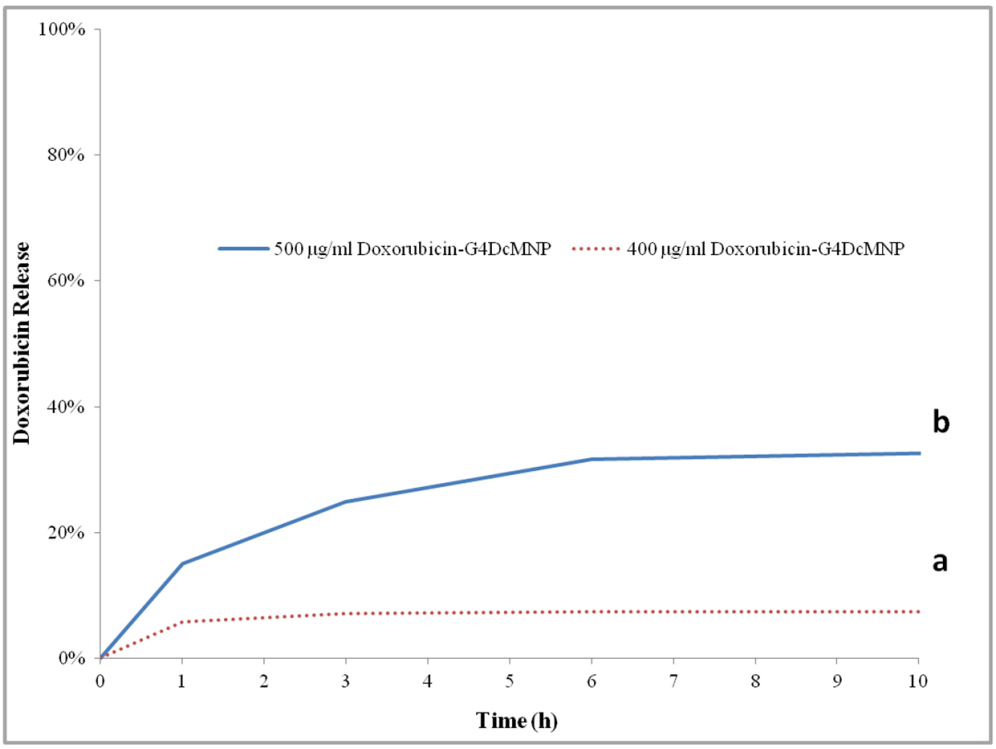

Figure 3.35 The stability of 400 µg/ml Doxorubicin-loaded G_4DcMNPs (a) and 500 µg/ml Doxorubicin-loaded G_4DcMNPs (b) in human blood serum.

3.3.6 Release study of Doxorubicin-Loaded DcMNPs

Doxorubicin (400 and 500 µg/ml) release studies were also performed in acetate buffer having pH 5.2 and 4.2 that mimics endosomal conditions. The release profiles of (G_2, G_3, and G_4) DcMNPs at pH 5.2 and pH 4.2 are given in Figures 3.35 and 3.36. The release studies were continued up to 90 h. Most of the drug was re-leased within first 15 h. Release of 400 µg/ml drug at first 15 h was approximately 70% (Figure 3. 36), and release of 500 µg/ml drug was nearly 80% (Figure 3. 37). In general, Doxorubicin release was higher at pH 4.2 compared with pH 5.2. There was no significant difference in Doxorubicin release between different generations of DcMNPs at pH 4.2 (Figs. 3. 36 b and 3. 37 b). However, in pH 5.2, the release profiles were changed by generation level of the NPs and the concentrations of the loaded drug. When we used highest concentration of Doxorubicin (500 µg/ml), the drug-released amount was approximately twofold more compared with the lower concentration (400 µg/ml) at pH 5.2 (Figure 3. 36 a and Figure 3.37 a).

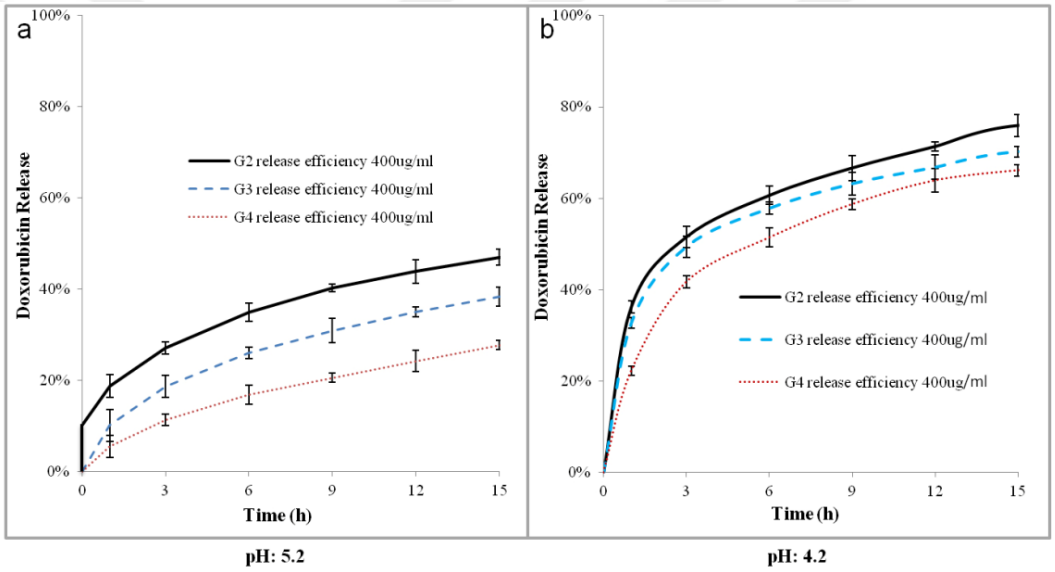

Figure 3.36 Release of 400 µg/ml Doxorubicin from (G_2, G_3 and G_4) DcMNPs at pH 5.2 (a) and pH 4.2 (b).

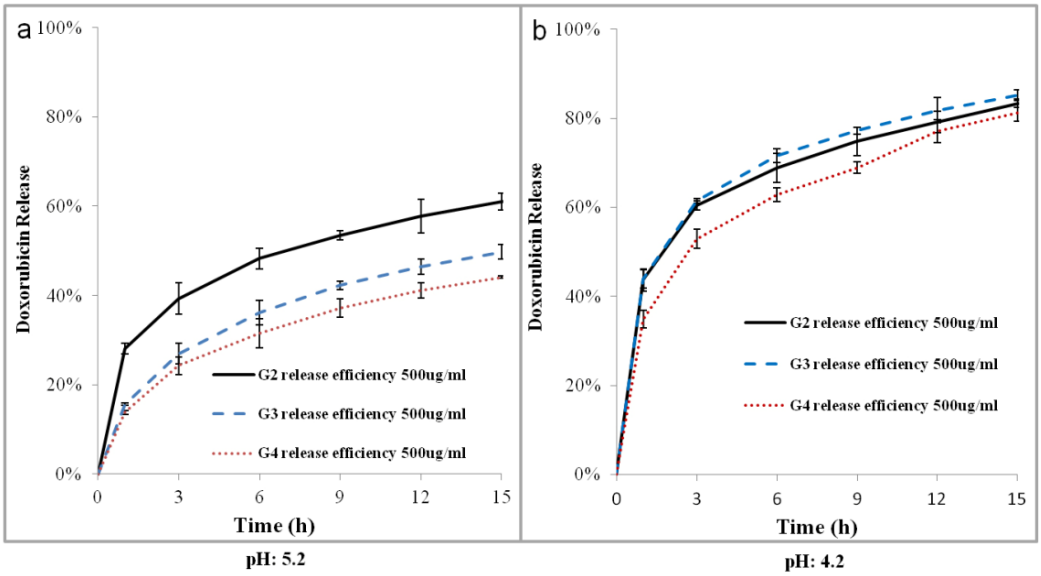

Figure 3. 37 Release of 500 µg/ml Doxorubicin from (G_2, G_3 and G_4) DcMNPs at pH 5.2 (a) and pH 4.2 (b).

3.3.7 Cellular Internalization of Doxorubicin-Loaded Dendrimer Coated Magnetic Nanoparticles

It was demonstrated by fluorescent microscopy that while fewer of the free Doxorubicin was taken up by the cells, after 4 hours most of the Doxorubicin loaded-DcMNPs were taken up by MCF7/ 1µM Dox cells. Doxorubicin-G_4DcMNPs containing MCF7/ 1µM Dox cells are shown in figure 3.38 a, and figure 3.38 b.

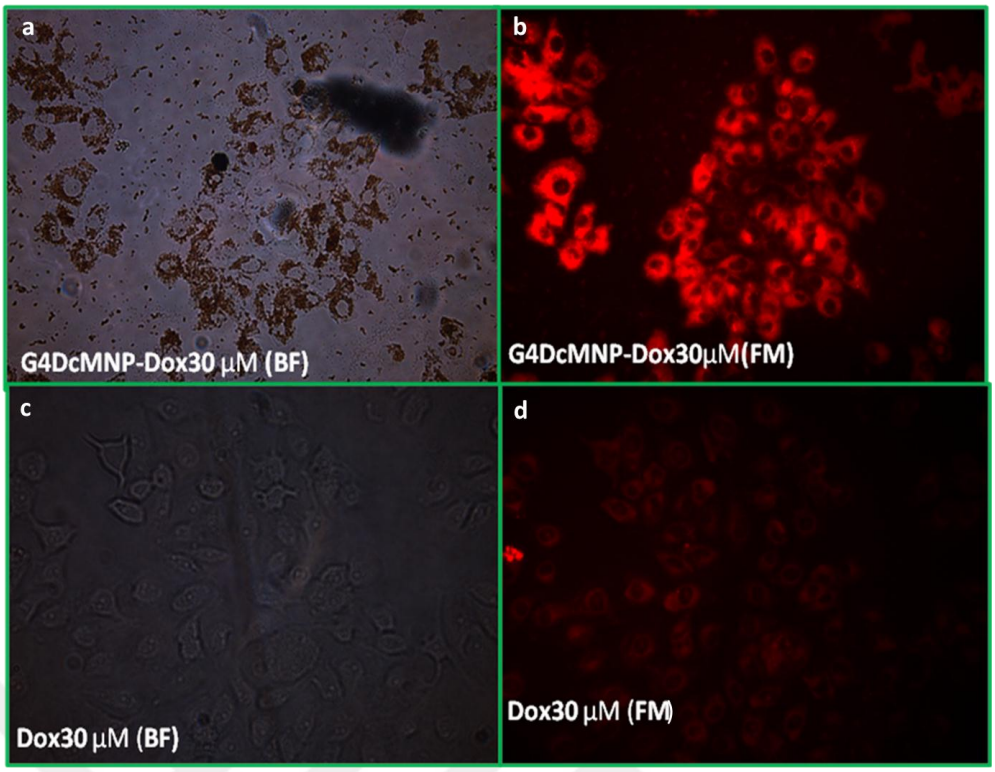

Figure 3.38 Bright field microscopy image of Doxorubicin Resistant MCF7 cells Treated with 30 µM (18 µg/ml) Doxorubicin which was loaded on G_4DcMNPs (a) fluorescent microscopy image of MCF7/ 1µM Doxorubicin Resistant cells Treated with 30 µM (18 µg/ml) Doxorubicin-loaded G_4DcMNPs (b). Bright field microscopy image of MCF7/ 1µM Doxorubicin Resistant cells Treated with 30 µM free Dox (c) and fluorescent microscopy image of MCF7/ 1µM Doxorubicin Resistant cells Treated with 30 µM free Doxorubicin (d)

3.3.8 Cytotoxicity Study of Doxorubicin-Loaded DcMNPs

To quantify the cytotoxic effects of empty G_4DcMNPs and Doxorubicin-loaded G_4DcMNPs on drug-resistant MCF7 cells, XTT cell viability assays were performed and inhibitory concentration 50 (IC50) values, which show the toxic dose of the Doxorubicin-loaded NPs, were calculated. The IC50 value for µM Doxorubicin resistant MCF7 cells by applying free Doxorubicin was calculated as 100 µg/ml (Figure 3.39). The similar result also previously reported by Kars `s research group as 107 µg/ml.

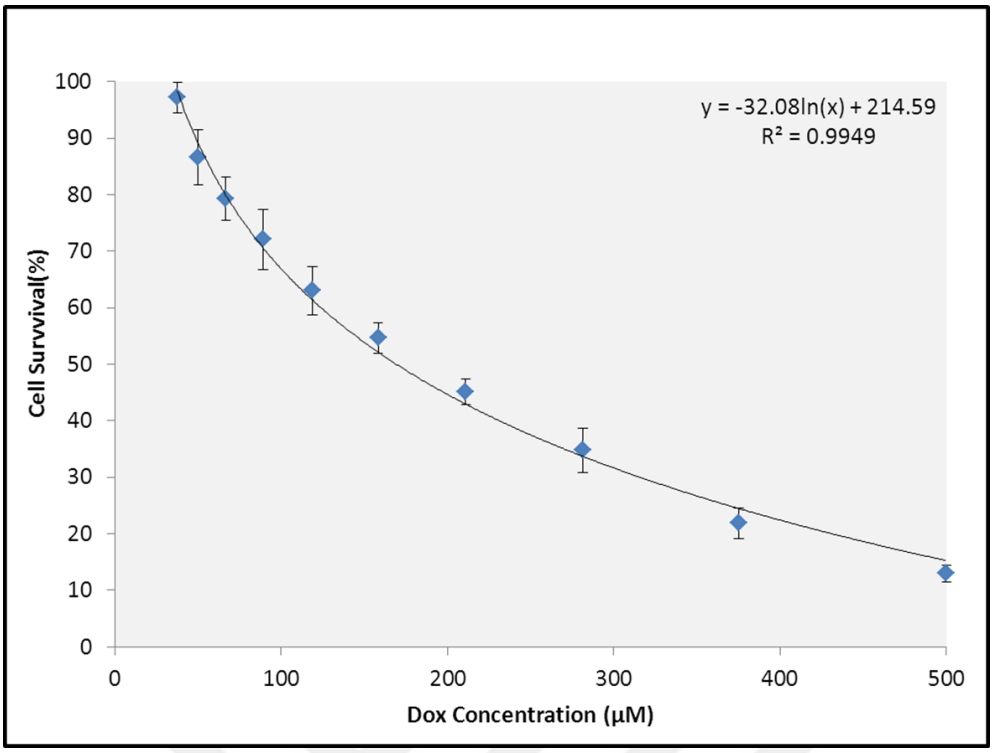

Figure 3.39 Doxorubicin cytotoxicity effect on Dox-resistant MCF7 cells.

Empty G_4DcMNPs were not found significantly cytotoxic up to 250 µg/ml (Figure 3.13). It was found that the released Doxorubicin from the NPs has the capacity to kill the MCF7 cells efficiently (Figure 3.40). This indicates that loading of the drug onto NPs did not change its effectiveness. In this work, the IC50 value of Doxorubicin-loaded G_4DcMNPs was calculated as 21 µg/ml. From the IC50 comparison values, it was seen that the loading of Doxorubicin onto G_4DcMNPs increased its efficacy of drug up to five folds. This indicates that the Doxorubicin resistant MCF7 cells became five-fold sensitized, when the drug was loaded into DcMNPs.

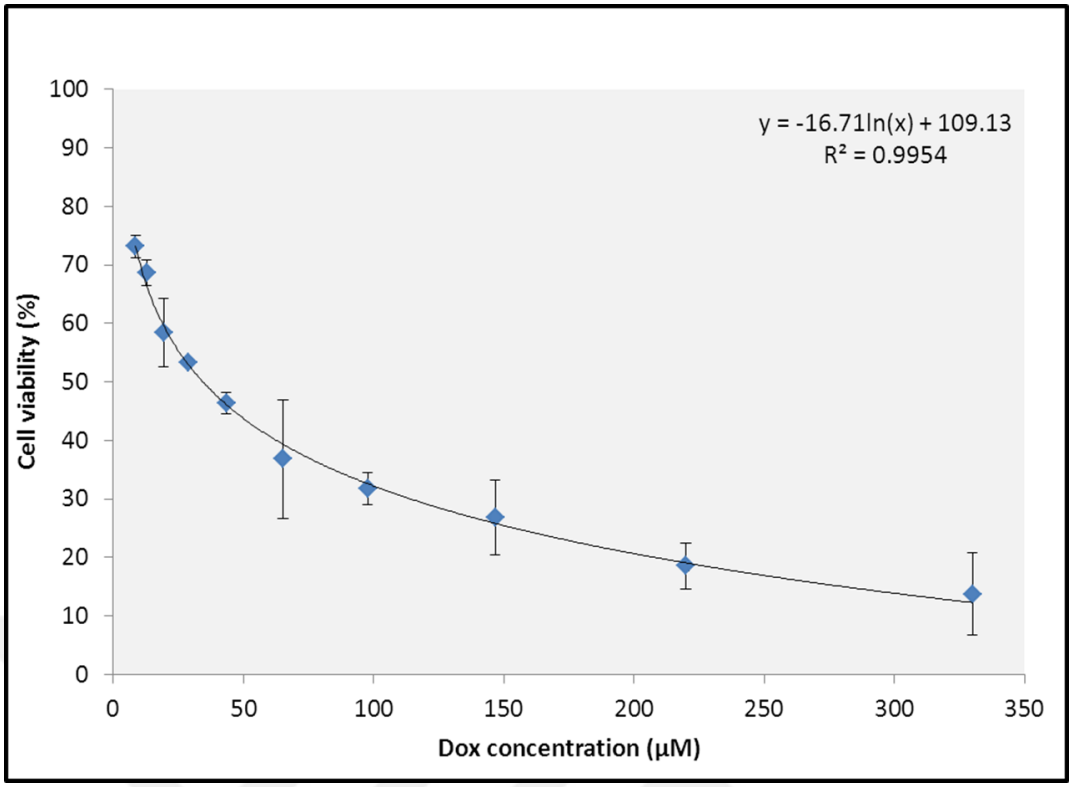

Figure 3.40 Cytotoxic effects of Doxorubicin-loaded G_4DcMNPs on MCF7/ 1µM Doxorubicin resistant cells.

3.4 Poly (I:C) Binding on Doxorubicin-Loaded DcMNPs

It was observed in section of Poly (I:C) loading on different generation that Poly (I:C) loading on lower generations is not efficient. The most efficient loading was related to G_7DcMNPs and the least was related to G_2DcMNPs. The loading on G_7DcMNPs was 3.5 folds more than G_4DcMNPs. Our results were parallel with the results of Tomalia *et al.*, Who demonstrated that higher generation of PAMAM dendrimers usually have rigid surface with higher number of functional groups at the surface to which different chemotherapeutic reagents can bind. On the other hand, the surface functional groups at the surface of G_4DcMNPs were flexible, through which the drug can enter into the cavities inside. From the result of Doxorubicin loading, it was observed that drugs like Doxorubicin could not be loaded on G_7DcMNPs. However, the most effective loading and release of Doxorubicin was on lower generations and especially G_4DcMNPs. This was because of the fact that unlike the lower generations of DcMNPs the distance between the branches at the surface of higher generation especially G_7DcMNPs are so low that the drug cannot enter into the empty cavities inside. In order to obtain most effective delivery systems, here we tried to bind and characterize Poly (I:C) on Doxorubicin-loaded- G_4DcMNPs (Figure 3.41).

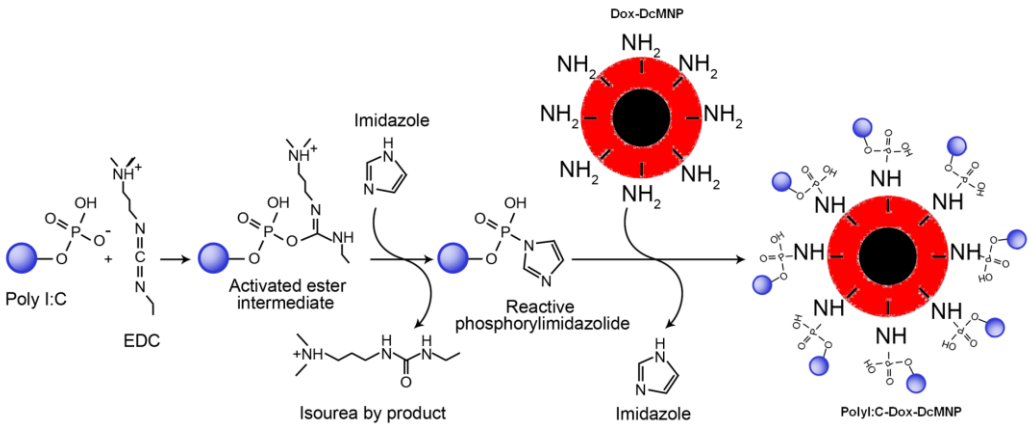

Figure 3.41 Schematic representation of Poly (I:C) modification of Doxorubicin-loaded DcMNPs.

3.4.1 Poly (I:C) Binding on G_4DcMNPs

Poly (I:C) were bound onto the surface of G4DcMNPs at pH 6 and pH 6.5. Polyacrylamide gel electrophoresis (PAGE) applied to analyze the binding efficiency of the Poly (I:C) functionalized dendrimer coated magnetic nanoparticles. The results demonstrated that for fully binding of Poly (I:C) onto the surface of G_4DcMNPs, the ratio of Poly (I:C):G_4DcMNPs should be 1:30 and 1:45 for pH 6 and pH 6.5, respectively. (Figure 3.42)

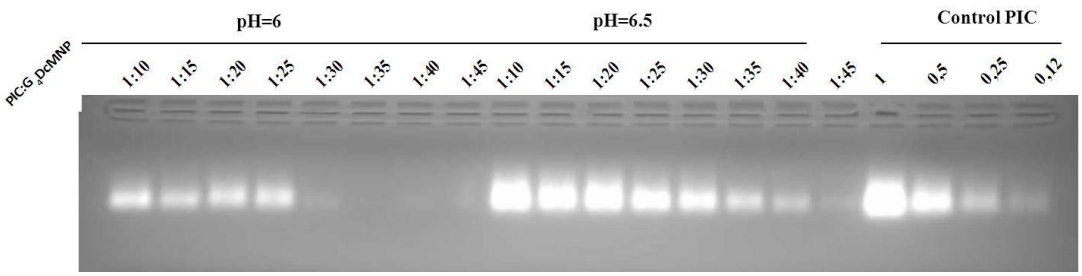

Figure 3.42 Agarose gel electrophoresis of loading optimization of poly on G_4DcMNPs at pH 6 and pH 6.5. Wells 1-8 demonstrate the loading of Poly (I:C) at pH 6. Wells 9-16 demonstrate the loading of Poly (I:C) at pH 6.5. Wells 17-20 demonstrate the control Poly (I:C) and different dilutions. 1 in the ratio represents 4 µg of Poly (I:C) or DcMNP.

3.4.2 The Amount of Loaded Doxorubicin on G_4DcMNPs Affects the Efficiency of Poly (I:C) Binding

The position of functional groups at the surface of DcMNPs is very important for binding of anticancer reagents here Poly (I:C). By increasing the amount of loaded Doxorubicin in the cavities of G_4DcMNPs the position of surface functional group will change Which may itself influence the binding efficiency of Poly (I:C).

In order to observe the effect of drug loading on Poly (I:C) binding, Doxorubicin were loaded on G_4DcMNPs at 400 µg/ml and 500 µg/ml concentrations. The Doxorubicin-loaded G_4DcMNPs were washed with 0.1 M MeIm (pH 6) to remove the PBS buffer and make the Doxorubicin-loaded G_4DcMNPs ready for Poly (I:C) binding. The percentage of released Doxorubicin was calculated through washing steps. Then Poly (I:C) binding procedure was performed on Doxorubicin-loaded G_4DcMNPs. as in section 2.3.3. It was observed that the total amount of released Doxorubicin during washing steps and Poly (I:C) binding procedure was only 8±2% of total amount of loaded Doxorubicin. Polyacrylamide gel electrophoresis (PAGE) applied to analyze the binding efficiency of the Poly (I:C) on 400 µg/ml and 500 µg/ml Doxorubicin-loaded G4DcMNPs. The results indicated that in order to fully bind Poly (I:C) on 500 µg/ml and 400 µg/ml Doxorubicin-loaded G4DcMNPs, the ratio of Poly (I:C):G_4DcMNPs should be as 1:10 and 1:20 respectively (Figure 3.43). The binding Poly (I:C) was efficient on 500 µg/ml Doxorubicin-loaded G_4DcMNPs in compared with 400 µg/ml Doxorubicin-loaded G_4DcMNPs. When we fully loaded the cavities of the G_4DcMNPs with Doxorubicin, the surface functional groups became more prone to bind to Poly (I:C).

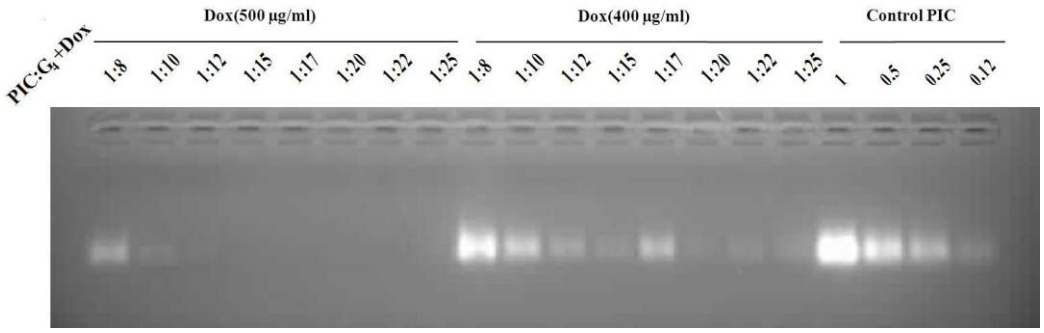

Figure 3.43 Agarose gel electrophoresis of loading optimization Poly on 500 µg/ml and 400 µg/ml Doxorubicin-loaded G_4DcMNPs at pH 6. Wells 1-8 demonstrate the loading of Poly (I:C) on 500 µg/ml Doxorubicin-loaded G_4DcMNPs. Wells 9-16 demonstrate the loading of Poly (I:C) on 400 µg/ml Doxorubicin-loaded G_4DcMNPs. Wells 17-20 demonstrate the control Poly (I:C) and different dilutions. 1 in the ratio represents 4 µg of Poly (I:C) or DcMNP.

3.4.3 PH Affects the Poly (I:C) Binding on Doxorubicin-Loaded G_4DcMNPs

The Doxorubicin-loaded G_4DcMNPs is sensitive to acidic pH. The acidic the condition is the more the release would be. Therefore, to determine the most efficient pH, binding of Poly (I:C) on G_4DcMNPs-Dox 500 were performed at pH 6 and pH 6.5 which are slightly acidic. This will results not only in efficient Poly (I:C) binding but also will prevent significant Doxorubicin release during the Poly (I:C) binding process. Polyacrylamide gel electrophoresis (PAGE) applied to analyze the binding efficiency of the Poly (I:C) on 500 µg/ml Doxorubicin-loaded G_4DcMNPs at pH 6 and pH 6.5. The results showed that the most efficient binding occurs at pH 6 (Figure 3.44). However changing the pH of MeIm buffer to

6.5 during the binding will decrease the binding efficiency slightly.

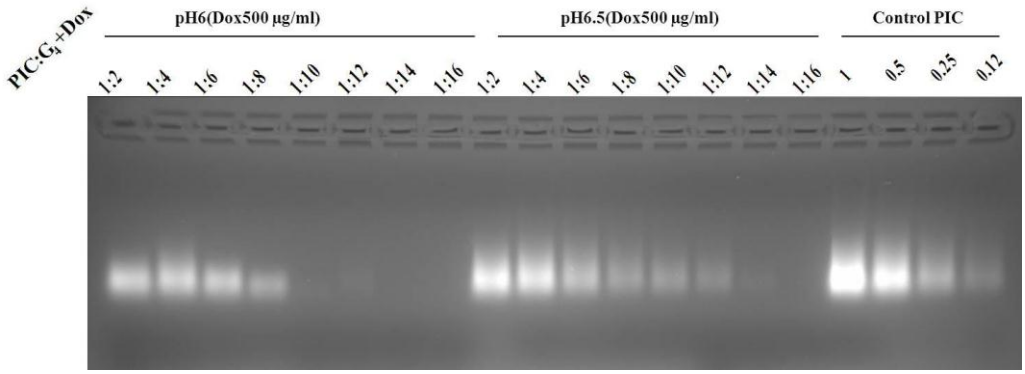

Figure 3.44 Agarose gel electrophoresis of binding optimization of poly on 500 µg/ml Doxorubicin-loaded G_4DcMNPs at pH 6 and pH 6.5. Wells 1-8 demonstrate the loading of Poly (I:C) on 500 µg/ml Doxorubicin-loaded G_4DcMNPs at pH 6. Wells 9-16 demonstrate the loading of Poly (I:C) on 500 µg/ml Doxorubicin-loaded G_4DcMNPs at pH 6.5. Wells 17-20 demonstrate the control Poly (I:C) and different dilutions. 1 in the ratio represents 4 µg of Poly (I:C) or DcMNP.

3.4.4 Doxorubicin Release from G_4DcMNPs and PIC-G_4DcMNPs

Doxorubicin release studies were performed in acetate buffer having pH 5.2 and 4.5 that mimics endosomal conditions. The release profiles of G_4DcMNPs and PIC-G_4DcMNPs at pH 5.2 and pH 4.5 are given in Figures 3.42. The release studies were continued up to 24 h. Release of 500 µg/ml Doxorubicin from G_4DcMNPs and PIC-G_4DcMNPs were analyzed using UV spectrophotometer. There was no significant difference in Doxorubicin release from Poly (I:C)-bound Doxorubicin-loaded G_4DcMNPs and Doxorubicin-loaded G_4DcMNPs (Figure 3.45). In general, Doxorubicin release was higher at pH 4.5 compared with pH 5.2.

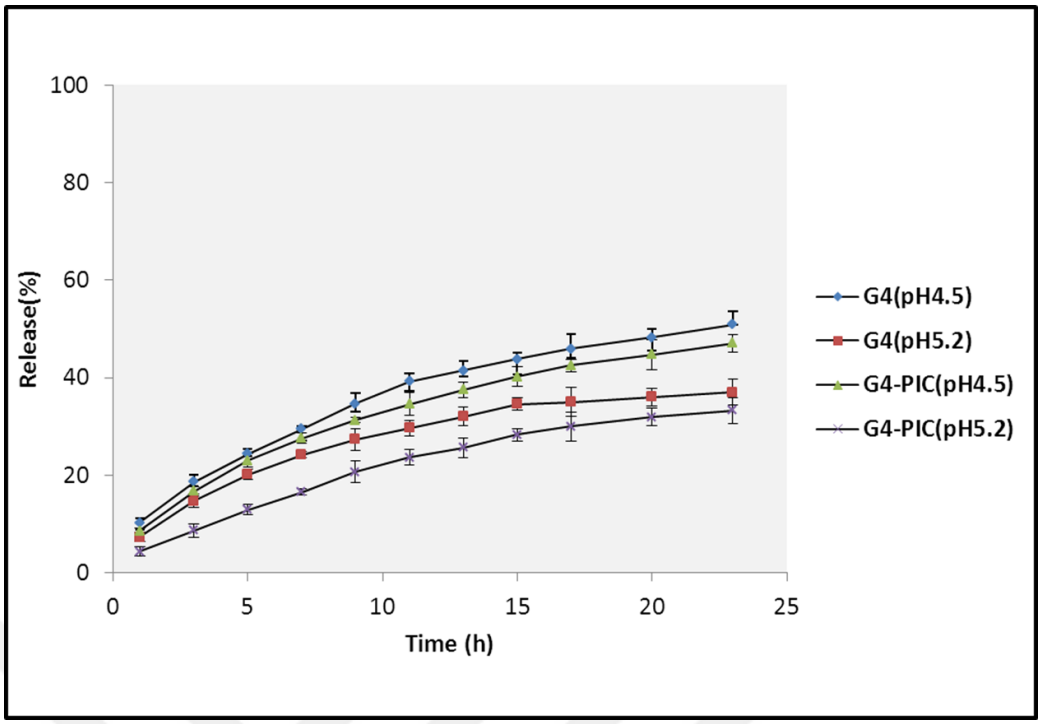

Figure 3.45 Release of 500 µg/ml Doxorubicin from G_4DcMNPs and G_4DcMNPs-PIC at pH 5.2 and pH 4.5.

3.4.5 Cytotoxicity Analysis of Poly (I:C)-Bound Doxorubicin-Loaded G_4DcMNPs

To quantify the cytotoxic effects of Poly (I:C)-bound Doxorubicin-loaded G4DcMNPs on Doxorubicin resistant MCF7 cells, XTT cell viability assays were performed and inhibitory concentration 50 (IC50) values were calculated. The IC50 value of Doxorubicin and Poly (I:C) for 1µM Doxorubicin resistant MCF7 cells by applying Poly (I:C)-bound Doxorubicin-loaded G_4DcMNPs were calculated as 12 µg/ml Doxorubicin (Figure 3.43) and 7 µg/ml Poly (I:C) (Figure 3.46).

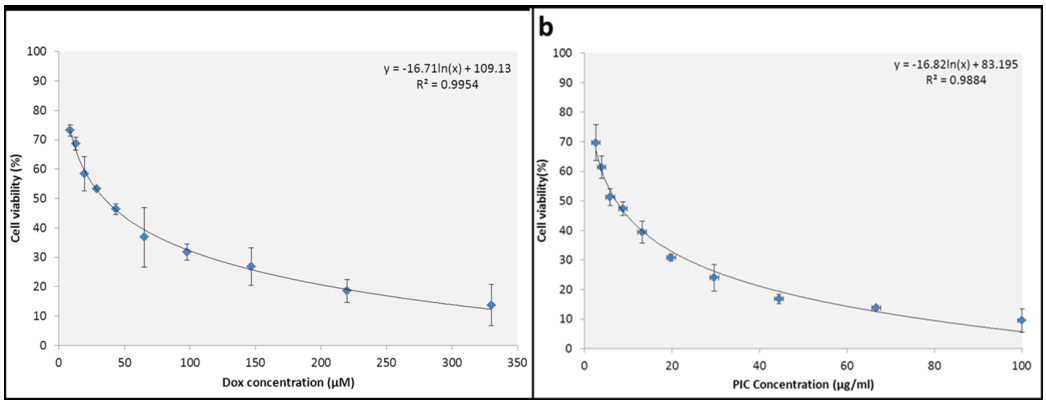

Figure 3.46 IC50 Value of Doxorubicin (a) and Poly (I:C) (b) in Poly (I:C) linked Doxorubicin-loaded DcMNPs were calculated as 12 µg/ml and 7 µg/ml.

The IC50 value for 1μM Doxorubicin resistant MCF7 cells by applying free Doxorubicin and Doxorubicin-loaded G4DcMNPs were previously calculated as 100 μg/ml and 21 μg/ml (Figure 3.36 and Figure 3.38). In addition, the cytotoxicity analysis of free Poly (I:C) and Poly (I:C)-bound DcMNPs were previously calculated as 450 μg/ml and 28 μg/ml (Figure 3.28). Comparison of these results with Doxorubicin-loaded DcMNPs (IC50 Dox = 21 μg/ml) and Poly (I:C)-bound Doxorubicin-loaded G_4DcMNPs (IC50 Dox=12 μg/ml and IC50 Poly (I:C) = 7 μg/ml) demonstrated that the loading of Doxorubicin can be a suitable way to overcome resistance mechanism (Table 3.7).

Table 3.7 IC_{50} values related to free Poly (I:C), Doxorubicin, Doxorubicin-loaded DcMNPs Poly (I:C) linked DcMNPs, and Poly (I:C)-bound Doxorubicin-loaded DcMNPs.

	IC_{50} of Free Dox	**IC_{50} of Free PIC**	**IC_{50} of G4DcMNP-Dox**	**IC_{50} of DcMNP-PIC**	**IC_{50} of DcMNP-Dox-PIC**
Dox	170 μg/ml	0 μg/ml	21 μg/ml	0 μg/ml	12 μg/ml
Poly I:C	0 μg/ml	450 μg/ml	0 μg/ml	28 μg/ml	7 μg/ml
DcMNP	0 μg/ml	0 μg/ml	270 μg/ml	400 μg/ml	145 μg/ml

Applying Poly (I:C)-bound Doxorubicin-loaded G_4DcMNPs on 1μM Doxorubicin resistant MCF7 cells improves the delivery system and have several advantageous on Doxorubicin-loaded G_4DcMNPs. Applying Poly (I:C)-bound Doxorubicin-loaded G_4DcMNPs on 1μM Doxorubicin resistant MCF7 cells will decrease the amount of applied Doxorubicin and makes the MCF7 Doxorubicin resistant cells 10 times more sensitive to Doxorubicin. It means that application of Doxorubicin together with Poly (I:C) will be two time more effective than when only Doxorubicin-loaded on DcMNPs. There may be two reasons for decreasing the cytotoxicity of drug-loaded nanoparticles in blood stream. When Poly (I:C) linked onto Doxorubicin-loaded DcMNPs, this will result in the modification of toxic amine group at the surface of dendrimeric nanoparticles into nontoxic $^{-}$OH groups. In addition, Binding of Poly (I:C) on the surface of Doxorubicin-loaded G_4DcMNPs decreased the amount of needed drug to kill 50 % of cancer cells. Therefore, the amounts of needed DcMNPs to deliver sufficient amount of anticancer drugs will be decreased. This will pave the way for decline in the cytotoxicity of delivery system, in the blood stream (Table 3.8). Obtained results demonstrated that, combination of Poly (I:C) and Doxorubicin will be superior to both Poly (I:C) and Doxorubicin-loaded DcMNPs. Entering inside the cell through endosome Poly (I:C) will bind to related TLR3 receptors and activate apoptotic pathways.

CHAPTER4

DISCUSSION

Magnetic nanoparticles, which were coated with PAMAM dendrimer, can be used to target-specific cancer cells in the presence of magnetic field. PAMAM dendrimers are hydrophilic, biocompatible, mono-disperse, and cascade branched macromolecules with highly flexible surface chemistry that facilitates functionalization. Dendrimer coating of MNPs reduces their agglomeration. It also provides cavities to load different anticancer drugs and surface functional groups to bind signaling molecules that can help targeted drug delivery. (Shukla *et al.*,.2005; Bhadra *et al.*, 2005; Khodadust et al. 2013; Pan *et al.*, 2007; Lai *et al.*, 2007; Brothers *et al.*, 1998)

Bare iron oxide nanoparticles were synthesized and coated with PAMAM to obtain different generations (G_1–G_7) of DcMNPs. Different parameters was optimized to synthesize DcMNPs with desired properties suitable for biomedical applications and drug delivery.

Bare nanoparticles were synthesized at different temperatures and different rates of ammonia addition. X-ray diffraction analysis proved that the synthesized MNPs at 90°C were corresponding to the characteristics of pure magnetite crystal (Fe_3O_4) having a cubic spinel structure.

In the FTIR spectrum of synthesized MNPs, Fe–O bond was observed at 570 cm^{-1} belonging to magnetite (Fe_3O_4). The stretching vibrations of Si–O–Fe and –CO–NH– bonds were observed at 980 and 1620 cm^{-1} after aminosilane modification. In dendrimer coated MNPs; stretching vibration of Si–O-Fe shifts to left side around 1020 cm^{-1} for G_7DcMNPs nanoparticles because of the presence of highly electronegative -CO-NH_2 groups. The new bonds of –CO–NH– were observed after synthesis of each dendrimer generations. Additional peaks were observed for vibrations of –CO– NH– in G_1DcMNPs at 1720 cm^{-1}, G_2DcMNPs at 1530 cm^{-1}, and G_3DcMNPs at 1450 cm^{-1} (Julian *et al.*, 1991). FTIR spectra of magnetite, aminosilane-modified magnetite, and different generations of dendrimer coated magnetite nanoparticles were compatible with the stepwise aminosilane modification and dendrimer coating processes.

The particle sizes of iron oxide nanoparticles and dendrimer coated magnetic nanoparticles visualized by TEM were in the range 3–13 and 11–21 nm, respectively. The size change of G_7DcMNPs was around eight nm after coating with PAMAM dendrimer. It was also demonstrated that the diameters of PAMAM dendrimers increase systematically at a rate of approximately one nm per generation (Svenson *et al.*, 2005).

The hydrodynamic diameters of dendrimer-coated nanoparticles were obtained as 45 ± 10 nm with a smaller size distribution than the value obtained for bare nanoparticles, which is 55 ± 15 in DLS measurements. The higher value of average size obtained in DLS (compared to TEM) arises because DLS measures the hydrodynamic radii of the particles, which include the solvent layer at the interface (Rahman *et al.*, 2012).

The agglomeration rate was very high in the bare Fe_3O_4 nanoparticles, which was also observed in DLS results and TEM images. The agglomeration occurs by the Van der Waals forces between the nanoparticles (Hoa *et al.*, 2009). One of the effective approaches for preventing particle agglomeration is to coat nanoparticles with polymers or other targeting agents, such as dendrimers taking into account their biocompatibility (Durmus *et al.*, 2009). Since the dispersity of nanoparticles was improved after the aminosilane modification and dendrimer-coating processes, the agglomeration of dendrimer-coated nanoparticles was expected to be reduced (Hoa *et al.*, 2009). A PAMAM coating was used to reduce magnetite agglomeration. The agglomeration of DcMNPs was reduced by increasing dendrimer layers at the surface of bare MNPs as observed in DLS and TEM results (Uzun *et al.*, 2010).

The ζ potential values of bare MNPs were calculated as -23.2 mV in PBS buffer pH 7.2, because of the plentiful OH^- ions. The ζ potential values of G_5DcMNPs and G_7DcMNPs were observed at 15.1 and 20.9 mV, respectively. This increase in ζ potential value is due to increase in positive charge of $–NH_3$ on the MNP surface through dendrimerization which also proves the success of PAMAM-coating process (Pan *et al.*, 2007).

Magnetic saturation value of the MNPs decreases as the size increases, which agrees with the literature (Rahman *et al.*, 2012).The decrease in the magnetic properties of the larger particles would be due to the increase in the volume/surface ratio in larger particles. Normally, we expect a reduction in magnetization of MNPs after modification with APTS. However, 5 % increase in magnetization of APTS-modified MNPs was observed when the magnetization time was 10 min. The increase of the sonication time to 30 min and adding of APTS at the 20th minute of sonication resulted in 20.5 % increase in magnetization. Increasing the time of ultrasonication and addition of APTS during sonication prevented the agglomeration of nanoparticles, which resulted in the improvement of magnetic properties and size distribution. VSM results of bare MNPs analyzed at 25 ^oC and 37 ^oC were obtained as 54.5 and 48.8 emu/g, respectively, which indicates a 10 % reduction in the magnetic strength of MNPs at body temperature.

The TGA curves of bare MNPs, G_0DcMNPs, G_5DcMNPs, and G_7DcMNPs points out the weight loss of nanoparticles at high temperatures. The results indicate that 17 % of the sample mass belongs to the dendrimer coating of fifth generation. Similarly, 22 % of the sample mass belongs to dendrimer coating of seventh generation. The increase in the organic content of nanoparticles observed in TGA analyses were the evidence of dendrimer growth when the PAMAM dendrimer coating was increased from G_5 to G_7.

General XPS scanning spectra of bare MNPs, G_0DcMNPs, G_5DcMNPs, and G_7DcMNPs demonstrated that peaks belonging to nitrogen and silane were not present in the spectrum of bare MNPs. These peaks were observed after aminosilane modification.

In the regional XPS scanning spectra of G_0DcMNPs, G_5DcMNPs, and G_7DcMNPs, the amounts of iron, oxygen, and silisium decrease, while the amounts of nitrogen and carbon increase exponentially throughout the dendrimer coating process. The decrease in the levels of iron, oxygen, and silisium atoms was due to the increase of the thickness of PAMAM layers at the surface of the nanoparticles.

The inverted light microscopy images demonstrated that DcMNPs were successfully taken up by MCF7 cells, even at low concentrations (Wuang *et al.,* 2007; Mahmoudi *et al.,* 2009). The main mechanism for the cellular internalization of MNPs is probably endocytosis (Gupta *et al.,* 2004).

MCF7 cells were treated with bare iron oxide nanoparticles, and DcMNPs. Bare iron oxide nanoparticles were not taken up by the cells because of their negative surface charge coming from the abundant OH^- ions which was also demonstrated by (Pan *et al.,* 2007). When magnetic nanoparticles were modified with different generations of PAMAM dendrimers, the positive charge increased with respect to the generation number because of the increasing amount of $–NH_3$ on the nanoparticle surface. XPS results showed that the amount of positively charged amine groups on the surface of DcMNPs was increased by dendrimer coating. Positively charged DcMNPs will be easily attached to negatively charged cell membrane, which will result in increased rate of cellular internalization. In the literature, there are parallel reports (Thorek *et al.,* 2008; Slowing *et al.,* 2006).

The performed cytotoxicity assays demonstrated that G_7DcMNPs and G_4DcMNPs were nontoxic up to 120 µg/ml and 250 µg/ml concentrations, respectively. The lower toxicity of G_4DcMNPs in compared with G_7DcMNPs was due to the fewer number of surface amine groups.. High generations of DcMNPs having abundant functional groups are usually used for ds RNA and oligonucleotide delivery systems (Boas *et al.,* 2001; Svenson *et al.,* 2005; Pan *et al.,* 2007) demonstrated that G_5DcMNPs could efficiently be used as delivery system for antisense surviving oligodeoxynucleotide (ODN) at 25 µg/ml concentration in cancer therapy. The toxicity observed at higher generations can be reduced by binding with such ligands. The lower generations of DcMNPs were generally used as drug delivery systems because of their highly branched and multi-cavity structures. Furthermore, the free amine functional groups in drug loaded DcMNPs can be modified with different molecules like folic acid (Thomas *et al.,* 2005) and PEG (Tang *et al.,* 2012; Singh *et al.,* 2008) to reduce their cytotoxicity.

The immobilization of Poly (I:C) onto nanoparticles is an important tool for the fabrication of functional therapeutic materials (Shukoor *et al.,* 2007; Khodadust *et al.,* 2013; Pan *et al.,* 2007). Due to their rapid clearance by nucleases, there is a need for carrier systems for Poly (I:C) treatment (Fischer *et al.,* 2009). Untargeted Poly (I:C) has already been applied as adjuvants in cancer directed human immunotherapy studies but by far not all applications

(Okada *et al.,* 2009; Butowski *et al.,* 2009; Jasani *et al.,* 2009). To have a successful therapeutic potential in cancer treatment Poly (I:C) has to be delivered intra-cellularly into endosomes and also to the cytosol, in a tumor targeted fashion. Up to now both liposomal and polymer based strategies have been developed which include antibody targeted or pH-sensitive liposomes (Milhaud *et al.,* 1989; Milhaud *et al.,* 1992). In one of the studies, linear polyethylenimine-based polymeric carrier was found as most effective in Poly (I:C) triggered killing of tumor cells which overexpress EGF-receptor (Schaffert *et al.,* 2011). In addition, combination of mushroom derived polysaccharide and Poly (I:C) forms stable nano-complexes and trigger sub-regulation of inflammatory cytokines in another study (Tincer *et al.,* 2011).

Recently, cationic lipid coated calcium phosphate nanoparticles constructed for co-delivery of zoledronic acid and Poly (I:C) was shown to have a better antitumor activity both *in vitro* and *in vivo* (Chen *et al.,* 2013). Magnetic nanoparticles are popular candidates for several biological applications including targeted cancer therapy studies since they can be targeted to the tumor site under magnetic field (Colombo *et al.,* 2012; Widder *et al.,* 1979). However, up to now there are limited number of reports about the loading studies of the Poly (I:C) on magnetic nanoparticles. Initially, Shukoor et al. (Shukoor *et al.,* 2007; Shukoor *et al.,* 2008) loaded Poly (I:C) onto γ-Fe_2O_3 nanoparticles through multifunctional polymeric ligand as a tool for targeting toll-like receptors. Recently, Poly (I:C) has been loaded on gold nanoparticles by using PEG bio-functional spacers and TAT peptide (Sanz *et al.,* 2012).

In second section of this research study, different generations of synthesized PAMAM dendron coated magnetic nanoparticles were efficiently linked for the first time with Poly (I:C). The optimum binding efficiencies and stabilities of Poly (I:C) at different pH conditions were discussed. Studying different pH (6, 7 and 7.5) values it was obtained that the loading efficiency of Poly (I:C) on DcMNPs were almost similar very low at pH 7 and 7.5 for generation 7. However at pH 6 the loading efficiency of Poly (I:C) on G_7DcMNPs were 3.5 fold higher than that of pH 7 and 7.5. At pH 7 MeIm buffer Poly (I:C) was not loaded on G_4DcMNPs even when the G_4DcMNPs ratios increased up to 35 fold with respect to Poly (I:C). However, at pH 6 MeIm buffer the loading efficiency of Poly (I:C) was obtained as about 80 % when the PIC:G_4DcMNPs ratio was 1:22. Although, unlike at pH 7 and pH 7.5, Poly (I:C) was also loaded on lower generations (G_3 and G_2) DcMNPs at pH 6, the loading efficiency was very low in these generations due to the small numbers of functional groups at the surface. These results contributed that loading of Poly (I:C) onto PAMAM DcMNPs at acidic pH was superior to neutral and basic pH. Yi Liu et al., demonstrated that pH-induces conformational change of PAMAM dendrimers from a “dense core” (high pH) to a “dense shell” (low pH) (Liu *et al.,* 2009). Therefore at acidic pH the surface amine functional groups of PAMAM dendrons would be more prone for Poly (I:C) binding than in basic and neutral pH. Results of this study confirm that efficient binding of Poly (I:C) on DcMNPs was performed when the activation and loading were performed at acidic pH. In addition, according to the literature nucleic acids should be activated in the presence of EDC at acidic pH for an efficient binding with amine and carboxyl groups (Sheehan *et al.,* 1961). Thereby higher loading efficiency may also be

partly related to the activation condition by EDC. The phosphoramide bound between Poly (I: C) and amine functional groups at the surface of DcMNPs were very sensitive to basic pH. The phosphoramide bound between the Poly (I:C) DcMNPs complex is stable at acidic condition up to pH 3 values. On the other hand, at pH 8.5 the bound between Poly (I:C) and DcMNPs starts to be hydrolyzed and the maximal hydrolysis was achieved at pH 9.4. The half-life of the bond between Poly (I:C) and surface amine groups of DcMNPs at pH 9.4 was obtained as 30 min. Poly(I:C)-DcMNPs bound was shown to be highly stable in powder form and aqueous form when stored at pH 6 (MeIm buffer), and pH 7 (PBS buffer and injection water) up to 4 weeks. These results demonstrate that the storage of the Poly (I:C) DcMNPs complex is safe in powder form, or in aqueous form at acidic to neutral pH. Recent findings demonstrated that dendrimers could cross cell membranes by endocytosis (Seib *et al.,* 2007). The release of Poly (I:C) from DcMNPs was not related to pH when the nanoparticles are inside the cells. Poly (I:C) is on the surface of DcMNPs where it can bind to receptors efficiently without its release. In endosome the Poly (I:C) at the surface of DcMNPs will bind to TLR3 receptors and induce apoptosis. In the case of their diffusion to the cytoplasm eventually they will bind to the cytoplasmic receptors of Poly (I:C) which are MDA-5 and RIG-1 proteins. This binding will activate some apoptotic proteins like PUMA and NOXA (Xiangzhong *et al.,* 2012; Kato *et al.,* 2006).

In 1984 it was reported that the phosphoramidase enzyme hydrolysis the bond between P and N in phosphoramide. Histochemical study for the demonstration of sites of phosphoramidase activity showed that small amounts of the enzyme are present in many normal tissues; however, large amounts are found in the grey matter of the central nervous system and in malignant epithelial tumors (Gomori *et al.,* 1948; Friedman *et al.,* 1954; Meyer *et al.,* 1957; Ludeman *et al.,* 1999). Therefore, in case of application of siRNA or Poly (I:C) (Khodadust *et al.,* 2013) bound-DcMNPs the phosphoramide bindings between phosphates group of siRNA or Poly (I:C) and amine groups of DcMNPs will be hydrolyzed by phosphoramidase enzymes, which are especially active in malignant cancer cells (Teicher et al., 2012).

In third section of thesis study, synthesized and characterized (G_2, G_3, G_4, G_5, G_6, and G_7) DcMNPs for the first time were most efficiently loaded with Doxorubicin. Initially, drug loading studies were performed with generation four in three different buffers [PBS (pH 7.2), TES (pH 7.3), and acetate (pH 5.0)] with two different drug concentrations (150 and 300 µg/ml) at room temperature. Doxorubicin incorporation ratio to G_4DcMNPs was 96% and 94% for 150 and 300 µg/ml Doxorubicin in PBS buffer, respectively. The most efficient drug loading was obtained in PBS buffer. Previously, Papagiannaros *et al*. loaded Doxorubicin to PAMAM dendrimer in TES and acetate buffers with 50% and 35% drug incorporation ratios, respectively (Papagiannaros *et al.,* 2005). The lower loading efficiency of Doxorubicin in Papagiannaros *et al*. study in the case of acetate buffer was because of the acidic pH of the buffer. However, the results of our study showed that at neutral pH, PBS buffer is superior to TES for Doxorubicin loading. In this study PBS buffer for the first time was shown as the most suitable buffer for Doxorubicin loading on DcMNPs. This result is parallel with the “like dissolves like” chemical rule because PBS and Doxorubicin have similar molecular structures (Schmid *et al.,* 2001). Therefore, it can be concluded that

because of the similarity in the structure, Doxorubicin can be easily dissolved and loaded on to DcMNPs in PBS buffer with respect to TES buffer.

Doxorubicin loading was efficient at lower generations (G_2, G_3 and G_4). G_4DcMNPs were found as the optimum generation for Doxorubicin loading. After fourth generation the distance between the surface branch groups decrease so much that Doxorubicin cannot path through and enter into the cavities inside. Therefore, at higher (G_5, G_6 and G_7) generations of DcMNPs because of the compact surface of the dendrimer with smaller cavities, loading efficiency and the stability of the drug were decreased. As a result, higher (G_5, G_6 and G_7) generations of DcMNPs were not found suitable for Doxorubicin loading. The maximum amount of drug loading was directly related to the shape and size of internal cavities of dendrimers. At a particular level of generation with increased terminal groups, PAMAM dendrimer will reach the compact packing limitation, which is called "de Gennes's dense packing." This situation will limit the drug loading into the cavities of NPs (Tsai *et al.*, 2011; Jansen *et al.*, 1994). Our results demonstrated that synthesized fourth generation of PAMAM dendrimer coated magnetic nanoparticles reached the compact packing limitation, which limited the drug loading into the cavities of higher (G_5, G_6 and G_7) generations.

The loading efficiencies of the drugs onto dendrimers are also related to various environmental conditions such as polarity, pH, and temperature (Tsai *et al.*, 1994). The loading was also performed at 4 ^{o}C (cold room) to see the temperature effect on loading efficiency. The loading percentage and the maximum loading efficiency were decreased at 4°C. This can be related to the decrease of cavity volume of the dendrimers at low temperatures.

In the literature, there are two different equations (Equation 3.1 and Equation 3.4) for drug loading efficiency study. The obtained results will be different. Therefore, in order to prevent complication the results of Equation 3.1 were discussed in details.

Doxorubicin loading, encapsulation efficiency, content and process yield percentages also calculated. From the results, lower generations were again shown similar and higher entrapment efficiencies. From the equation 3.4, lower generations demonstrated higher loading efficiencies. Although the drug entrapment was the same in G_2, G_3 and G_4DcMNPs, the drug loading efficiency increased when the generation number decreased. This is because; the dendrimer amount is the main factor when we apply equation 3.4 for drug loading efficiency study.

The stability studies of Doxorubicin-loaded MNPs (G_2, G_3 and G_4) were carried out both in PBS (pH 7.4, 37 B°C) buffer and human serum. The results indicated that Doxorubicin-loaded MNPs were highly stable up to 8 weeks in PBS buffer. This is a desirable property, which provides an advantage in the storage of Doxorubicin-loaded DcMNPs. In human serum, the results were similar with those in PBS buffer for 400 µg/ml Doxorubicin-loaded NPs, indicating a significant stability under physiological conditions. This would be especially an important property for *in vivo* applications, when the release of the drug was not desired until the drug loaded NPs are delivered to tumor site. In case of 500 µg/ml

Doxorubicin-loaded NPs, 30% of the drug was released within the first 15 h in human serum, which was in contrast with the results obtained in PBS. It is probable that the cavities, which are close to the surface of DcMNPs, were totally filled with drug at 500 µg/ml Doxorubicin concentration (the maximum loaded dose). In contrast to PBS buffer, human serum contains many organic molecules, which may interact with DcMNPs surface, causing the drug to be released more easily. These results showed that in human serum, the most stable Doxorubicin loading concentration onto G_4DcMNPs was 400 µg/ml. As it was also emphasized in the literature, the stability of drug loaded MNPs is a very important parameter for the preservation of the drug in the active form throughout its shelf life (Min *et al.*, 2008). In addition, the drug loaded MNPs should be stable in the bloodstream to limit the damage to healthy tissue during its targeting period. On the contrary, instability of drug loaded NPs would release the drug before being delivered to the target site (Ducry *et al.*, 2010).

The release efficiencies of Doxorubicin-loaded MNPs were investigated at PBS buffers with two different pH values, 5.2 and 4.2, that mimic endosomal conditions. Most of the drug (approximately 80%) was released within first 15 h from all of the generations in pH 4.2 buffer. However, in pH 5.2 buffer, the release profile was changed because of the generation number of the NPs. The release of Doxorubicin from G_4DcMNPs was slower compared with the release from lower generation NPs (G_2, G_3). Although Doxorubicin can be loaded on to G_2DcMNPs -G_3DcMNPs, they release most of the drug rapidly in pH 5.2 because of their flexible interior properties. Therefore, G_2DcMNPs and G_3DcMNPs were more suitable for the delivery of drugs such as vinca alkaloids (Clarke *et al.*, 1999) and taxenes (Jahnson *et al.*, 1963), which show their effect in cytoplasm. PAMAM dendrimers with primary amines as surface groups exhibit extended conformations upon lowering the pH because of electrostatic repulsion between surface primary amines, thus forcing the dendritic branches apart (Lee *et al.*, 2002; Chen *et al.*, 2000). The repulsions of the tertiary amine groups of the G_4DcMNPs at late endosomal pH 4.2 were optimal for drug release. The slow release makes G_4DcMNPs more attractive for Doxorubicin delivery. Doxorubicin, which was loaded to G_4DcMNPs, could be successfully delivered to the cell's late endosome near to the nucleus where Doxorubicin shows its anticancer activity.

Using low generations (G_2 and G_3) as drug carrier systems cause the release and escape of the Doxorubicin from endosome near to the membrane of the cells. Therefore, Doxorubicin will be caught and pumped out by resistance mechanism. It is known that P-glycoprotein (multidrug resistance protein-1) acts as a pump to extrude the Doxorubicin out of the cell (Abam *et al.*, 2009; Zyad *et al.*, 1994). By releasing the drug in low pH (late endosome) away from the cell membrane and efflux pumps, it will be possible to overcome the MDR-1-related resistance. As a result, G_4DcMNPs could be the ideal DcMNPs system for Doxorubicin.

It was also demonstrated that Doxorubicin-loaded G_4DcMNPs were fivefold more toxic on Doxorubicin resistant MCF7 cells compared with free Doxorubicin. These results confirmed that the loaded Doxorubicin were active when released. Loading of Doxorubicin on DcMNPs also help to overcome the drug resistance and sensitize resistant cells.

Poly (I:C) binding on higher generations (G_7DcMNPs) was efficient (Khodadust *et al.*, 2013) due to having rigid surface with higher number of functional groups on the surface (Esfand *et al.*, 2001). However, drug loading was achieved more efficiently at lower generations (Khodadust *et al.*, 2013). This is because of the fact that lower generations have flexible scaffolding structure through which the drug can enter into the cavities inside (Esfand *et al.*, 2001). In addition, the maximum amount of entrapped Doxorubicin was directly proportional to the shape and the size of the drugs, as well as to the amount, shape and size of the available internal DcMNPs cavities (Esfand *et al.*, 2001; Khodadust *et al.*, 2013).

In last section of thesis study, in order to obtain most effective delivery system Poly (I:C) was bound on Doxorubicin-loaded G_4DcMNPs at pH 6 and pH 6.5 values. The Doxorubicin-loaded G_4DcMNPs are sensitive to acidic pH and most efficient Poly (I:C) binding occurs at pH 6 (Khodadust *et al.*, 2013). Results of our study demonstrated that the Doxorubicin could enter into the cavities of G_4DcMNPs at neutral pH in PBS buffer. The release starts at acidic pH and maximum release was achieved in pH 4.2 (Khodadust *et al.*, 2013). This is because at neutral pH only the primary amine groups were protonated (Prabal *et al.*, 2005) which makes the gyration radius suitable for the entrance of drugs while at pH 4.2 the gyration radius is so high (Prabal *et al.*, 2005) which lets most of the drugs to scape and release from the cavities of nanoparticles. At slightly acidic pH the surface amine functional groups of PAMAM dendrons would be more prone for Poly (I:C) binding than in neutral and basic pH. This is because, like other nucleic acids, the most efficient activation of the phosphate groups of Poly (I:C) with EDC occurs at acidic environment (Sheehan *et al.*, 1961). The binding of Poly (I:C) was more efficient at highest amount (500 µg/ml) of Doxorubicin-loaded G_4DcMNPs. This is because of the fact that the amount of loaded Doxorubicin on G_4DcMNPs effects the gyration radius and also the position of surface functional groups as a results it influences the efficiency of Poly (I:C) binding. The position of functional groups at the surface of DcMNPs are very important for binding of Poly (I:C). In the case of the cavities of the G_4DcMNPs were fully loaded with the drug, the surface functional groups became more rigid like in the case of higher generations (G_7DcMNPs) and they became more prone to bind to Poly (I:C). On the other hand, Doxorubicin release from G_4DcMNPs and Poly (I:C) loaded G_4DcMNPs was not significantly different. In general, Doxorubicin release was higher at more acidic pH values. Therefore only small amount of Doxorubicin was lost during washing with MeIm buffer (5 %) and binding of Poly (I:C) (5%) at pH 6.

Binding of Poly (I:C) on Dox-G_4DcMNPs will decrease the toxic effect of the nanoparticle when in the blood stream. This is because the surface amine(NH_2-) functional groups which are the main reason for the toxicity of PAMAM dendrimers (Sadekar *et al.*, 2012) will be covered with Poly (I:C) (by making phosphoramide bound) and will turn to OH- groups which are not toxic. This phosphoramide bound is very stable bounding in blood streams. In addition, in 1984 it was reported that the phophoramidase enzyme hydrolyzes the bond between P and N in phosphoramide. Hystochemical study for the demonstration of sites of phosphoramidase activity showed that Small amounts of the enzyme are present in many

normal tissues; however, large amounts are found in the grey matter of the central nervous system and in malignant epithelial tumors (Gomori *et al.,* 1948; Friedman *et al.,* 1954; Meyer *et al.,* 1957; Ludeman *et al.,* 1999).

When we compared the *in vitro* cytotoxic effect of Doxorubicin, Poly (I:C) and Poly (I:C)-bound Doxorubicin-loaded DcMNPs with each other, it was observed that Poly (I:C)-bound Doxorubicin-loaded DcMNPs show the most cytotoxic effect on MCF7/Dox cells. The results demonstrated that applying Poly (I:C)-bound Doxorubicin-loaded G_4DcMNPs will improve the delivery system by increasing the biocompatibility of the complex when in blood stream and increasing the toxicity when inside tumor cells. Poly (I:C) binding on the surface of DcMNPs may also increase the stability of Doxorubicin-loaded nanoparticles by preventing the drug release in blood stream. In addition, applying Poly (I:C) linked Doxorubicin-loaded DcMNPs, lowers the amount of required nanoparticles for drug delivery. Poly (I:C) modification of Doxorubicin-loaded DcMNPs will also decrease the toxicity of nanoparticles by turning toxic amine group to water soluble and nontoxic –OH groups. However, after entering inside the tumor cells the Poly (I:C) will be released from the surface by phosphoramidase enzyme which is highly expressed in tumor cells and will increase the cytotoxicity of the system inside the tumor cells. It means, applying Poly (I:C)-bound- Doxorubicin-loaded DcMNPs will make the system more safe when in blood stream and more toxic when they are inside the tumor cells. Therefore, Poly (I:C)-bound Doxorubicin-loaded DcMNPs can be used as a novel and really suitable system for sensitization of Doxorubicin resistant cells. *In vivo* characterization of this system will help to overcome the drug resistant mechanism of breast cancer, which is one of the main obstacles in breast cancer therapy. It may also open new ideas about combinational-targeted cancer therapy.

CHAPTER 5

CONCLUSIONS

1. This was a novel detailed optimization study about synthesis and characterization of different generation of PAMAM dendrimer coated iron oxide nanoparticles.

2. Results related to the characterization of DcMNPs demonstrated that the synthesized DcMNPs, with their functional groups, symmetry perfection, size distribution, improved magnetic properties, and nontoxic characteristics could be suitable nano-carriers for targeted cancer therapy upon loading with various anticancer agents.

3. This Was the first reported case of successful Poly (I:C) loading onto different generations of PAMAM dendrimer coated magnetic nanoparticles. According to the results, Acidic reaction conditions were found as superior to basic and neutral for binding of Poly (I:C). In addition, having more functional groups at the surface, higher generations (G_7, G_6, G_5) of PAMAM DcMNPs were found more suitable as a delivery system for Poly (I:C).

4. The release of Poly (I:C) from DcMNPs was not related to pH when the nanoparticles are inside the cells. In endosome the Poly (I:C) at the surface of DcMNPs will bind to TLR3 and in the case of their diffusion to the cytoplasm, they will bind to the cytoplasmic receptors of MDA-5 and RIG-1 and induce apoptosis.

5. In vitro cytotoxicity study on different breast-cancer cell lines demonstrated that Poly (I:C)-bound DcMNPs are more effective than free Poly (I:C). However, the most efficient cytotoxicity of Poly (I:C)-bound DcMNPs was observed in Doxorubicin resistant MCF7 cells. Therefore, Poly (I:C)-bound DcMNPs application seem to be a suitable replacement drug for the treatment of Doxorubicin resistant cells.

6. PBS buffer with neutral pH for the first time reported as the most suitable loading buffer for Doxorubicin loading on different generation of DcMNPs. Doxorubicin loading, release, and stability studies on these nanoparticles (NPs) demonstrated that Doxorubicin could be loaded on G_2, G_3 and G_4DcMNPs with 97% efficiency. Therefore, generations (G_2, G_3, G_4) of PAMAM DcMNPs were shown as the efficient drug carrier systems while higher generation G_5, G_6 and G_7DcMNPs were not suitable for Doxorubicin delivery. For the success of the drug-loaded delivery systems, the right balance between plasma stability and efficient drug release at the target site is critical. PH-responsive polymers and dendrimers mimic biological systems wherein an alteration in pH value results in the conformational changes of delivery systems. As a result, pH-responsive drug carriers have the potential to provide selective drug release at therapeutic targets including tumors and in acidic intracellular vesicles such as endosomes and lysosomes. Doxorubicin, being a DNA-

targeting drug, needs to be released near the nucleus. Among the lower generations, G_4 could be the ideal DcMNPs system for Doxorubicin delivery. Doxorubicin could be successfully delivered to the cell's late endosome near to the nucleus where the drug shows its anticancer activity. Doxorubicin-loaded DcMNPs are five times more cytotoxic than free Doxorubicin. Therefore, application of Doxorubicin-loaded G_4DcMNPs may help to overcome Doxorubicin resistance mechanism in MCF7/Dox cells.

7. This Was the first reported case of successful Poly (I:C) binding on Doxorubicin-loaded DcMNPs. Doxorubicin loading on lower generation of DcMNPs made them more suitable for Poly (I:C) binding. Loading of Doxorubicin into the cavities of G_4DcMNPs up to 10 fold increases the binding efficiency of Poly (I:C) to the surface functional groups. Poly (I:C) binding on Doxorubicin-loaded G_4DcMNPs was superior to Doxorubicin and Poly (I:C) loaded DcMNPs in terms of its cytotoxic effect on MCF7/Dox cells. When we compared the *in vitro* cytotoxic effect of Doxorubicin, Poly (I:C), Doxorubicin-loaded DcMNPs, Poly (I:C)-bound DcMNPs and Poly (I:C)-bound Doxorubicin-loaded DcMNPs with each other, it was observed that Poly (I:C)-bound Doxorubicin-loaded DcMNPs show the most cytotoxic effect on MCF7/Dox cells. Binding of Poly (I:C) to amine groups at the surface of Doxorubicin-loaded DcMNPs will decrease the cytotoxicity of the system in the blood streams and increase its biocompatibility. This may also increase the dispersivity of the system in blood stream. TEM results demonstrated that Poly (I:C) binding on DcMNPs increases their dispersivity. Phosphoramidase enzyme which can break the linkage between P groups of Poly (I:C) and N groups of DcMNPs are highly active in tumor cells. Therefore, Poly (I:C) binding onto surface of Doxorubicin-loaded DcMNPs will not only sensitize Doxorubicin resistant cells but also make the system specific to tumor cells and cause apoptosis of the drug resistant MCF7 cells with lower amounts of Doxorubicin.

REFERENCES

Abaan, O. D., Mutlu, P. K., Baran, Y., Atalay, C., & Gunduz, U. (2009). Multidrug resistance mediated by MRP1 gene overexpression in breast cancer patients. *Cancer investigation*, *27*(2), 201-205.

Arruebo, M., Fernández-Pacheco, R., Ibarra, M. R., & Santamaría, J. (2007). Magnetic nanoparticles for drug delivery. Nano today, 2(3), 22-32.

áBaker Jr, J. R. (2005). Tumor angiogenic vasculature targeting with PAMAM dendrimer–RGD conjugates. *Chemical communications*, (46), 5739-5741.

Alexiou, C., Arnold, W., Klein, R. J., Parak, F. G., Hulin, P., Bergemann, C., ... & Luebbe, A. S. (2000). Locoregional cancer treatment with magnetic drug targeting. Cancer research, 60(23), 6641-6648.

Bhadra, D., Yadav, A. K., Bhadra, S., & Jain, N. K. (2005). Glycodendrimeric nanoparticulate carriers of primaquine phosphate for liver targeting. *International journal of pharmaceutics*, *295*(1), 221-233..

Borges, O., Silva, M., de Sousa, A., Borchard, G., Junginger, H. E., & Cordeiro-da-Silva, A. (2008). Alginate coated chitosan nanoparticles are an effective subcutaneous adjuvant for hepatitis B surface antigen. *International immunopharmacology*, *8*(13), 1773-1780.

Bosman, A. W., Janssen, H. M., & Meijer, E. W. (1999). About dendrimers: structure, physical properties, and applications. *Chemical Reviews*, *99*(7), 1665-1688.

Brothers II, H. M., Piehler, L. T., & Tomalia, D. A. (1998). Slab-gel and capillary electrophoretic characterization of polyamidoamine dendrimers. *Journal of Chromatography A*, *814*(1), 233-246.

Bruce, I. J., Taylor, J., Todd, M., Davies, M. J., Borioni, E., Sangregorio, C., & Sen, T. (2004). Synthesis, characterisation and application of silica-magnetite nanocomposites. *Journal of magnetism and magnetic materials*, *284*, 145-160.

Burgess, D. J., Doles, J., Zender, L., Xue, W., Ma, B., McCombie, W. R., ... & Hemann, M. T. (2008). Topoisomerase levels determine chemotherapy response in vitro and in vivo. *Proceedings of the National Academy of Sciences*,*105*(26), 9053-9058.

Butowski, N., Lamborn, K. R., Lee, B. L., Prados, M. D., Cloughesy, T., DeAngelis, L. M., ... & Chang, S. M. (2009). A North American brain tumor consortium phase II study of poly-ICLC for adult patients with recurrent anaplastic gliomas. *Journal of neuro-oncology*, *91*(2), 183-189.

Chen, L., Ding, Y., Wang, Y., Liu, X., Babu, R. J., Ravis, W. R., & Yan, W. (2013). Codelivery of zoledronic acid and doublestranded RNA from core-shell nanoparticles. *International journal of nanomedicine*, *8*, 137.

Clementi, M. E., Giardina, B., Di Stasio, E., Mordente, A., & Misiti, F. (2003). Doxorubicin-derived metabolites induce release of cytochrome C and inhibition of respiration on cardiac isolated mitochondria. *Anticancer research*, *23*(3B), 2445.

Cole, S. P., Sparks, K. E., Fraser, K., Loe, D. W., Grant, C. E., Wilson, G. M., & Deeley, R. G. (1994). Pharmacological characterization of multidrug resistant MRP-transfected human tumor cells. *Cancer Research*, *54*(22), 5902-5910.

Colombo, M., Carregal-Romero, S., Casula, M. F., Gutierrez, L., Morales, M. P., Böhm, I. B., ... & Parak, W. J. (2012). Biological applications of magnetic nanoparticles. *Chemical Society Reviews*, *41*(11), 4306-4334.

Crozier, W. J. (1921). " Homing" Behavior in Chiton. *The American Naturalist*,*55*(638), 276-281.

Desai, K. G. H., & Park, H. J. (2005). Preparation and characterization of drug- loaded chitosan–tripolyphosphate microspheres by spray drying. Drug development research, 64(2), 114-128.

Dobson, J. (2006). Gene therapy progress and prospects: magnetic nanoparticle-based gene delivery. Gene therapy, 13(4), 283-287.

Dobson, J. (2006). Magnetic nanoparticles for drug delivery. Drug Development Research, 67(1), 55-60.

Du, X., Poltorak, A., Wei, Y., & Beutler, B. (2000). Three novel mammalian toll-like receptors: gene structure, expression, and evolution. *European cytokine network*, *11*(3), 362-71.

Ducry, L., & Stump, B. (2009). Antibody− drug conjugates: linking cytotoxic payloads to monoclonal antibodies. *Bioconjugate chemistry*, *21*(1), 5-13.

Dung, T. T., Danh, T. M., Duc, N. H., & Chien, D. M. (2009, September). Preparation and characterization of magnetic nanoparticles coated with polyethylene glycol. In *Journal of Physics: Conference Series* (Vol. 187, No. 1, p. 012048). IOP Publishing.

Durmus, Z., Kavas, H., Toprak, M. S., Baykal, A., Altınçekiç, T. G., Aslan, A., ... & Coşgun, S. (2009). L-lysine coated iron oxide nanoparticles: synthesis, structural and conductivity characterization. *Journal of Alloys and Compounds*,*484*(1), 371-376.

Esfand, R., & Tomalia, D. A. (2001). Poly (amidoamine)(PAMAM) dendrimers: from biomimicry to drug delivery and biomedical applications. *Drug discovery today*, *6*(8), 427-436.

Ferlay, J., Shin, H. R., Bray, F., Forman, D., Mathers, C., & Parkin, D. M. (2010). Estimates of worldwide burden of cancer in 2008: GLOBOCAN 2008.*International journal of cancer*, *127*(12), 2893-2917.

Ferrari, M. (2005). Cancer nanotechnology: opportunities and challenges.*Nature Reviews Cancer*, *5*(3), 161-171.

Fischer, S., Schlosser, E., Mueller, M., Csaba, N., Merkle, H. P., Groettrup, M., & Gander, B. (2009). Concomitant delivery of a CTL-restricted peptide antigen and CpG ODN by PLGA microparticles induces cellular immune response. *Journal of drug targeting*, *17*(8), 652-661.

Friedman, O. M., Klass, D. L., & Seligman, A. M. (1954). N-Phosphorylated Derivatives of Diethanolamine1. *Journal of the American Chemical Society*,*76*(3), 916-917.

Gao, F., Pan, B. F., Zheng, W. M., Ao, L. M., & Gu, H. C. (2005). Study of streptavidin coated onto PAMAM dendrimer modified magnetite nanoparticles. *Journal of Magnetism and Magnetic materials*, *293*(1), 48-54.

Gao, J., Gu, H., & Xu, B. (2009). Multifunctional magnetic nanoparticles: design, synthesis, and biomedical applications. *Accounts of chemical research*, *42*(8), 1097-1107.

Germann, U. A., Pastan, I., & Gottesman, M. M. (1993, February). P-glycoproteins: mediators of multidrug resistance. In *Seminars in cell biology* (Vol. 4, No. 1, pp. 63-76). Academic Press.

Gnanaprakash, G., Mahadevan, S., Jayakumar, T., Kalyanasundaram, P., Philip, J., & Raj, B. (2007). Effect of initial pH and temperature of iron salt solutions on formation of magnetite nanoparticles. *Materials chemistry and physics*, *103*(1), 168-175.

Gomori, G. (1948, December). Histochemical Demonstration of Sites of Phosphamidase Activity. In *Proceedings of the Society for Experimental Biology and Medicine. Society for Experimental Biology and Medicine (New York, NY)* (Vol. 69, No. 3, pp. 407-409). Royal Society of Medicine.

Gupta, A. K., & Gupta, M. (2005). Synthesis and surface engineering of iron oxide nanoparticles for biomedical applications. *Biomaterials*, *26*(18), 3995-4021.

Häfeli, U. O. (2004). Magnetically modulated therapeutic systems. International journal of pharmaceutics, 277(1), 19-24.

Hansson, G. K., & Edfeldt, K. (2005). Toll to be paid at the gateway to the vessel wall. *Arteriosclerosis, thrombosis, and vascular biology*, *25*(6), 1085-1087.

Hemmi, H., Takeuchi, O., Kawai, T., Kaisho, T., Sato, S., Sanjo, H., ... & Akira, S. (2000). A Toll-like receptor recognizes bacterial DNA. *Nature*,*408*(6813), 740-745.

Hergt, R., Dutz, S., Müller, R., & Zeisberger, M. (2006). Magnetic particle hyperthermia: nanoparticle magnetism and materials development for cancer therapy. *Journal of Physics: Condensed Matter*, *18*(38), S2919.

Ho, K. M., & Li, P. (2008). Design and synthesis of novel magnetic core-shell polymeric particles. *Langmuir*, *24*(5), 1801-1807.

Hyeon, T. (2003). Chemical synthesis of magnetic nanoparticles. *Chemical Communications*, (8), 927-934.

Iagaru, A., Masamed, R., Keesara, S., & Conti, P. S. (2007). Breast MRI and18F FDG PET/CT in the management of breast cancer. *Annals of nuclear medicine*, *21*(1), 33-38.

Ishikawa, T., Kumagai, M., Yasukawa, A., Kandori, K., Nakayama, T., & Yuse, F. (2002). Influences of metal ions on the formation of γ-FeOOH and magnetite rusts. *Corrosion science*, *44*(5), 1073-1086.

Jasani, B., Navabi, H., & Adams, M. (2009). Ampligen: a potential toll-like 3 receptor adjuvant for immunotherapy of cancer. *Vaccine*, *27*(25), 3401-3404.

Johnsen, S., & Lohmann, K. J. (2008). Magnetoreception in animals. *Physics Today*, *61*, 29.

Johnson, I. S., Armstrong, J. G., Gorman, M., & Burnett, J. P. (1963). The vinca alkaloids: a new class of oncolytic agents. *Cancer Research*, *23*(8 Part 1), 1390-1427.

Julian JM, Anderson DG, Brandau AH, McGinn JR, Millon AM (1991) In: Brezinski DR (ed) An infrared spectroscopy atlas for the coatings industry 1 federation of societies for coating technology, 4th edn. Blue Bell, Pennsylvania Vols I and II

Kato, H., Takeuchi, O., Sato, S., Yoneyama, M., Yamamoto, M., Matsui, K., ... & Akira, S. (2006). Differential roles of MDA5 and RIG-I helicases in the recognition of RNA viruses. *Nature*, *441*(7089), 101-105.

Kawai, T., & Akira, S. (2010). The role of pattern-recognition receptors in innate immunity: update on Toll-like receptors. *Nature immunology*, *11*(5), 373-384.

Kawai, T., Takahashi, K., Sato, S., Coban, C., Kumar, H., Kato, H., ... & Akira, S. (2005). IPS-1, an adaptor triggering RIG-I-and Mda5-mediated type I interferon induction. *Nature immunology*, *6*(10), 981-988.

Khodadust, R., Mutlu, P., Yalcın, S., Unsoy, G., & Gunduz, U. (2013). Polyinosinic: polycytidylic acid loading onto different generations of PAMAM dendrimer-coated magnetic nanoparticles. *Journal of Nanoparticle Research*,*15*(8), 1-12.

Khodadust, R., Unsoy, G., Yalcın, S., Gunduz, G., & Gunduz, U. (2013). PAMAM dendrimer-coated iron oxide nanoparticles: synthesis and characterization of different generations. *Journal of Nanoparticle Research*,*15*(3), 1-13.

Kim, D. H., Lee, S. H., Kim, K. N., Kim, K. M., Shim, I. B., & Lee, Y. K. (2005). Cytotoxicity of ferrite particles by MTT and agar diffusion methods for hyperthermic application. Journal of magnetism and magnetic materials,293(1), 287-292.

Kim, D. K., Mikhaylova, M., Zhang, Y., & Muhammed, M. (2003). Protective coating of superparamagnetic iron oxide nanoparticles. Chemistry of Materials,15(8), 1617-1627.

Kiyama, M. (1974). Conditions for the formation of Fe3O4 by the air oxidation of Fe (OH) 2 suspensions. Bull. Chem. Soc. Jpn, 47(7), 1646-1650.

Kjaer, A. (2006). Molecular imaging of cancer using PET and SPECT. In New trends in cancer for the 21st century (pp. 277-284). Springer Netherlands..

Kodama, R. H. (1999). Magnetic nanoparticles. Journal of Magnetism and Magnetic Materials, 200(1), 359-372.

Kohler, N., Fryxell, G. E., & Zhang, M. (2004). A bifunctional poly (ethylene glycol) silane immobilized on metallic oxide-based nanoparticles for conjugation with cell targeting agents. *Journal of the American Chemical Society*, *126*(23), 7206-7211.

Krishnan, K. M., Pakhomov, A. B., Bao, Y., Blomqvist, P., Chun, Y., Gonzales, M., ... & Roberts, B. K. (2006). Nanomagnetism and spin electronics: materials, microstructure and novel properties. Journal of materials science,41(3), 793-815.

Kumar, H., Kawai, T., Kato, H., Sato, S., Takahashi, K., Coban, C., ... & Akira, S. (2006). Essential role of IPS-1 in innate immune responses against RNA viruses. *The Journal of experimental medicine*, *203*(7), 1795-1803.

Lai, P. S., Lou, P. J., Peng, C. L., Pai, C. L., Yen, W. N., Huang, M. Y., ... & Shieh, M. J. (2007). Doxorubicin delivery by polyamidoamine dendrimer conjugation and photochemical internalization for cancer therapy. *Journal of Controlled Release*, *122*(1), 39-46.

Landmark, K. J. (2008). Dendrimer-coated Iron-oxide Nanoparticles as Targeted MRI Contrast Agents. ProQuest.

Lee, I., Athey, B. D., Wetzel, A. W., Meixner, W., & Baker, J. R. (2002). Structural molecular dynamics studies on polyamidoamine dendrimers for a therapeutic application: effects of pH and generation. *Macromolecules*, *35*(11), 4510-4520.

Li, K. C., Pandit, S. D., Guccione, S., & Bednarski, M. D. (2004). Molecular imaging applications in nanomedicine. Biomedical Microdevices, 6(2), 113-116.

Lida, H., Takayanagi, K., Nakanishi, T., & Osaka, T. (2007). Synthesis of Fe< sub> 3</sub> O< sub> 4</sub> nanoparticles with various sizes and magnetic properties by controlled hydrolysis. Journal of colloid and interface science,314(1), 274-280.

Liu, Y., Bryantsev, V. S., Diallo, M. S., & Goddard Iii, W. A. (2009). PAMAM dendrimers undergo pH responsive conformational changes without swelling.*Journal of the American Chemical Society*, *131*(8), 2798-2799.

Lowenstam, H. A. (1962). Magnetite in denticle capping in recent chitons (Polyplacophora). Geological Society of America Bulletin, 73(4), 435-438.

Lu, A. H., Salabas, E. E., & Schüth, F. (2007). Magnetic nanoparticles: synthesis, protection, functionalization, and application. Angewandte Chemie International Edition, 46(8), 1222-1244.

Lübbe, A. S., Alexiou, C., & Bergemann, C. (2001). Clinical applications of magnetic drug targeting. Journal of Surgical Research, 95(2), 200-206.

Lübbe, A. S., Bergemann, C., Brock, J., & McClure, D. G. (1999). Physiological aspects in magnetic drug-targeting. Journal of Magnetism and Magnetic Materials, 194(1), 149-155.

Lübbe, A. S., Bergemann, C., Huhnt, W., Fricke, T., Riess, H., Brock, J. W., & Huhn, D. (1996). Preclinical experiences with magnetic drug targeting: tolerance and efficacy. Cancer research, 56(20), 4694-4701.

Lübbe, A. S., Bergemann, C., Riess, H., Schriever, F., Reichardt, P., Possinger, K., ... & Huhn, D. (1996). Clinical experiences with magnetic drug targeting: a phase I study with 4′-epiDoxorubicin in 14 patients with advanced solid tumors. Cancer research, 56(20), 4686-4693.

Ludeman, S. M. (1999). The chemistry of the metabolites of cyclophosphamide.*Current pharmaceutical design*, *5*, 627-644.

Mahmoudi, M., Simchi, A., Milani, A. S., & Stroeve, P. (2009). Cell toxicity of superparamagnetic iron oxide nanoparticles. *Journal of colloid and interface science*, *336*(2), 510-518.

Maiti, P. K., Çagin, T., Lin, S. T., & Goddard, W. A. (2005). Effect of solvent and pH on the structure of PAMAM dendrimers. *Macromolecules*, *38*(3), 979-991.

Matsumoto, M., Funami, K., Oshiumi, H., & Seya, T. (2003). Toll-like receptor 3: a link between toll-like receptor, interferon and viruses. *Microbiology and immunology*, *48*(3), 147-154.

McBain, S. C., Yiu, H. H. P., El Haj, A., & Dobson, J. (2007). Polyethyleneimine functionalized iron oxide nanoparticles as agents for DNA delivery and transfection. *Journal of Materials Chemistry*, *17*(24), 2561-2565.

Meijer, E. W., Jansen, J. F. G. A., & De Brabander-van den Berg, E. M. M. (1994). Encapsulation of guest molecules into a dendritic box. *Science*, *266*, 1226-1229.

Meyer, J., & Weinmann, J. P. (1957). Occurrence of Phosphamidase Activity in Keratinizing Epithelia1. *Journal of Investigative Dermatology*, *29*(6), 393-405.

Milhaud, P. G., Compagnon, B., Bienvenue, A., & Philippot, J. R. (1992). Interferon production by L929 and HeLa cells enhanced by polyriboinosinic acid-polyribocytidylic acid pH-sensitive liposomes. *Bioconjugate chemistry*, *3*(5), 402-407.

Milhaud, P. G., Machy, P., Lebleu, B., & Leserman, L. (1989). Antibody targeted liposomes containing poly (rI)· poly (rC) exert a specific antiviral and toxic effect on cells primed with interferons α/β or γ. *Biochimica et Biophysica Acta (BBA)-Biomembranes*, *987*(1), 15-20.

Min, K. H., Park, K., Kim, Y. S., Bae, S. M., Lee, S., Jo, H. G., ... & Kwon, I. C. (2008). Hydrophobically modified glycol chitosan nanoparticles-encapsulated camptothecin enhance

the drug stability and tumor targeting in cancer therapy.*Journal of Controlled Release*, *127*(3), 208-218.
Minotti, G., Recalcati, S., Mordente, A., Liberi, G., Calafiore, A. M., Mancuso, C., ... & Cairo, G. (1998). The secondary alcohol metabolite of Doxorubicin irreversibly inactivates aconitase/iron regulatory protein-1 in cytosolic fractions from human myocardium. *The FASEB journal*, *12*(7), 541-552.

Mizota, M., & Maeda, Y. (1986). Magnetite in the radular teeth of chitons.Hyperfine Interactions, 29(1-4), 1423-1426.

Mohapatra, S. C., & Ahmad, S. (2012). Fe< sub> 3</sub> O< sub> 4</sub> inverse spinal super paramagnetic nanoparticles. *Materials Chemistry and Physics*, *132*(1), 196-202.

Mordente, A. L. V. A. R. O., Meucci, E. L. I. S. A. B. E. T. T. A., Silvestrini, A. N. D. R. E. A., Martorana, G. E., & Giardina, B. R. U. N. O. (2009). New developments in anthracycline-induced cardiotoxicity. *Current medicinal chemistry*, *16*(13), 1656-1672.

Mornet, S., Vasseur, S., Grasset, F., & Duguet, E. (2004). Magnetic nanoparticle design for medical diagnosis and therapy. *Journal of Materials Chemistry*, *14*(14), 2161-2175.

Mosbach, K., & Schröder, U. (1979). Preparation and application of magnetic polymers for targeting of drugs. *FEBS letters*, *102*(1), 112-116.

Nedkov, I., Merodiiska, T., Kolev, S., Krezhov, K., Niarchos, D., Moraitakis, E., ... & Takada, J. (2002). Microstructure and magnetic behaviour of nanosized Fe3O4 powders and polycrystalline films. Monatshefte für Chemie/Chemical Monthly, 133(6), 823-828.

Neuberger, T., Schöpf, B., Hofmann, H., Hofmann, M., & von Rechenberg, B. (2005). Superparamagnetic nanoparticles for biomedical applications: possibilities and limitations of a new drug delivery system. Journal of Magnetism and Magnetic Materials, 293(1), 483-496.

Nie, S., Xing, Y., & Kim, G. J. (2007). and Jonathan W. Simons. Annual Review of Biomedical Engineering, 9, 257-88.

Okada, H. (2009). Brain Tumor Immunotherapy with Type-1 Polarizing Strategies. *Annals of the New York Academy of Sciences*, *1174*(1), 18-23.

Olowe, A. A., & Genin, J. M. R. (1991). The mechanism of oxidation of ferrous hydroxide in sulphated aqueous media: Importance of the initial ratio of the reactants. Corrosion science, 32(9), 965-984.

Olson, R. D., Mushlin, P. S., Brenner, D. E., Fleischer, S., Cusack, B. J., Chang, B. K., & Boucek, R. J. (1988). Doxorubicin cardiotoxicity may be caused by its metabolite, Doxorubicinol. *Proceedings of the National Academy of Sciences*, *85*(10), 3585-3589.

Pan, B. F., Gao, F., & Gu, H. C. (2005). Dendrimer modified magnetite nanoparticles for protein immobilization. *Journal of colloid and interface science*, *284*(1), 1-6.

Pan, B., Cui, D., Sheng, Y., Ozkan, C., Gao, F., He, R., ... & Huang, T. (2007). Dendrimer-modified magnetic nanoparticles enhance efficiency of gene delivery system. *Cancer research*, *67*(17), 8156-8163.

Pankhurst, Q. A., Connolly, J., Jones, S. K., & Dobson, J. (2003). Applications of magnetic nanoparticles in biomedicine. Journal of physics D: Applied physics, 36(13), R167.

Papagiannaros, A., Dimas, K., Papaioannou, G. T., & Demetzos, C. (2005). Doxorubicin–PAMAM dendrimer complex attached to liposomes: cytotoxic studies against human cancer cell lines. *International journal of pharmaceutics*,*302*(1), 29-38.

Patri, A. K., Majoros, I. J., & Baker Jr, J. R. (2002). Dendritic polymer macromolecular carriers for drug delivery. *Current Opinion in Chemical Biology*,*6*(4), 466-471.

Pritchard, K. I., Messersmith, H., Elavathil, L., Trudeau, M., O'Malley, F., & Dhesy-Thind, B. (2008). HER-2 and topoisomerase II as predictors of response to chemotherapy. *Journal of Clinical Oncology*, *26*(5), 736-744.

Reetz, M. T., Zonta, A., Vijayakrishnan, V., & Schimossek, K. (1998). Entrapment of lipases in hydrophobic magnetite-containing sol-gel materials: magnetic separation of heterogeneous biocatalysts. *Journal of Molecular Catalysis A: Chemical*, *134*(1), 251-258.

Refait, P., & Génin, J. M. (1993). The oxidation of ferrous hydroxide in chloride-containing aqueous media and Pourbaix diagrams of green rust one. Corrosion science, 34(5), 797-819.

Riu, D. H., Oh, K. S., Lee, H. J., Shin, D. K., Jeong, Y. K., & Lee, J. H. (2006). Nano Magnetite Particles Prepared under the Combined Addition of Urea and Ammonia. Key Engineering Materials, 317, 203-206.

Rouhollah, K., Pelin, M., Serap, Y., Gozde, U., & Ufuk, G. (2013). Doxorubicin loading, release, and stability of polyamidoamine dendrimer-coated magnetic nanoparticles. *Journal of pharmaceutical sciences*.

Sadekar, S., & Ghandehari, H. (2012). Transepithelial transport and toxicity of PAMAM dendrimers: Implications for oral drug delivery. Advanced drug delivery reviews, 64(6), 571-588.

Šafařík, I., & Šafaříková, M. (2002). Magnetic nanoparticles and biosciences. In *Nanostructured Materials* (pp. 1-23). Springer Vienna.

Salaun, B., Greutert, M., & Romero, P. (2009). Toll-like receptor 3 is necessary for dsRNA adjuvant effects. *Vaccine*, *27*(12), 1841-1847.

Salem, M. L., El-Naggar, S. A., Kadima, A., Gillanders, W. E., & Cole, D. J. (2006). The adjuvant effects of the toll-like receptor 3 ligand polyinosinic-cytidylic acid poly (I: C) on antigen-specific CD8+ T cell responses are partially dependent on NK cells with the induction of a beneficial cytokine milieu.*Vaccine*, *24*(24), 5119-5132.

Salvador, A., Igartua, M., Hernández, R. M., & Pedraz, J. L. (2012). Combination of immune stimulating adjuvants with poly (lactide-co-glycolide) microspheres enhances the immune response of vaccines. *Vaccine*, *30*(3), 589-596.

Sanz, V., Conde, J., Hernández, Y., Baptista, P. V., Ibarra, M. R., & Jesús, M. (2012). Effect of PEG biofunctional spacers and TAT peptide on dsRNA loading on gold nanoparticles. *Journal of Nanoparticle Research*, *14*(6), 1-9.

Schaffert, D., Kiss, M., Rödl, W., Shir, A., Levitzki, A., Ogris, M., & Wagner, E. (2011). Poly (I: C)-mediated tumor growth suppression in EGF-receptor overexpressing tumors using EGF-polyethylene glycol-linear polyethylenimine as carrier. *Pharmaceutical research*, *28*(4), 731-741.

Schlosser, E., Mueller, M., Fischer, S., Basta, S., Busch, D. H., Gander, B., & Groettrup, M. (2008). TLR ligands and antigen need to be coencapsulated into the same biodegradable microsphere for the generation of potent cytotoxic T lymphocyte responses. *Vaccine*, *26*(13), 1626-1637.

Schmid, R. (2002). Recent advances in the description of the structure of water, the hydrophobic effect, and the like-dissolves-like rule. In *Highlights in Solute-Solvent Interactions* (pp. 59-90). Springer Vienna.

Schultheiss-Grassi, P. P., & Dobson, J. (1999). Magnetic analysis of human brain tissue. BioMetals, 12(1), 67-72.

Schulz, O., Diebold, S. S., Chen, M., Näslund, T. I., Nolte, M. A., Alexopoulou, L., ... & e Sousa, C. R. (2005). Toll-like receptor 3 promotes cross-priming to virus-infected cells. *Nature*, *433*(7028), 887-892.

Seib, F. P., Jones, A. T., & Duncan, R. (2007). Comparison of the endocytic properties of linear and branched PEIs, and cationic PAMAM dendrimers in B16f10 melanoma cells. *Journal of controlled release*, *117*(3), 291-300.

Senyei, A., Widder, K., & Czerlinski, G. (1978). Magnetic guidance of drug-carrying microspheres. Journal of Applied Physics, 49(6), 3578-3583

Sheehan, J., Cruickshank, P., & Boshart, G. (1961). Notes-A Convenient Synthesis of Water-Soluble Carbodiimides. *The Journal of Organic Chemistry*,*26*(7), 2525-2528.

Shen, T., Weissleder, R., Papisov, M., Bogdanov, A., & Brady, T. J. (1993). Monocrystalline iron oxide nanocompounds (MION): physicochemical properties. *Magnetic Resonance in Medicine*, *29*(5), 599-604.

Shir, A., Ogris, M., Wagner, E., & Levitzki, A. (2005). EGF receptor-targeted synthetic double-stranded RNA eliminates glioblastoma, breast cancer, and adenocarcinoma tumors in mice. *PLoS medicine*, *3*(1), e6.

Shubayev, V. I., Pisanic II, T. R., & Jin, S. (2009). Magnetic nanoparticles for theragnostics. Advanced drug delivery reviews, 61(6), 467-477.

Shukoor, M. I., Natalio, F., Ksenofontov, V., Tahir, M. N., Eberhardt, M., Theato, P., ... & Tremel, W. (2007). Double-Stranded RNA Polyinosinic–Polycytidylic Acid Immobilized onto γ-Fe2O3 Nanoparticles by Using a Multifunctional Polymeric Linker. *Small*, *3*(8), 1374-1378.

Shukoor, M. I., Natalio, F., Metz, N., Glube, N., Tahir, M. N., Therese, H. A., ... & Tremel, W. (2008). dsRNA-Functionalized Multifunctional γ-Fe2O3 Nanocrystals: A Tool for Targeting Cell Surface Receptors. *Angewandte Chemie International Edition*, *47*(25), 4748-4752.

Singh, P., Gupta, U., Asthana, A., & Jain, N. K. (2008). Folate and Folate− PEG− PAMAM Dendrimers: Synthesis, Characterization, and Targeted Anticancer Drug Delivery Potential in Tumor Bearing Mice. *Bioconjugate chemistry*, *19*(11), 2239-2252.

Singhal, S. S., Singhal, J., Sharma, R., Singh, S. V., Zimniak, P., Awasthi, Y. C., & Awasthi, S. (2003). Role of RLIP76 in lung cancer Doxorubicin resistance: I. The ATPase activity of RLIP76 correlates with Doxorubicin and 4-hydroxynonenal resistance in lung cancer cells. *International journal of oncology*, *22*(2), 365.

Slowing, I., Trewyn, B. G., & Lin, V. S. Y. (2006). Effect of surface functionalization of MCM-41-type mesoporous silica nanoparticles on the endocytosis by human cancer cells. *Journal of the American Chemical Society*,*128*(46), 14792-14793.

Sugimoto, T., & Matijević, E. (1980). Formation of uniform spherical magnetite particles by crystallization from ferrous hydroxide gels. Journal of Colloid and Interface Science, 74(1), 227-243.

Sun, C., Lee, J. S., & Zhang, M. (2008). Magnetic nanoparticles in MR imaging and drug delivery. *Advanced drug delivery reviews*, *60*(11), 1252-1265.

Svenson, S. (2009). Dendrimers as versatile platform in drug delivery applications. *European Journal of Pharmaceutics and Biopharmaceutics*, *71*(3), 445-462.

Svenson, S., & Tomalia, D. A. (2012). Dendrimers in biomedical applications—reflections on the field. *Advanced drug delivery reviews*.

Tabeta, K., Georgel, P., Janssen, E., Du, X., Hoebe, K., Crozat, K., ... & Beutler, B. (2004). Toll-like receptors 9 and 3 as essential components of innate immune defense against mouse cytomegalovirus infection. *Proceedings of the National Academy of Sciences of the United States of America*, *101*(10), 3516-3521.

Takeda, K., Kaisho, T., & Akira, S. (2003). Toll-like receptors. *Annual review of immunology*, *21*(1), 335-376.

Tang, Y., Li, Y. B., Wang, B., Lin, R. Y., van Dongen, M., Zurcher, D. M., ... & Qi, R. (2012). Efficient in vitro siRNA delivery and intramuscular gene silencing using PEG-modified PAMAM dendrimers. *Molecular pharmaceutics*, *9*(6), 1812-1821.

Tartaj, P., del Puerto Morales, M., Veintemillas-Verdaguer, S., González-Carreno, T., & Serna, C. J. (2003). The preparation of magnetic nanoparticles for applications in biomedicine. Journal of Physics D: Applied Physics, 36(13), R182..

Teicher, B. A., Linehan, W. M., & Helman, L. J. (2012). Targeting cancer metabolism. Clinical Cancer Research, 18(20), 5537-5545.

Thomas, T. P., Majoros, I. J., Kotlyar, A., Kukowska-Latallo, J. F., Bielinska, A., Myc, A., & Baker, J. R. (2005). Targeting and inhibition of cell growth by an engineered dendritic nanodevice. *Journal of medicinal chemistry*, *48*(11), 3729-3735.

Thorek, D. L., & Tsourkas, A. (2008). Size, charge and concentration dependent uptake of iron oxide particles by non-phagocytic cells. *Biomaterials*,*29*(26), 3583-3590.

Thorn, C. F., Oshiro, C., Marsh, S., Hernandez-Boussard, T., McLeod, H., Klein, T. E., & Altman, R. B. (2011). Doxorubicin pathways: pharmacodynamics and adverse effects. Pharmacogenetics and genomics,21(7), 440.

Thorne, M. J. (1968). Studies on homing in the chiton Acanthozostera gemmata. Marine and Freshwater Research, 19(2), 151-160.

Tincer, G., Yerlikaya, S., Yagci, F. C., Kahraman, T., Atanur, O. M., Erbatur, O., & Gursel, I. (2011). Immunostimulatory activity of polysaccharide–poly (I: C) nanoparticles. *Biomaterials*, *32*(18), 4275-4282.

Tomalia, D. A., Baker, H., Dewald, J., Hall, M., Kallos, G., Martin, S., ... & Smith, P. (1985). A new class of polymers: starburst-dendritic macromolecules.*Polym. j*, *17*(1), 117-132.

Tomalia, D. A., Baker, H., Dewald, J., Hall, M., Kallos, G., Martin, S., ... & Smith, P. (1986). Dendritic macromolecules: synthesis of starburst dendrimers.*Macromolecules*, *19*(9), 2466-2468.

Tripathi, A., Gupta, R., & Saraf, S. A. (2010). PLGA nanoparticles of anti tubercular drug: drug loading and release studies of a water in-soluble drug. Int J PharmTech Res, 2(3), 2116-2123.

Tsai, H. C., & Imae, T. (2010). Fabrication of dendrimers toward biological application. *Progress in molecular biology and translational science*, *104*, 101-140.

Unsoy, G., Yalcin, S., Khodadust, R., Gunduz, G., & Gunduz, U. (2012). Synthesis optimization and characterization of chitosan-coated iron oxide nanoparticles produced for biomedical applications. *Journal of Nanoparticle Research*, *14*(11), 1-13.

Uzun K, C¸ evik E, S¸ enel M, So¨zeri H, Baykal A, Abasıyanık FM, Toprak SM (2010) Covalent immobilization of invertase on PAMAM-dendrimer modified superparamagnetic iron oxide nanoparticles. J Nanopart Res 12(8):3057–3067

Veiseh, O., Gunn, J. W., & Zhang, M. (2010). Design and fabrication of magnetic nanoparticles for targeted drug delivery and imaging. *Advanced drug delivery reviews*, *62*(3), 284-304.

Vercammen, E., Staal, J., & Beyaert, R. (2008). Sensing of viral infection and activation of innate immunity by toll-like receptor 3. *Clinical microbiology reviews*, *21*(1), 13-25.

Villaverde, A. (2011). *Nanoparticles in translational science and medicine*. Academic Press.

Vince, J. E., & Tschopp, J. (2010). IRF-3 partners Bax in a viral-induced dance macarbre. *The EMBO Journal*, *29*(10), 1627.

Weber, A., Kirejczyk, Z., Besch, R., Potthoff, S., Leverkus, M., & Häcker, G. (2009). Proapoptotic signalling through Toll-like receptor-3 involves TRIF-dependent activation of caspase-8 and is under the control of inhibitor of apoptosis proteins in melanoma cells. *Cell Death & Differentiation*, *17*(6), 942-951.

Weinstein, D. M., Mihm, M. J., & Bauer, J. A. (2000). Cardiac peroxynitrite formation and left ventricular dysfunction following Doxorubicin treatment in mice. *Journal of Pharmacology and Experimental Therapeutics*, *294*(1), 396-401.

Weiss, R. B. (1992). The anthracyclines: will we ever find a better Doxorubicin?. In *Seminars in oncology* (Vol. 19, No. 6, pp. 670-686).

Whitesides, G. M. (2003). The'right'size in nanobiotechnology. *Nature biotechnology*, *21*(10), 1161-1165.

Widder, K. J., Senyei, A. E., & Ranney, D. F. (1979). Magnetically responsive microspheres and other carriers for the biophysical targeting of antitumor agents. *Adv. Pharmacol. Chemother*, *16*, 213-271.

Widder, K. J., Senyei, A. E., & Scarpelli, D. G. (1978, June). Magnetic microspheres: a model system for site specific drug delivery in vivo. In Proceedings of the Society for Experimental Biology and Medicine. Society for Experimental Biology and Medicine (New York, NY) (Vol. 158, No. 2, pp. 141-146). Royal Society of Medicine.

Willard, M. A., Kurihara, L. K., Carpenter, E. E., Calvin, S., & Harris, V. G. (2004). Chemically prepared magnetic nanoparticles. International Materials Reviews, 49(3-4), 3-4.

Wojnowski, L., Kulle, B., Schirmer, M., Schlüter, G., Schmidt, A., Rosenberger, A., ... & Hasenfuss, G. (2005). NAD (P) H oxidase and multidrug resistance protein genetic polymorphisms are associated with Doxorubicin-induced cardiotoxicity. *Circulation*, *112*(24), 3754-3762.

Wu, J., Wang, Y. S., Yang, X. Y., Liu, Y. Y., Yang, J. R., Yang, R., & Zhang, N. (2012). Graphene oxide used as a carrier for adriamycin can reverse drug resistance in breast cancer cells. *Nanotechnology*, *23*(35), 355101.

Wuang, S. C., Neoh, K. G., Kang, E. T., Pack, D. W., & Leckband, D. E. (2007). Synthesis and functionalization of polypyrrole-Fe3O4 nanoparticles for applications in biomedicine. *Journal of Materials Chemistry*, *17*(31), 3354-3362.

Xu, C., & Sun, S. (2007). Monodisperse magnetic nanoparticles for biomedical applications. Polymer International, 56(7), 821-826.

Zhao, X., Ai, M., Guo, Y., Zhou, X., Wang, L., Li, X., & Yao, C. (2012). Poly I: C-Induced Tumor Cell Apoptosis Mediated by Pattern-Recognition Receptors.*Cancer Biotherapy and Radiopharmaceuticals*, *27*(9), 530-534.

Zyad, A., Bénard, J., Tursz, T., Clarke, R., & Chouaib, S. (1994). Resistance to TNF-α and adriamycin in the human breast cancer MCF7 cell line: relationship to MDR1, MnSOD, and TNF gene expression. *Cancer research*, *54*(3), 825-831.

CURRICULUM VITAE

Rouhollah KHODADUST

PhD on BSc, DEPARTMENT OF BIOTECHNOLOGY
Address: Department of Biological Scince, Middle East Technical University, 06800 Çankaya Ankara/TURKEY
Tel :+90 (312) 210-5184 & +90(531) 5563440
E-mail: hodadust_r@yahoo.com
Date of Birth & Place: 07.02.1981 Ardebil-Iran

Academic Qualifications

University	Education Field	Education Period	Degree	CumGPA
METU Ankara-Turkey	Biotechnology	01.07.2008-04.09.2013	PhD	3.43/4.00
METU Ankara-Turkey	Biotechnology	2007- 2008	Master	3.57/4.00
METU Ankara-Turkey	English Language	2006-2007	Proficiency	76.5/100
Istanbul University Istanbul-Turkey	Turkish Language	2004-2005	Proficiency	perfect
Tehran University of Medical Sciences Tehran-Iran	Medical Enthomolgy	1997-2001	Bachelor (BSc)	3.14/4.00

Languages

Azerbaycani: Fluent (Mother tongue)
Turkish: Fluent
Persian: Fluent
English: Excellent
Arabic: Beginner

Professional Positions Held

Institution: Ardabil University of Medical Science, Ardebil, Iran
Job Title: Responsible for the control of Malaria disease
Date: 2002-2004

Honors and Awards

- Success Award by the *Rector of Ardabil University of Medical Science* for being the main responsible person of the team of controlling Malaria disease in Iran-Azerbaijan Border for great success in controlling malaria disease and decreasing the disease cases from 542 cases to zero in less than three years (2002-2004)

- METU Graduate Courses Performance Award (2008-2009)

- 2215 – TUBITAK-Graduate Scholarship Program for International Students (2009-2013)

Publications
[Refereed SCI/SSCI Journal Articles]

Ünsoy,G., Yalçın,S., **Khodadust,R.,** Gündüz,G., Gündüz,U., "Synthesis optimization and characterization of chitosan-coated iron oxide nanoparticles produced for biomedical applications." *Journal of Nanoparticle Research.,* Vol:14, No: 964 (2012). (**SCI/SSCI**)

Khodadust,R., Ünsoy,G., Yalçın,S., Gündüz,G., Gündüz,U., "PAMAM Dendrimer Coated Iron Oxide Nanoparticles: Synthesis and Characterization of Different Generations" *Journal of Nanoparticle Research* Vol:15, No: 1488, 2013, (**SCI/SSCI**)

Khodadust,R., Mutlu,P., Yalçın,S., Ünsoy,G., Gündüz,U., "Doxorubicin loading, release and stability of PAMAM dendrimer coated magnetic nanoparticle" *Journal of Pharmaceutical Sciences.*, DOI 10.1002/jps.23524 (**SCI /SSCI**)

Khodadust,R., Mutlu,P., Yalcin.S., Uusoy,G., Gunduz,U., "Polyinosinic:Polycytidylic Acid Loading onto Different Generation of PAMAM Dendrimer coated Magnetic Nanoparticles" *Journal of Nanoparticle Research*, Vol:15, No: 1860, 2013, (**SCI /SSCI**)

Azar, N. T. P., Mutlu, P., **Khodadust, R.,** & Gunduz, U. Poly (amidoamine)(PAMAM) Nanoparticles: Synthesis and Biomedical Applications. *Hacettepe J. Biol. & Chem.*, 2013, 41 (3), 289-299

Yalçın,S., **Khodadust,R.,** Ünsoy,G., Garip,I.C., Mumcuoğlu, Z.D., Gündüz,U. "Synthesis and characterization of Poly-hydroxybutyrate (PHB) coated magnetic nanoparticles: toxicity analyses on different cell lines." *Synthesis and Reactivity in Inorganic, Metal-Organic, and Nano-Metal Chemistry* ID LSRT-2013-0374.R1 (Accepted)

Yalçın,S., Khodadust,R., Ünsoy,G., Mutlu,P., Gündüz,U. "Poly-Hydroxy Butyrate (PHB) Coated Magnetic Nanoparticles For Doxorubicin Release" International Journal of Nanomedicine (Submitted)

Oral Presentaiton

Khodadust,R., Ünsoy,G., Yalçın,S., Mutlu,P., Gündüz,U., Synthesis of dendrimeric magnetic nanoparticles and imaging studies using IgG-FITC . *" NANOMEDICINE:FROM MOLECULES TO DIAGNOSIS AND THERAPY,* Rome CONSIGLIO NAZIONALE DELLE RICERCHE October, 1 - 3, 2012", Rome, (2012), SL4.

Khodadust,R., Yalçın,S., Ünsoy,G., Gündüz,G., Gündüz,U., Synthesis and Characterization of Dendrimer Coated Magnetic Nanoparticles for Drug Delivery. "*BIOMED 2011, XVIIth International Symposium on Biomedical Science and Technology", ,* (2011), p.O-22.

Khodadust, R., Gündüz,G., Gündüz,U., Dendrimer Modified Superparamagnetic İron Oxide Nanoparticle Synthesis for Targeted Cancer Therapy. *"NANOTR VII , 7 th Nanoscience and Nanotechnology Conference*, June 27-July 01, Istanbul",Turkey,(2011),.

[Refereed Proceedings]
International

Yalçın,S., Ünsoy,G., Mutlu,P., **Khodadust,R.**, Gündüz,U., The identification of cytotoxicity of various polymers coated magnetic iron oxide nanoparticles in MCF7 cells. " *NANOMEDICINE:FROM MOLECULES TO DIAGNOSIS AND THERAPY,* Rome CONSIGLIO NAZIONALE DELLE RICERCHE October, 1 - 3, 2012", Rome, (2012), P30.

Ünsoy,G., Yalçın,S**.,** **Khodadust,R.,** Mutlu,P., Gündüz,G., Gündüz,U., Clellular internalization of Chitosan Coated Magnetic Nanoparticles ByMCF7 Cells. " *ISOPS 10 th INTERNATINAL SYMPOSIUM ON PHARMACEUTICAL SCIENCES* June, 26-29, 2012", Ankara, (2012), P240.

Ünsoy,G., Yalçın,S., **Khodadust,R.,** Mutlu,P., Gündüz,U., Determination of loading and release efficiencies of Doxorubicin by using chitosan coated of magnetic nanoparticles designed for targeted drug delivery " *NANOMEDICINE:FROM MOLECULES TO DIAGNOSIS AND THERAPY,* Rome CONSIGLIO NAZIONALE DELLE RICERCHE October, 1 - 3, 2012",Rome , (2012), P26.

Yalçın,S., Ünsoy,G., Mutlu,P., **Khodadust,R.,** Gündüz,U., Loading, release, stability of anti cancer drug from in situ formation PHB coated magnetic nanoparticles . " NANOMEDICINE:FROM MOLECULES TO DIAGNOSIS AND THERAPY, Rome CONSIGLIO NAZIONALE DELLE RICERCHE October, 1 - 3, 2012", Rome, (2012), P28.

Yalçın,S., Ünsoy,G., Mutlu,P., **Khodadust,R.,** Gündüz,U., Preparation of antibody-FITC binding dextran coated magnetic nonoparticles for imaging and cancer therapy" *NANOMEDICINE:FROM MOLECULES TO DIAGNOSIS AND THERAPY,* Rome CONSIGLIO NAZIONALE DELLE RICERCHE October, 1 - 3, 2012",Rome , (2012), P29.

Ünsoy,G., Yalçın,S., **Khodadust,R.,** Mutlu,P., Taghavipourianazar,N., Gündüz,U., IN SITU Synthesis and Characterization of Chitosan Coated Iron Oxide Nanoparticles and Loading of Doxorubicin. " *NANOCON 4 th INTERNATIONAL CONFERENCE*, Oct 23 – 25, 2012, Brno, Czech Republic, EU, PE11. (Full paper)

Yalçın,S., Ünsoy,G., **Khodadust,R.,** Mutlu,P., Taghavipourianazar,N., Gündüz,U., The Cytotoxicity Analysis of PHB Coated Magnetic Nanoparticles on Sensaitive and Doxorubicin Resistant MCF7 Cell Lines. *" NANOCON 4 th INTERNATIONAL CONFERENCE*, Oct 23 – 25, 2012, Brno, Czech Republic, EU, PD5. (full paper)

Khodadust,R., Mutlu,P., Yalçın,S., Ünsoy,G., Taghavipourianazar,N.,Gündüz,U., Loading Efficiency Optimization of Doxorubicin on Dendrimer Coated Magnetic Nanoparticles Using Different Buffers. " *NANOCON 4 th INTERNATIONAL CONFERENCE*, Oct 23 – 25, 2012, Brno, Czech Republic, EU, PA72. (full paper)

Ünsoy,G., **Khodadust,R.,** Yalçın,S., Gündüz,G., Gündüz,U., Characterization of Etoposide Loaded Magnetic Nanoparticles Prepared for Drug Delivery. *"BIOMED 2011, XVIIth International Symposium on Biomedical Science and Technology,* Nov.23-25", , (2011), p.P-16.

Yalçın,S., Ünsoy,G., **Khodadust,R.,** Gündüz,G., Gündüz,U., Synthesis and Characterization of Dextran Coated Magnetic Nanoparticles for Anti-Cancer Agent Delivery in Cancer Therapy. *"BIOMED 2011, XVIIth International Symposium on Biomedical Science and Technology,* Nov.23-25, Ankara",, (2011), p.P-20.

Khodadust,R., Mutlu,P., Gündüz,U., The cytotoxic effect of Doxorubicin-loaded Dendrimer Coated Magnetic Nanoparticles on MCF7 cell line. "*BIOMED 2011,XVII th International Symposium on Biomedical Science and Technology,* Nov.23-25, Ankara", , (2011), p.P-28.

Ünsoy,G., Yalçın,S., **Khodadust,R.,** Mutlu,P., Gündüz,U., Preperatin of Fluoroscent IgG Monoclonal Antibody Conjugated Chitosan Coated Magnetic Nanoparticles For Cncer Theragnostics . *"NANOTR VIII , 8 th Nanoscience and Nanotechnology Conference & 3 th World Congress IANM, June 25-29 01Ankara", ,* (2012), pp-342.

Yalçın,S., Ünsoy,G., **Khodadust,R.,** Mutlu,P., Mumcuoğlu,D., Gündüz,U., Cellular Internalization of Polyhydroxybutyrate (PHB) Coated Magnetic Nanoparticles in MCF7 Cell Lines. *"NANOTR VIII , 8 th Nanoscience and Nanotechnology Conference & 3 th World Congress IANM,* June 25-29 01Ankara", , (2012), pp-264.

Khodadust,R., Mutlu,P., Yalçın,S., Ünsoy,G., Gündüz,U., The Cytotoxic Analysis of Free Doxorubicin and DoxorubicinLoaded Dendrimer Coated Magnetic Nanoparticles on Sensitive and Doxorubicin Resistant MCF7 Cell Lines . *"NANOTR VIII , 8 th Nanoscience*

and Nanotechnology Conference & 3 th World Congress IANM, June 25-29 01Ankara", , (2012), p-262.

Ünsoy,G., Yalçın,S., Khodadust,R., Mutlu,P., Gündüz,G., Gündüz,U., Clellular internalization of Chitosan Coated Magnetic Nanoparticles ByMCF7 Cells. " *ISOPS 10 th INTERNATINAL SYMPOSIUM ON PHARMACEUTICAL SCIENCES* June, 26-29, 2012", Ankara, (2012), P240.

Yalçın,S., **Khodadust,R**., Ünsoy,G., Mutlu,P., Garip,C., Gündüz,U., Synthesis and Characterization of Polyhydroxybutyrate (PHB) Coated Magnetic Nanoparticles for Anti-Cancer Agent Delivery in Cancer Therpay . *" ISOPS 10 th INTERNATINAL SYMPOSIUM ON PHARMACEUTICAL SCIENCES* June, 26-29, 2012", Ankara, (2012), P256.

Khodadust,R., Ünsoy,G., Yalçın,S., Mutlu,P., Gündüz,G., Gündüz,U., Synthesis of IgG Monoclonal Antibody Conjugated Fluoroscent Dendrimer Coated Magnetic Nanoparticles For Cancer Therapy. " *ISOPS 10 th INTERNATINAL SYMPOSIUM ON PHARMACEUTICAL SCIENCES* June, 26-29, 2012", Ankara, (2012), P271

[Refereed Proceedings]
National

Keskin T., Tansık G., Yakar A., Unsoy G., **Khodadust R.,** Gündüz U.,, In vitro Cytotoxic Studies of Polymer Coated Magnetic Nanoparticles for Anti-Cancer Drug Delivery. *"6th Nanoscience and Nanotechonology Conference,* Conference Book, 15-18 June, 2010, Çeşme,İzmir",Turkey , (2010), s.470.

Yakar A., Unsoy G., **Khodadust R.,** Tansık G., Keskin T., Gündüz U., Preparation of PLGA and Chitosan-modified PLGA Coated Magnetite Nanoparticles. *"6th Nanoscience and Nanotechonology Conference*, Conference Book, 15-18 June, 2010, Çeşme, İzmir", Turkey, (2010), s.477.

Yakar A., Tansık G., **Khodadust R.,** Keskin T., Unsoy G., Gündüz U.,, Synthesis of Magnetic Nanoparticles as a Targeting System for Drug Delivery. *"6th Nanoscience and Nanotechonology Conference, Conference* Book, 15-18 June, 2010, Çeşme, İzmir", Turkey, (2010), s.476.

Khodadust,R., Erdem,M., Gündüz,U., Liposomal Delivery of Poly (I:C) on Sensitive and 1000Dox Resistant MCF7 Cell Line ."*NANOTR VII , 7 th Nanoscience and Nanotechnology Conference,* June 27-July 01, Istanbul", , (2011), s.

Project Collaborations

A.

1. Research fund project (BAP1) Funding agency: BAP1(Excluding thesis supports). Project code: BAP: 08-11-2012-012. Project name: The in vivo cytotoxicity analysis of synthesized polymer coated magnetic nanoparticles prepared for Targeted cancer therapy application purposes: institution: METU-GATA From Month:1 Year: 2012 to Month: 12 Year: 2012

2. Research fund project (BAP1) Funding agency: BAP1 (Excluding thesis supports). Project code: BAP: 07-02-2012-001. Project name: Suppression of Survivin gene expression in cancer cell line with siRNA loaded Magnetic Nanoparticles: institutions: METU From Month:1 Year: 2012 to Month: 12 Year: 2012

3. Research fund project (BAP1) Funding agency: BAP1 (Excluding thesis supports). Project code: BAP: 08-11-2012-012. Project name: The in vivo cytotoxicity analysis of synthesized polymer coated magnetic nanoparticles prepared for Targeted cancer therapy application purposes: Institutions: METU-GATA from Month: 1 Year: 2012 to Month: 12 Year: 2012- extended to Month: 12 Year: 2013

4. Research fund project (BAP1) Funding agency: BAP1 (Excluding thesis supports). Project code: BAP-08-11-2013-018 Project name: Immunocytochemistry analysis of Doxorubicin-loaded chitosan-coated magnetic nanoparticles on cancer cell line. METU-GATA From Month:1 Year: 2013 to Month: 12 Year: 2013

5. Project work (NATIONAL) Funding agency: TUBİTAK Projects. Project code: TBAG: 109T949. Project name: Idarubicin loaded magnetic nanoparticles synthesis and cytotoxicity analysis on MCF7 breast cancer cell line: institution: METU From Month:4 Year: 2010 to Month:7 Year: 2012

6. Research fund project (BAP1) Funding agency: BAP1(Excluding thesis supports). Project code: BAP-07-02-2010-06. Project name: Dendrimer coated Magnetic nanoparticles application for drug targeting in cancer therapy: institution: METU From Month:1 Year: 2010 to Month: 12 Year: 2010- extended to Month: 12 Year: 2013

B.

1.close collaboration with a team of Tehran University of Medical Sciences working on a project under the name of "bionomics of malaria vectors in a resurgent malaria region bordered with Turkey"(the chairperson of the team was Prof. Dr. Hasan Vatandoost). 2002-2004

2. Collaboration with team from Tehran pastor Institute on projects related to malaria diseases 2002-2004

3. Collaboration with team from Meshkinshahr Kalaazar (Leshmaniosis) Research Institute on projects related to Kalaazar disease(the president of Institute was prof. Dr. Mehdi Mohebali) 2002-2004